QATAR UNIVERSITY

COLLEGE OF ENGINEERING

ADVANCED DSP ALGORITHMS FOR MODERN WIRELESS COMMUNICATION TRANSCEIVERS

BY

LUTFI ZUHAIR LUTFI SAMARA

A Dissertation Submitted to

the Faculty of the College of Engineering

in Partial Fulfillment of the Requirements for the Degree of

Doctorate of Philosophy in Electrical Engineering

June 2019

COMMITTEE PAGE

The members of the Committee approve the Dissertation of

Lutfi Zuhair Lutfi Samara defended on April 18, 2019.

Prof. Ridha Hamila
Dissertation Supervisor

Prof. Sofiène Tahar
Committee Member

Prof. Mohsen Guizani
Committee Member

Dr. Aiman Erbad
Committee Member

Approved:

Abdelmagid Hamouda, Dean, College of Engineering

ABSTRACT

Samara, Lutfi, Zuhair, Lutfi, Doctorate : June : 2019.

Doctorate of Philosophy in Electrical Engineering.

Title: Advanced DSP Algorithms for Modern Wireless Communication Transceivers.

Supervisor of Thesis: Prof. Ridha Hamila.

A higher network throughput, a minimized delay and reliable communications are some of many goals that wireless communication standards, such as the fifth-generation (5G) standard and beyond, intend to guarantee for its customers. Hence, many key innovations are currently being proposed and investigated by researchers in the academic and industry circles to fulfill these goals. This dissertation investigates some of the proposed techniques that aim at increasing the spectral efficiency, enhancing the energy efficiency, and enabling low latency wireless communications systems. The contributions lay in the evaluation of the performance of several proposed receiver architectures as well as proposing novel digital signal processing (DSP) algorithms to enhance the performance of radio transceivers. Particularly, the effects of several radio frequency (RF) impairments on the functionality of a new class of wireless transceivers, the full-duplex transceivers, are thoroughly investigated. These transceivers are then designed to operate in a relaying scenario, where relay selection and beamforming are applied in a relaying network to increase its spectral efficiency. The dissertation then investigates the use of greedy algorithms in recovering orthogonal frequency division multiplexing (OFDM) signals by using sparse equalizers, which carry out the equalization in a more efficient manner when the low-complexity single tap OFDM equalizer can no longer recover the received signal due to severe interferences. The proposed sparse equalizers are shown to perform close to conventional optimal and dense equalizers when the OFDM signals are impaired by interferences caused by the insertion of an insufficient cyclic prefix and RF impairments.

DEDICATION

To my family.

ACKNOWLEDGEMENTS

The research work reported in this dissertation was carried out between 2014 and 2019 at the Department of Electrical Engineering, Qatar University, Doha, Qatar. This dissertation was made possible by the graduate student research award (GSRA) grant #2-1-0601-14011 from the Qatar National Research Fund (QNRF) (a member of Qatar Foundation). I am grateful for the opportunity that QNRF has granted me to complete my doctoral studies.

I would like to thank Prof. Ridha Hamila for his guidance throughout the years of my studies at Qatar University. I was involved with Prof. Ridha all the way from my undergraduate studies in 2010 until my doctoral dissertation defense. I would also like to thank Prof. Naofal Al-Dhahir and Dr. Tamer Khattab for their support throughout my research work.

I would also like to thank my defense committee Dr. Aiman Erbad, Prof. Mohsen Guizani and Prof. Sofiène Tahar for their time and useful comments.

Finally, I would like to thank my co-workers A. Abdellatif, A. Al-abbasi, A. Gouissem, F. Sonnara, M. Mokhtar at Qatar University for their help and useful discussions, and for providing me with a friendly work atmosphere at the Research and Graduate Studies workplace.

TABLE OF CONTENTS

LIST OF TABLES

LIST OF FIGURES

ACRONYMS

5G	Fifth generation
ADC	Analog-to-digital converter
AF	Amplify-and-forward
AWGN	Additive white Gaussian noise
BER	Bit Error Rate
BPSK	Binary phase-shift keying
CFO	Carrier-frequency offset
CIR	Channel impulse response
CM/A	Complex multiplication/addition (CM/A)
CP	Cyclic prefix
CPE	Common phase error
CSI	Channel-state information
DF	Decode-and-forward
DFE	Decision-feedback equalizer
DFT	Discrete Fourier transform
DSP	Digital signal processing
ETC	Equal tap channel
FD	Full-duplex
FEC	Forward error correction
FFT	Fast Fourier transform
FIR	Finite impulse response
FRO	Free-running oscillator
HD	Half-duplex

I/Q	In-phase/quadrature
ICI	Inter-carrier interference
IEEE	Institute of electrical and electronics engineers
IQI	In-phase/quadrature imbalance
IRR	Image-rejection ratio
IRS	Impulse response shortening
ISI	Inter-user interference
LE	Linear equalizer
LNSR	Limited number of selected relays
LNSR-ℓ_1	Limited Number of Selected Relays - ℓ_1-norm
LNSR-**ZF**	Limited number of selected relays - Zero forcing
LTE	long-term evolution
MEC	Maximum expected coherence
MIMO	Multiple-input multiple-output
MMSE	Minimum mean-squared error
MSE	Mean-squared error
OFDM	Orthogonal Frequency Division Multiplexing
OIR	Overall impulse response
OMP	Orthogonal matching pursuit
OSRS	Optimal single relay selection
OSRS-**BF**	Optimal single relay selection with beamforming
OST	One-step thresholding
PLL	Phase-locked loop
PN	Phase noise
QAM	Quadrature Amplitude Modulation

RF	Radio frequency
Rx	Receiver
SI	Self-interference
SINR	Signal-to-interference plus noise ratio
SNR	Signal-to-interference ratio
TDE	Time-domain equalizers
Tx	Transmitter
UNSR	Unlimited number of selected relays
UNSR-ℓ_1	Unlimited Number of Selected Relays - ℓ_1-norm
UNSR-**ZF**	Unlimited number of selected relays - Zero forcing
WCC	Worst-case coherence
WiMax	Worldwide interoperability for microwave access
ZF	Zero forcing

NOTATIONS

$A_{i,j}$	The element of the Matrix $\mathbf{A}$ in the i^{th} row and j^{th} column.
a_i	The i^{th} element of the vector $\mathbf{a}$.
$\underset{i \in S}{\overset{K}{\text{argmax}}}(\mathbf{a})$	The arguments of the K largest elements.
Bold upper case symbols.	Matrices.
Bold lower case symbols.	Vectors.
$\text{card}(.)$	The cardinality operator.
$\text{diag}(\mathbf{A})$	The main diagonal vector of the matrix $\mathbf{A}$.
$\text{diag}(\mathbf{v})$	A diagonal matrix with its diagonals being $\mathbf{v}$.
$\mathbb{E}\{.\}$	The statistical expectation operator.
$\mathbf{F}$	The FFT matrix.
$\mathbf{I}_N$	The identity matrix of size $N \times N$.
ℓ_p-norm and $\|\|.\|\|_p$	The p-norm operator.
$\Re\{.\}$	The real operator.
$\text{Tr}(.)$	The trace operator.
$\text{vec}(.)$	The matrix vectorization operator.
$\mathbf{0}_N$	The all-zero matrix of size $N \times N$.
$(.)^H$	The complex-conjugate transpose operator.
$(.)^T$	The transpose operator.
$(.)^{-1}$	The inverse operator.
$(.)^*$	The complex conjugate operator.
$\|.\|$	The absolute value operator.
$\odot$	The element-wise (Hadamard) product operator.
$\oslash$	The element-wise division operator.
$\otimes$	The Kroenecker product operator.
$\perp$	The statistical independence operator.
$\lceil . \rceil$	The round up operator.

CHAPTER 1: INTRODUCTION

1.1. Overview and Motivation

Today, the academic and industrial circles are compelled to propose efficient and novel solutions to cope with the increasing demand on wireless communication applications. New wireless communication standards such as the filth generation (5G) standard are supposed to promote the most suitable of the proposed solutions to support high capacity figures, taking into considerations several constraints such as communication delay and energy efficiency.

In general, this dissertation discusses two main topics that are inline with the goals that the new wireless communication standards consider. The first is the new class of transceivers, the full-duplex (FD) transceivers, which can potentially double the spectral efficiency of wireless communications. The second is efficient signal equalization techniques that decrease the complexity of the detection of signals.

More specifically, the effects of radio frequency (RF) impairments in full-duplex (FD) transceivers are thoroughly investigated both in a bidirectional communication scenario and one-way dual-hop relaying networks. The analytical investigations quantify the performance of the transceiver by measuring the amount of residual self-interference (SI).

Then, the problem of multiple relay selection and beamforming in one-way dual-hop relaying networks is investigated, where the relay is assumed to use FD transceivers and adopts the amplify-and-forward (AF) protocol.

The dissertation further proposes the use of several digital signal processing (DSP) approaches in the detection of wireless signals. In particular, greedy algorithms are exploited to approximate complex signal equalizers while still maintaining an acceptable performance. The approximation here aims at reducing the complexity of the equalization process. The proposed equalizers, which are named as sparse equalizers in this dissertation, account for the effects of phase noise (PN) due to RF non-idealities

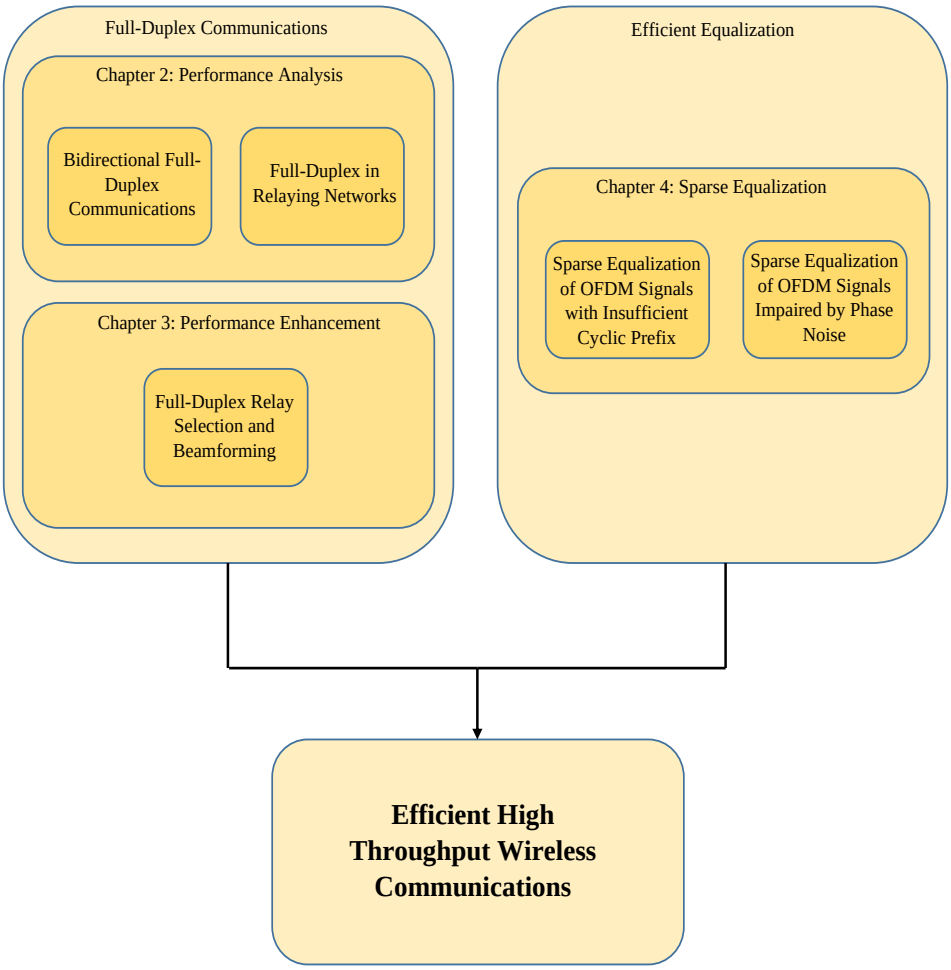

Figure 1.1: Overview of the dissertation.

[1], and inter-symbol interference (ISI) and inter-carrier interference (ICI) which result from using insufficient cyclic prefix (CP) [2].

Hence, overall, this dissertation aims at enhancing the performance of wireless communications to support applications that require high data throughout. The combination of FD communications and efficient equalization can help in improving the performance of wireless communications, and hence potentially meeting the requirements of new wireless communication standards. Fig. 1.1 depicts the overall structure of the conducted research work reported in the dissertation, as well as the link between different chapters/sections.

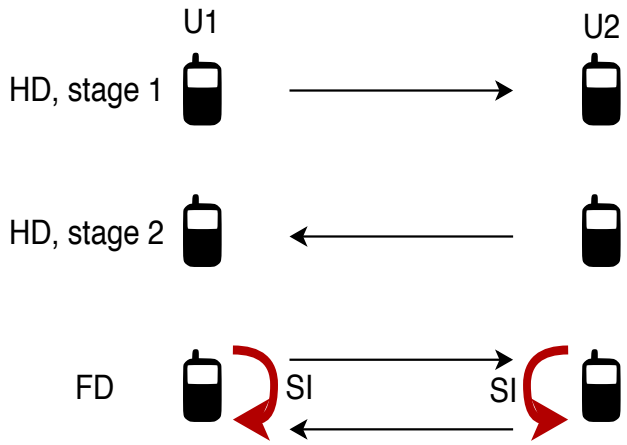

Figure 1.2: FD bidirectional communication example.

1.2. Background

Traditionally, it has been long thought that carrying out wireless communications is possible only if data is properly duplexed using e.g. time or frequency division duplexing (TDD and FDD). The orthogonalization of the exchanged signals should be carefully carried out to insure that a communicating transceiver will not interfere with itself. Hence, a wireless node should be either transmitting or receiving data on a frequency band of interest, otherwise the receiver will not be able to detect an incoming signal of interest that has more than 100 dB lower power than that of the transmitted one. One way of dropping the orthogonalization constraint is for the transceiver to use the transmitted data to cancel out the resulting SI. Fig. 1.2 explains the differences between the traditional TDD and its FD counterpart. The SI is highlighted with a red arrow. The literature contains a considerable amount of contributions regarding SI cancellation, combining active and passive approaches in the wireless propagation domain [3], radio-frequency [4] and base-band domains [5]. Hardware verifications of FD transceivers were also carried out in the literature mainly to test the achievable amount of SI suppression, where for instance, suppression levels of more than 100 dB was reported in [6]. Network service providers are mainly interested in applying FD communications to potentially double the spectral efficiency. For instance, Fig. 1.2

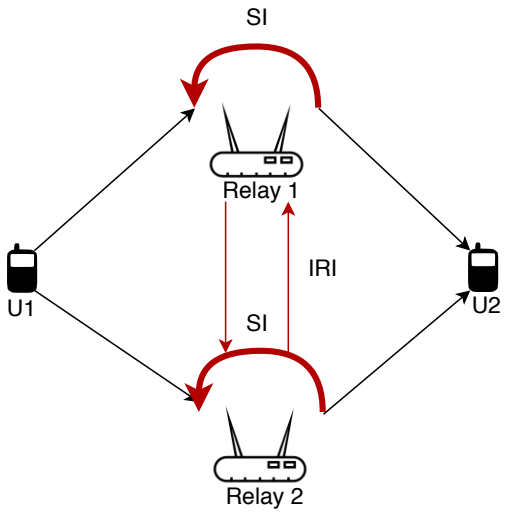

Figure 1.3: FD communications when deployed by relays.

shows a bidirectional communication between the nodes U1 and U2. Assuming a TDD duplexing approach, the half-duplex (HD) scheme needs either of the nodes to seize transmitting in order to be able to detect the signal of interest. However, if SI is canceled sufficiently, simultaneous transmission and reception between U1 and U2 can occur, hence doubling the spectral efficiency.

Moreover, Fig. 1.3 depicts a scenario where a relay operates in a FD mode to connect between U1 an U2. In the case of utilizing both relays to forward the message, both relays not only suffer from SI, but from inter-relay interference (IRI). Hence, although FD communications may increase the spectral efficiency if the SI is dealt with, IRI suppression schemes should be devised to fully exploit the FD communication scheme. Fig. 1.4 depicts a base-station (BS) simultaneously transmitting and receiving data related to two users, U1 and U2. Although the SI is the main bottleneck hindering the network from operating with a satisfactory performance, inter-user interference strategies should be deployed to fully exploit the FD communication scheme. As previously mentioned, the SI is the main obstacle hindering a communication node from exploiting the advantage that FD communications can offer. Hence, this dissertation focuses on the effects hardware imperfections on the cancellation of SI.

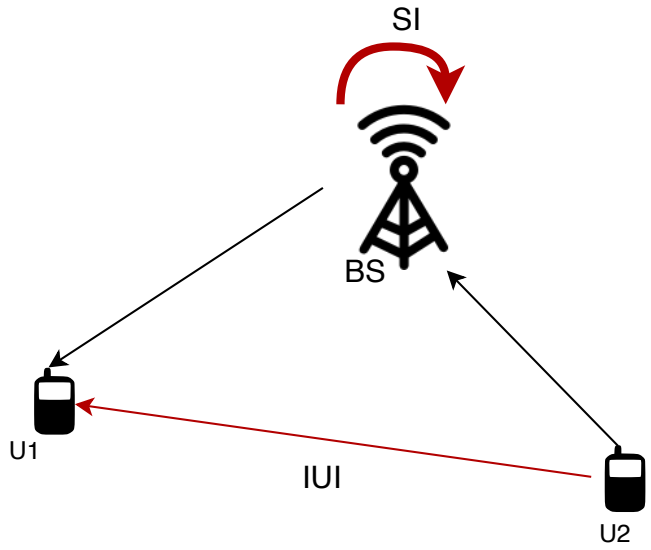

Figure 1.4: FD base-station serving multiple nodes.

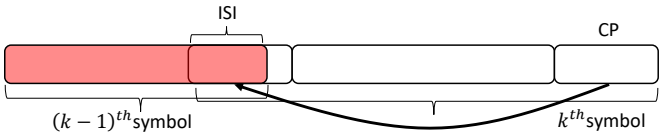

Figure 1.5: CP-based OFDM signal.

An important aspect to consider in wireless communications is the complexity of detecting the received signal. An efficient approach for high data rate communications is orthogonal frequency division multiplexing (OFDM). Although the concept of OFDM has been tackled long ago [7], it continues to draw attention in today's research community due to its effectiveness in providing high data rate communications [8, 9]. One fundamental design consideration in OFDM is to pre-process the data in real time with efficient recovery. Hence, each OFDM symbol has redundant data appended to it to minimize ISI. Fig. 1.5 depicts an OFDM symbol with redundant data appended to it. In the physical layer communication jargon, this redundant data is referred to as CP.

Although the CP is beneficial since it reduces/nulls out ISI, and hence making the detection through equalization much simpler, it wastes spectral and energy efficiency.

Another major source of interference in OFDM signals is the PN occurring due to the imperfections of the local oscillator at the transceiver. PN is known as a major

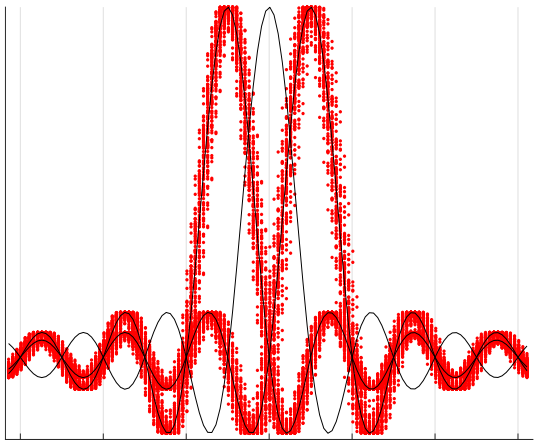

Figure 1.6: OFDM signal affected by ICI due to PN.

performance limiter, and hence must be accounted for to support high data rate communications. Fig. 1.6 shows an example of an OFDM signal, where a subcarrier in the middle is affected by the interferences of the neighboring subcarriers caused by PN, hence destroying the orthogonality between them. This dissertation evaluates the performance of FD transceiver architecture under different practical constraints. Since a transceiver has an additional interference to consider (SI), more practical and efficient equalization methods should be considered to cope with the increasing complexity of FD transceivers. The dissertation proposes novel efficient equalization methods considering different types of interferences. Although the proposed equalization methods are not designed specifically for FD transceivers, their efficiency makes them a potential candidate to be used in such transceivers where equalization complexity becomes a priority. Hence, this dissertation offers several methods to increase the performance of communication systems while maintaining an affordable complexity. The next section presents a thorough review of the related works.

1.3. Related Work

1.3.1. Radio-frequency Impairments in Full-duplex Transceivers

RF impairments, also known as hardware phenomenological effects [10], are defects that occur due to imperfections in the fabrication process of RF hardware. These imperfections are considered to be a source of performance deterioration in modern wireless communication systems, especially in multi-carrier communications [11]. Hence, researchers have been eager to device techniques that quantify the effects of these impairments and eventually mitigate them in the most efficient manner.

Recently, FD radio transceivers have gained an increasing interest in the research and industrial circles [12, 13]. An FD radio transceiver is capable of simultaneously transmitting (Tx) and receiving (Rx) data on the same frequency and time resources to achieve higher spectral efficiency compared to half-duplex transmission that suffers from rate loss due to transmitting/receiving over orthogonal time slots or frequency bands. However, an FD radio transceiver suffers from inevitable SI due to co-located Tx and Rx antennas which limits the transceiver from realizing its potential gains.

The investigation of the effects of RF impairments on FD transceivers is carried out for two different communication scenarios. The first is a bidirectional case, where two nodes communicate directly, and the second involves a relaying node between the two communicating node, as will be detailed next.

Effects of Radio-frequency Impairments on a Full-duplex Bidirectional Link

Let there be two communicating nodes, where the two nodes adopt a FD communication scenario using OFDM signals. OFDM is a broadband data modulation that is adopted in several wireless communications standards due to its robustness against frequency selective channels and its simple single tap equalizer that can be easily realized using fast Fourier transform (FFT). However, in direct conversion transceivers, OFDM is highly sensitive to RF impairments such as PN, in-phase/quadrature (I/Q) imbalance (IQI) and carrier-frequency offset (CFO). Such impairments destroy the orthogonal-

ity between the subcarriers which results in ICI and require sophisticated equalization techniques to restore the performance.

On the other hand, SI becomes the dominating factor when it comes to evaluating its performance. Several algorithms have been recently proposed to mitigate the effects of SI. Mitigating SI can occur in the wireless-propagation-domain, where the co-located transmit and receive antennas are either isolated, or more advanced transmit Tx/Rx beamforming techniques are developed to null the SI signal [14, 15, 16]. However, separating Tx and Rx may not be applicable due to space limitations while nulling the SI may result in degradation to the signal of interest as described in [14], [15]. Consequently, the mitigation is moved to the receiver front-end over two stages, namely, analog and digital-domain SI mitigation techniques. The former procedure creates an image of the transmitted signal with adjusted gain, phase and delay to subtract it from the received signal. Estimating such parameters for multipath SI channel suppression in the analog-domain is not an easy task. Hence, only the direct path SI component is suppressed in this stage [14, 15, 16], nevertheless, other methods that involve the implementation of a multi-tap analog-domain SI canceler are implemented as in e.g. [17]. Channel-state information (CSI) estimation is better performed in the digital domain, so mitigating the rest of the multipath SI channel components is executed in the digital domain. Although the SI mitigation is more flexible in the digital domain, the analog-to-digital converter's (ADC) dynamic range forms a bottleneck in the SI mitigation process [14]. Several FD radio transceivers have been implemented [18, 19, 20], yet, they are investigated in a supervised laboratory environment, and may not be appropriate as off-the-shelf FD transceivers.

In [21], the authors analyzed the harmful effects of a single RF impairment on the SI cancellation capability of a FD radio transceiver node. Specifically, they investigated the deterioration caused by PN and they compared two FD transceiver architectures where a common and two distinct oscillators are used for both the Tx and Rx chains. Their analysis showed the advantage of using a common oscillator over using two distinct oscillators for both Tx and Rx chains to obtain a lower residual SI power.

In practice, the Tx and Rx chains may suffer from several RF impairments [22] and the references therein. The distortions from the power amplifier non-linearity in the transmit chain and IQI in transmit/receive chains are studied for an FD OFDM radio transceiver in [22]. It was shown that image component of the SI signal due to IQI adversely affects the performance of FD OFDM radio transceivers.

Effects of Radio-frequency Impairments on a Full-duplex Amplify-and-forward Relay

An interesting application of the FD technology is also in relaying networks [23, 24, 25, 26, 27, 28, 29]. A considerable effort has been made to address the fusion of these techniques in which the potential gains and inevitable drawbacks of this fusion were thoroughly investigated. For example, in [23], an elaborate analysis of various SI cancellation techniques was performed in MIMO-OFDM decode-and-forward (DF) relay networks, where several spatial suppression schemes were presented. In [24], an optimal relay gain that maximizes the end-to-end signal-to-interference-plus-noise ratio (SINR) is derived along with outage probability expressions. Moreover, in [25] and [26], exact outage probability and channel capacity expressions were derived respectively for one-way FD AF relaying network along with optimal single relay selection. Furthermore, in [27], various performance metrics, namely the bit-error rate (BER), outage probability, and the ergodic capacity are derived for two-way FD dual-hop relaying network. Based on these analytical closed-form expressions, single relay selection is performed. Furthermore, the optimal power allocation and the optimal choice of the duplexing scheme (HD or FD mode) were obtained. This hybrid system is also reported in [28] for AF and DF relaying schemes and in [29] for DF relay networks.

Various articles have investigated the effects of RF impairments on a FD AF relay. For instance, in [30], the effect of transceiver PN was investigated for a FD AF relay, where it was shown that if the relay was not carefully synchronized in time, PN had a detrimental effect on the performance of the relay. Moreover, in [31], optimization of the transmit power of a FD relay adopting the AF relaying protocol under the effect of imperfect receiver electronics was investigated. However, the residual SI was not

modeled as an incremental term that could cause oscillations at the relay. It is worth noting that investigating the residual SI power is insightful since even if a compensation scheme is present at the relay, the compensation is not always accurate and would result in significant residual errors [32].

1.3.2. Full-Duplex Transceivers in Relaying Networks

The effects of RF impairments on the SI cancellation capabilities of a FD AF relay is an interesting aspect to analyze. However, it is also important to investigate other potential communication improvements using DSP algorithms, such as beamforming in relay networks and the possibility of multiple relay selection, specifically in AF relay networks that adopts a FD communication scheme.

Relaying information from a source to a destination is a well-established technology that has various benefits in wireless communication networks such as increasing the spatial diversity of wireless communications. If the relay in the network operates in a FD mode and utilizes the AF protocol, the residual SI could cause the relay to enter in an oscillation stage, which could be detrimental to the communication link.

FD relaying, which adopts both the AF and DF protocols, has been widely addressed in the literature, and its performance as a function of residual SI has been thoroughly investigated as mentioned in Section 1.3.1, as for instance, the work in [24], which investigated maximizing the network's SINR by selecting an optimal relay gain, or the work in [27], which performed single relay selection based on different analyzed metrics. These contributions have used a constant amplification factor at the AF relay that guarantees the stability of the relay. Hence, it is interesting to investigate the use of a variable beamforming coefficient that is adaptive to the residual SI, and perform multiple relay selection to enhance the end-to-end performance of the relaying network. Such techniques have been widely proposed in the literature. For instance, in half-duplex AF relaying networks, multiple relay selection and beamforming were implemented efficiently. The idea was to formulate the system's SINR and maximize it while constraining the number of selected relays. This type of constraint, which was

referred to as the cardinality constraint, requires the search over all possible subsets of relays that results in a maximized SINR, which is computationally exhaustive. Hence, the authors in [33] proposed a reduced-complexity approach by relaxing the cardinality constraint. Therefore, it is interesting to cast this problem into one that involved the use of FD relays.

1.3.3. Efficient Signal Equalization

In this dissertation, one of the aims is to design efficient signal equalizers that are less complex to realize and more efficient to implement than conventional optimal equalizers. Specifically, the dissertation tackles two major problems: Equalization of OFDM signals affected by ISI and ICI due to the insertion of an insufficient CP, and the joint equalization of the multipath channel and PN in OFDM systems. The dissertation proposes several approaches using DSP techniques to handle the resulting interferences.

Equalization of OFDM Signals with Insufficient Cyclic Prefix

The CP is appended to OFDM signals to combat ISI and ICI induced by the communication channel, which limits its spectral efficiency. Therefore, inserting an insufficient CP and equalizing the resulting ICI and ISI is a method that has been circulating the literature for a while, aiming at increasing the efficiency of OFDM systems.

The CP overhead in OFDM can be significant, especially for long range transmission. For instance, in LTE/LTE Advanced [34], the extended CP length represents 25% of the useful data transmission time. Thus, by reducing the CP length, significant improvement in bandwidth efficiency can be obtained. The reduced complexity modulation/demodulation of OFDM is based on nulling the ISI and ICI by the insertion of a CP at the beginning of the OFDM symbol with a duration that is greater than the delay spread imposed by the channel. However, the reduction in the complexity is gained at the expense of the inefficient usage of the time available to communicate data and power consumption. The loss of time and power resources can be quantified by the fraction $\frac{v}{v+N}$, where v is the length of the inserted CP and N is the number of OFDM

subcarriers [35]. One can increase the efficiency of OFDM systems by increasing N or reducing v, but this is generally not practical since N is usually constrained in many communication standards by a fixed and relatively small number, and v is chosen such that it is greater than or equal to L, which is the length of the delay spread in samples that is imposed by the channel condition.

Plenty of research articles proposed the insertion of a CP with a length of v, where $v < L$, and design various equalization techniques to rectify the loss of performance caused by the insertion of a short CP. In [2, 36], the modeling of the ISI and ICI resulting from inserting an insufficient CP has been analyzed, along with an implementation of a zero-forcing (ZF) decision feedback equalizer (DFE) equalizer to compensate for the effects of ISI and ICI. The equalizer assumes a negligible noise at the receiver, which causes a performance degradation if the receiver noise is high, and hence in [37], a minimum mean squared error (MMSE) DFE which inherently considers the receiver noise has been proposed along with forward error correction (FEC) to improve the performance of the equalizer. Furthermore, time-domain equalizers (TEQ) have been proposed with the aim of impulse response shortening (IRS), i.e. shortening the overall impulse response (OIR), which is the convolution of the impulse response of the equalizer and the channel, conditioned on maximizing different received signal evaluation metrics such as the BER or the SINR [38, 39], and in [40, 41, 42], TEQ is applied to shorten, implicitly or explicitly, the effective length of the channel impulse response (CIR). However, even if the introduction of an equalizer compensates for the loss of performance, this compromises the simplicity of the OFDM transceiver design, and hence its utility. Recently, a channel independent interference nulling scheme using precoding for multiple-input multiple-output (MIMO)-OFDM systems with insufficient CP was introduced in [43], and furthermore, iteratively estimating the CIR and using a trellis-based equalization scheme has been proposed for MIMO-OFDM systems in [44, 9].

Moreover, sparse approximations of finite impulse response (FIR) channel equalizers have been investigated due to their significant complexity reductions while still

performing close to non-sparse optimal equalizers. For example, in [45], a framework for designing sparse FIR equalizers is proposed using greedy algorithms, and an interesting application of self far-end crosstalk cancellation was shown for systems adopting discrete multitone modulation, while in [46], a reduced complexity sparsest FIR equalizer was derived for single-carrier linear channel equalizers. The authors in [46] extended their work for the design of sparse FIR MIMO linear and decision-feedback equalizers [47]. However, to the best of the authors' knowledge, no work has previously addressed a sparse equalizer design for OFDM signals suffering from ICI and ISI due to the insertion of an insufficient CP.

Equalization of OFDM Signals Affected by Phase Noise

A major performance and complexity limitation in direct-conversion broadband wireless transceivers is PN resulting from the inevitable imperfections in the fabrication process of the crystal oscillator. As a result, PN induces ICI in OFDM transceivers.

A plethora of articles exists in the literature where the problems of modeling, analyzing, estimating and compensating the effects of PN on OFDM signals are investigated. For example, while the works in [48, 49] numerically studied the capacity of OFDM systems impaired by PN, in [50], the effects of the Wiener PN and frequency-selective channels on OFDM signals were analyzed in terms of capacity and SINR. Furthermore, the authors in [51] built on the work in [50] by assuming that no information about the common phase error (CPE) is available at the receiver. Thus, several bounds on the rate were derived by treating the ICI induced by PN as noise, arguing that OFDM detection complexity should be kept minimal by only considering the CPE at the detection stage.

Concerning the estimation and mitigation of PN, in [52, 53] the authors considered the estimation and mitigation of the CPE, while PN-induced ICI was ignored. Since the PN-induced ICI is known to have a detrimental effect on the performance of OFDM systems, the work in [54] considered the ICI introduced by PN which was iteratively estimated and then compensated for both Wiener and Ornstein-Uhlenbeck

models. In this approach, the PN waveform was estimated and equalized in a decision feedback manner. In [55], the authors extended the work in [54] by proposing a more accurate estimate of ICI where a significant improvement in terms of the symbol error rate is demonstrated.

It is well known that PN changes from one OFDM symbol to another, thus, PN estimates should be updated for each OFDM symbol to maintain a satisfactory performance, which is computationally demanding for both iterative estimation and equalization approaches. Hence, the authors in [1] proposed a non-iterative joint channel and PN estimation technique where the PN is estimated by maximizing a constrained quadratic objective function independent of the CSI. The improvement shown in [1] is not only limited to a better estimation technique, but also results in a complexity reduction for the PN estimation process. Moreover, in [56], the constraints imposed to solve the optimization problem formulated to estimate the PN components in the received signal was modified to account for the PN's spectral characteristics. The authors showed that accounting for the PN's spectral characteristics improved the accuracy of the PN estimates. However, the estimation was conducted in an iterative fashion which imposes a significant delay on the detection time. Therefore, the work in [57] proposed a non-iterative channel PN estimation scheme which significantly reduces the complexity of the estimation process.

In addition to complexity reduction, the joint sparse channel equalization and PN compensation approach offers some additional advantages over the conventional non-sparse equalizers. The use of a smaller number of (non-zero) coefficients enables more rapid adaptation of the equalizer entries to the varying channel and PN conditions, and as a result, the equalizer can afford using imperfect oscillators and could adapt to rapidly varying channel conditions.

1.4. List of Contributions

This section highlights the contributions that form the contents of this dissertation. Each contribution is contained in one of three main chapters, where each chapter

is further divided into several sections to explicitly highlight each of the contributions. Chapters 2 and 3 focus on the deployment of FD transceivers in bidirectional and relaying communication scenarios, respectively. Even though Chapter 3 still discusses FD transceivers, it was not merged with Chapter 2 since the approach there revolves around DSP more than the performance analysis of FD transceivers. Chapter 4 then tackles a different set of problems, which is efficient signal equalization. The contributions are detailed in the following sections.

1.4.1. Contributions to the Performance Analysis of Bidirectional Full-Duplex Communication Systems

In this dissertation, the contributions regarding the performance of a bidirectional FD system affected by RF impairments are summarizes as follows:

- The effects of the presence of both PN and IQI on an OFDM waveform that operates in a FD transceiver are mathematically modeled.
- A closed-form expression of the average residual SI power is derived in FD OFDM transceivers to show its functional dependency on IQI and PN levels.
- With perfect digital-domain cancellation and for small PN and IQI levels, the effects of PN and IQI is shown to be decoupled and the average residual SI power is shown to be linearly proportional to the parameters of the RF impairments.

Chapter 2, Section 2.1, elaborates on the details behind the contributions, and this work resulted in the publication in [58].

1.4.2. Contributions to the Performance Analysis of Full-Duplex Transceivers Deployed in Cooperative Networks

Concerning the one-way dual-hop FD relay network, where a mediating IQI affected relay is assumed to adopt the AF protocol, the main contributions which are detailed in Chapter 2 (Section 2.2) are listed as follows:

- The effect of IQI on the transceiver of a FD AF relay when SI cancellation is applied is mathematically modeled.
- The relay's amplification factor is closely investigated and its maximum theoretical limit that prevents the system from entering in an oscillation stage is derived.
- An amplification factor that controls the transmit power at the relay is derived when the relay is affected by IQI.
- A lower bound on the average residual SI power is derived, where it is shown that the average residual SI power is bounded by a sum of scaled Gamma functions.

The above contribution resulted in the submission of the article mentioned in Appendix C (Journal number 6).

1.4.3. Contributions to the Design of Relay Selection and Beamforming Schemes in Full-duplex Cooperative Networks

Chapter 3 discusses the contributions related to multiple relay selection and beamforming in AF FD dual-hop relay networks, which are:

- The effects of residual SI in a FD AF relay is mathematically modeled by considering the cumulative SI resulting from the relay operating in a FD mode. The modeling is based on using the exact varying beamforming coefficient, which is usually modeled as a fixed parameter for the sole purpose of preventing oscillations at the relay [24, 27].
- Assuming the availability of perfect CSI and second order statics of the residual SI, the beamforming coefficient is designed while aiming at minimizing the mean-squared error (MSE) at the destination, and then sparsity inducing optimization problems are used to perform relay selection.
- The proposed beamforming and multiple relay selection technique is shown to be a hybrid FD and alternate relaying system, where it is shown that the switch-

ing rate is mainly dependent on the SI cancellation capability of receivers at the relays.

The above contributions resulted in the publication of the article in [59].

1.4.4. Contributions to the Design of Sparse Equalizers for OFDM Signals With Insufficient Cyclic Prefix

Concerning the sparse equalization of OFDM with insufficient CP, the following are the main contributions:

- A reduced-complexity time-domain sparse DFE equalizer is proposed for OFDM signals with insufficient CP.
- The equalizer is designed to offer a complexity-performance trade-off by either setting a desired number of active entries or by targeting a specific amount of loss in terms of SINR.
- The worst-case coherence (WCC) metric of the sparsifying dictionary is investigated and the simulations show that it is suitable for designing the sparse equalizers with more likelihood of successfully retrieving the non-zero entries.

The above contributions are detailed in Chapter 4, Section 4.1, and resulted in the publication of the article in [60].

1.4.5. Contributions to the Design of Sparse Equalizers for OFDM Signals Impaired by Phase Noise

For the joint equalization of the multipath channel and PN, the key contributions (discussed in details in Chapter 4, Section 4.2) are listed as follows:

- A novel low-complexity sparse design framework is proposed for joint PN mitigation and channel equalization in direct-conversion OFDM receivers. The proposed approach exploits the inherent sparse characteristics of the ICI in the frequency domain to significantly reduce the complexity of the proposed design

method at a negligible performance loss. It is important to mention that, in this work, no PN and channel estimation operations are performed. Hence, to emulate a practical scenario, the derived equalizer is generalized to account for the inaccurate estimations of the PN and channel quantities.

- The maximum expected coherence (MEC) metric is analyzed, which quantifies the performance of the sparsifying matrix, to point to the likelihood of success in providing the sparse approximation of the conventional non-sparse high-complexity optimum equalizer design.

- The simulation results show that allowing for a little performance loss results in a significant implementation complexity reduction. Consequently, the power consumption of devices that use sparse equalizers decreases since a smaller number of complex multiplication/addition (CM/A) operations are required. In addition, the proposed approach shows better performance compared to the state-of-the-art designs.

The above contributions resulted in the publication of the article in [61].

Chapter 5 finally concludes the whole dissertation, where each topic is explicitly concluded and some possible future work is discussed.

The listed contributions resulted in the dissemination of journal articles and conference proceedings which are summarized in Appendix C.

1.5. Chapter Summary

Now that each topic that is discussed in this dissertation has been introduced, the related works have been thoroughly discussed and each contribution was specifically highlighted, the next chapters discuss in details each and every approach adopted to achieve the final results, along with their respective verifications using Monte-Carlo computer simulations.

FD communications allows for the simultaneous transmission and reception of signals on the same frequency band, thus possibly doubling the spectral efficiency. This could be achieved by using a novel class of transceivers, specifically the FD transceivers. The main obstacle towards exploiting the FD communication scheme is the SI resulting from the co-location of the transmitter and the receiver. Thus, the main objective of a transceiver designer is to completely cancel out the SI. However, this is not necessarily possible due to the inaccuracy of the SI cancellation scheme. In this chapter, the effects of RF impairments on the SI cancellation is thoroughly investigated in different communication scenarios. The sections below elaborate on the details.

2.1. Residual Self-interference Analysis in Bidirectional Communication Transceivers

This section presents the details behind the performance analysis of FD transceiver affected by PN and IQI. The performance of the transceiver is quantified by the residual SI level after different stages of SI cancellation, as will be discussed in the next sections.

2.1.1. System Model

Denoting $x_p(t) = \Re\{x(t)e^{jw_m t}\}$ as the PN and IQI free pass-band transmitted signal, where $\Re\{.\}$ denotes the real operator, the IQI and PN impaired transmitted signal can be written as follows

$$\begin{aligned} x_p(t) = {} & x_I(t)\alpha_{I,tx}\cos(w_m t + \phi_{tx}(t) + \theta_{I,tx}) \\ & - x_Q(t)\alpha_{Q,tx}\sin(w_m t + \phi_{tx}(t) + \theta_{Q,tx}), \end{aligned} \tag{2.1}$$

where $x(t) = x_I(t) + jx_Q(t)$ is the base-band undistorted Tx signal with average energy of $\mathbb{E}\{|x(t)|^2\} = \mathcal{E}_x$, $\mathbb{E}\{.\}$ is the statistical expectation operator, and $w_m = 2\pi f_m$ is the angular oscillator frequency. The I and Q oscillator's gain imbalance levels are denoted by $\alpha_{I,tx}$ and $\alpha_{Q,tx}$, respectively, while the phase mismatch levels at the I and

Q branches are termed by $\theta_{I,tx}$ and $\theta_{Q,tx}$, respectively. The transmitter PN process is denoted by $\phi_{tx}(t)$ with a 3-dB bandwidth denoted by β. The free-running oscillator (FRO) model [62] is used since it simplifies the analysis and has a similar performance to more practical PN process models such as the phase-locked loop (PLL) PN model [21]. The received SI after performing analog cancellation to suppress the direct path signal is given by

$$y_p(t) = ax_p(t-\delta) - \hat{a}x_p(t-\hat{\delta}) + \sum_{c=1}^{L} a_c x_p(t-\delta_c), \tag{2.2}$$

where L denotes the number of multipath channel taps between the co-located Tx and Rx antennas, and $a_c \sim \mathcal{CN}(0, \sigma_{a,c}^2)$, $\forall\ c\ \in\ \{1,\ \cdots,\ L\}$, represents the channel tap coefficient. Those channel coefficients are assumed to be independent of one another with δ_c representing the delay of the c^{th} channel tap. The direct path channel gain between the Tx and Rx antennas is $a \sim \mathcal{CN}(0, \sigma_a^2)$ with a delay denoted by δ. The estimated direct path channel gain and its delay are denoted by $\hat{a}$ and $\hat{\delta}$, respectively.

Down-converting the received signal, and after some mathematical manipulations, the received signal after ideal low-pass filters in the I and Q branches can be written as follows

$$\begin{aligned}
\tilde{y}(t) &= \mu_{rx} e^{-j\phi_{rx}(t)} y(t) + \nu_{rx} e^{j\phi_{rx}(t)} y^*(t), \\
&\approx ap(t) e^{-jw_m\delta} \left(\mu_{rx}\mu_{tx} s(t) + \mu_{rx}\nu_{tx} s^*(t)\right) \\
&- \hat{a}p(t) e^{-jw_m\hat{\delta}} \left(\mu_{rx}\mu_{tx} s(t) + \mu_{rx}\nu_{tx} s^*(t)\right) \\
&+ \sum_{c=1}^{L} a_c p_c(t) e^{-jw_m\delta_c} \left(\mu_{rx}\mu_{tx} s_c(t) + \mu_{rx}\nu_{tx} s_c^*(t)\right) \\
&+ a^* p'(t) e^{jw_m\delta} \nu_{rx}\mu_{tx}^* s^*(t) - \hat{a}^* p'(t) e^{jw_m\hat{\delta}} \nu_{rx}\mu_{tx}^* s^*(t) \\
&+ \sum_{c=1}^{L} a_c^* p_c'(t) e^{jw_m\delta_c} \nu_{rx}\mu_{tx}^* s_c^*(t),
\end{aligned} \tag{2.3}$$

where $y(t) = y_I(t) + jy_Q(t)$ is the base-band equivalent signal of $y_p(t)$ and

$$\begin{aligned} p(t) &= e^{j(\phi_{tx}(t-\delta)-\phi_{rx}(t))},\ p'(t) = e^{-j(\phi_{tx}(t-\delta)+\phi_{rx}(t))}, \\ p_c(t) &= e^{j(\phi_{tx}(t-\delta_c)-\phi_{rx}(t))},\ p'_c(t) = e^{-j(\phi_{tx}(t-\delta_c)+\phi_{rx}(t))}, \end{aligned} \tag{2.4}$$

and $\phi_{rx}(t)$ denotes the receiver PN process, $s(t) = x(t-\delta)$ and $s_c(t) = x(t-\delta_c)$. Assuming good delay estimation of the main tap, i.e. $\delta \approx \hat{\delta}$, then $s(t) \approx x(t-\hat{\delta})$, $\phi_{tx}(t-\delta) \approx \phi_{tx}(t-\hat{\delta})$ and $s(t+\delta-\hat{\delta}) \approx s(t)$. The quantities $p(t)$, $p'(t)$, $p_c(t)$ and $p'_c(t)$ denote the PN effect on the received signal. Moreover, $\mu_{rx} = 1/2\left(\alpha_{I,rx}e^{-j\theta_{I,rx}} + \alpha_{Q,rx}e^{-j\theta_{Q,rx}}\right)$ and $\nu_{rx} = 1/2\left(\alpha_{I,rx}e^{j\theta_{I,rx}} - \alpha_{Q,rx}e^{j\theta_{Q,rx}}\right)$ model the base-band receiver IQI parameters, where $\alpha_{I,rx}$, $\alpha_{Q,rx}$, $\theta_{I,rx}$ and $\theta_{Q,rx}$ are the receiver I and Q branches gain and phase imbalances, respectively. It is worth mentioning that the terms that are multiplied by $\nu_{rx}\nu^*_{tx}$ are omitted from the analysis since they yield a relatively small contribution to the overall interference. Sampling Eq. (2.3) every T_s periods, and assuming $a_0 = a - \hat{a}e^{jw_m(\delta-\hat{\delta})}$ and $a^*_0 = a^* - \hat{a}^*e^{-jw_m(\delta-\hat{\delta})}$, (2.4) becomes

$$\begin{aligned} \tilde{y}(nT_s) = &\sum_{c=0}^{L} a_c e^{j(\phi_{tx}((n-c)T_s-\delta)-\phi_{rx}(nT_s)-w_m(cT_s+\delta))} \\ &\times (\mu_{rx}\mu_{tx}s((n-c)T_s) + \mu_{rx}\nu_{tx}s^*((n-c)T_s)) \\ &+ \sum_{c=0}^{L} a^*_c e^{-j(\phi_{tx}((n-c)T_s-\delta)+\phi_{rx}(nT_s)-w_m(cT_s+\delta))} \\ &\times \nu_{rx}\mu^*_{tx}s^*((n-c)T_s). \end{aligned} \tag{2.5}$$

Taking the FFT of (2.5), the result is

$$\begin{aligned} Y(k) = &\sum_{c=0}^{L}\sum_{l=0}^{N-1} a_c e^{-j(w_m(cT_s+\delta)+2\pi kc/N)} \\ &\times (\mu_{rx}\mu_{tx}S[l] + \mu_{rx}\nu_{tx}S^*[l']) \times P^1_{k-l} \\ &+ \sum_{c=0}^{L}\sum_{l=0}^{N-1} a^*_c e^{j(w_m(cT_s+\delta)+2\pi kc/N)}\nu_{rx}\mu^*_{tx}S^*[l'] \times P^2_{k-l}, \end{aligned} \tag{2.6}$$

where

$$P_{k-l}^{1} = \frac{1}{N}\sum_{n=0}^{N-1} e^{j(\phi_{tx}((n-c)T_s-\delta)-\phi_{rx}(nT_s)-2\pi(k-l)n/N)}, \quad (2.7)$$

$$P_{k-l}^{2} = \frac{1}{N}\sum_{n=0}^{N-1} e^{-j(\phi_{tx}((n-c)T_s-\delta)+\phi_{rx}(nT_s)-2\pi(k-l)n/N)}, \quad (2.8)$$

and DFT $\{s[n]\} = S[l]$ and DFT $\{s^*[n]\} = S[l']$, where DFT$\{.\}$ denotes the discrete Fourier transform (DFT) operator, and assigning $l' = N - l + 2$, and $0 \leqslant l \leqslant N-1$ for $0 \leqslant k \leqslant N-1$ [63]. Finally, the digital-domain cancellation stage is performed by applying

$$\begin{aligned} Z(k) = &\sum_{c=0}^{L}\sum_{l=0}^{N-1} a_c e^{-j(w_m(cT_s+\delta)+2\pi kc/N)} \\ &\times (\mu_{rx}\mu_{tx}S[l] + \mu_{rx}\nu_{tx}S^*[l']) \times P_{k-l}^{1} \\ &+ \sum_{c=0}^{L}\sum_{l=0}^{N-1} a_c^* e^{j(w_m(cT_s+\delta)+2\pi kc/N)}\nu_{rx}\mu_{tx}^* S^*[l'] \times P_{k-l}^{2} \\ &- \sum_{c=0}^{L} \hat{a}_c e^{-j(w_m(cT_s+\hat{\delta})+2\pi kc/N)} \times \hat{\mu}_{rx}\hat{\mu}_{tx}S[l]\hat{P}_0^1, \end{aligned} \quad (2.9)$$

where $\hat{a}_c$ is the estimate of the c^{th} SI channel coefficient, $\hat{\mu}_{rx}$ and $\hat{\mu}_{tx}$ are the estimates of the IQI parameters μ_{rx} and μ_{tx}, while the estimation of the PN CPE is denoted by $\hat{P}_0$. Suppressing the cross-leakage between the subcarriers due to PN or the image subcarrier interference caused by IQI is complicated because it is not easy to estimate the equivalent channels [21]. Therefore, with perfect digital cancellation, i.e., suppressing the CPE and IQI's effects at the k^{th} subcarrier excluding the image effect, there is still inevitable residual SI. Similar effects are observed in [21] due to the presence of PN only.

2.1.2. Average Residual Self-interference Analysis

Assuming that the channel, transmitted data and PN are independent random processes, taking the mean of the squared absolute value of $Z(k)$, the average residual

SI power can be written as

$$\begin{aligned}\mathbb{E}\{|Z(k)|^2\} = \frac{1}{N^2}\Bigg[&|\mu_{rx}|^2|\mu_{tx}|^2\sum_{c=0}^{L}\sigma_{a,c}^2\sum_{\substack{l=0\\l\neq k}}^{N-1}\mathcal{E}_l\\ &\times\left(-N+\sum_{n=0}^{N-1}2(N-n)e^{(-4\pi n\beta T_s)}\cos\Big(\frac{2\pi(k-l)n}{N}\Big)\right)\\ &+\left(|\mu_{rx}|^2|\nu_{tx}|^2+|\nu_{rx}|^2|\mu_{tx}|^2\right)\sum_{c=0}^{L}\sigma_{a,c}^2\sum_{l=0}^{N-1}\mathcal{E}_l\\ &\times\left(-N+\sum_{n=0}^{N-1}2(N-n)e^{(-4\pi n\beta T_s)}\cos\Big(\frac{2\pi(k-l)n}{N}\Big)\right)\\ &+|\mu_{rx}|^2|\mu_{tx}|^2\mathcal{E}_k\sigma_\epsilon^2\left(-N+\sum_{n=0}^{N-1}2(N-n)e^{(-4\pi n\beta T_s)}\right)\Bigg],\end{aligned} \tag{2.10}$$

where σ_ϵ^2 denotes the variance of the error in estimating the effective SI channel which is a function of the amount of digital-domain cancellation [21]. Basically, most of SI cancellation schemes rely on creating an image of the transmitted signal by estimating the equivalent SI channel that captures the effects of RF impairments of the Tx and Rx chains. Here, the accuracy of the analog and digital domains SI cancellation schemes is modeled by two parameters, κ and d, respectively. This approach is widely adopted in the literature as in e.g. [21], [22] where κ and d denote the error varaince of analog-domain and digital-domain cancellation, respectively. The error variance σ_ϵ^2 is equal to $\kappa \times d$ [21].

It is worth mentioning that several cross-terms arise while deriving (2.10), and it can be shown that they vanish to zero (proof is in Appendix A). Further, it can be shown that $\mathbb{E}\{|P_{k-l}^1|^2\} = \mathbb{E}\{|P_{k-l}^2|^2\} = \mathbb{E}\{|P_{k-l}|^2\}$. The closed form expression of $\mathbb{E}\{|P_k|^2\}$, which is used in (2.10), is given by [21]

$$\mathbb{E}\{|P_k|^2\} = -\frac{1}{N} + \frac{2}{N^2}\sum_{n=0}^{N-1}(N-n)e^{-4\pi n\beta T_s}\cos\frac{2\pi kn}{N}. \tag{2.11}$$

Next, to get more insights on the effects of IQI and PN, a perfect digital-domain cancellation is assumed, i.e., $\sigma_\epsilon^2 = 0$, and the same IQI levels at both Tx and Rx oscillators. Moreover, for practical IQI levels, $1 + 2\frac{|\nu|^2}{|\mu|^2} \approx 1$ and the total channel taps power is demoted by $\sigma_{total}^2 = \sum_{c=0}^{L} \sigma_{a,c}^2$. Rearranging the terms in (2.10) yields

$$\mathbb{E}\{|Z(k)|^2\} \approx \frac{1}{N^2}\left(C_1 + 2C_2\frac{|\nu|^2}{|\mu|^2}\right), \tag{2.12}$$

where

$$C_1 = |\mu|^4\sigma_{total}^2 \sum_{\substack{l=0 \\ l\neq k}}^{N-1} \mathcal{E}_l \times \tag{2.13}$$
$$\left(-N + \sum_{n=0}^{N-1} 2(N-n)e^{(-4\pi n\beta T_s)}\cos\Big(\frac{2\pi(k-l)n}{N}\Big)\right),$$

and

$$C_2 = |\mu|^4\sigma_{total}^2(-N + \sum_{n=0}^{N-1} 2(N-n)e^{-4\pi n\beta T_s}). \tag{2.14}$$

It is evident from (2.12) that the asymptotic average residual SI power, i.e. when $\sigma_\epsilon^2 = 0$, is linearly proportional to $\frac{|\nu|^2}{|\mu|^2}$ termed as the IQI image rejection ratio (IRR). It is worth mentioning that in C_1 and C_2, for practical IQI levels, $|\mu|^4 \approx 1$ and, hence, they are independent of IQI levels. Moreover, for small β, the term $e^{-4\pi n\beta T_s}$ can be approximated by $1-4\pi n\beta T_s$, and for practical values of T_s and N, C_2 can be simplified as follows

$$C_2 \approx \sigma_{total}^2\left(N^2 - \frac{4\pi\beta T_s}{3}N(N^2-1)\right) \approx \sigma_{total}^2 N^2, \tag{2.15}$$

where C_2 is shown to be approximately independent of β. Therefore, the slope C_2 is fixed and dependent only on the total channel taps power and the number of subcarriers. Furthermore, after straight forward manipulations, C_1 can then be approximated by

$$C_1 \approx \sigma_{total}^2\beta \sum_{\substack{l=0 \\ l\neq k}}^{N-1} \mathcal{E}_l \times \frac{8\pi T_s N}{1-\cos(\frac{2\pi(k-l)}{N})}. \tag{2.16}$$

Interestingly, the approximation of C_1 shows that the average residual SI power linearly depends on β. This demonstrates that, with perfect digital-cancellation, the PN and IQI effects are decoupled. Moreover, in addition to the average SI power being linearly proportional to the IQI IRR, it is also linear in PN 3-dB bandwidth for small PN levels as shown in (2.16).

2.1.3. Numerical Results

An OFDM system with 256 subcarriers is considered, where 128 of them are active and the rest are nulls. The sampling frequency is 15.36 MHz and the subcarrier spacing is 60 KHz. At the receiver, the average symbol energy is set to $\mathcal{E}_l = 0$ dB so that the residual SI is given in dBs, in relation to it. The carrier frequency is selected to be $f_m = 2.1$ GHz. The power delay profile of the SI channel has a total of five taps with the values of -30, -65, -70, $-\infty$, -75 dBs, based on the SI channel assumptions in [21]. The separation between the Tx and Rx antennas of the transceiver is set to be 20 cm, which corresponds to a delay of $\delta = 0.67$ ns [21]. It is also assumed that the amount of attenuation that the signal experiences due to antenna separation is 30 dB. Moreover, the amount of signal attenuation due to analog and digital-domain cancellation is $\kappa = 30$ dB and $d = 50$ dB, respectively. These values are then used in the calculation of σ_ϵ^2. In the case of an impairments free transceiver, the residual SI power should be equal to -80 dB. A symmetric IQI case is assumed, i.e. $\alpha_{I,tx/rx} = 1 + \bar{\alpha}_{tx/rx}$, $\alpha_{Q,tx/rx} = 1 - \bar{\alpha}_{tx/rx}$, $\theta_{I,tx/rx} = -\frac{\theta_{tx/rx}}{2}$ and $\theta_{Q,tx/rx} = \frac{\theta_{tx/rx}}{2}$, where $\bar{\alpha}_{tx/rx}$ is defined in log scale by applying $\alpha_{tx/rx} = 10\log(1 + \bar{\alpha}_{tx/rx})$.

In Fig. 2.1, the residual SI power is plotted versus the digital-domain cancellation parameter d. It shows the effect of changing the IRR for IQI and β for the PN. Moreover, this figure shows a perfect match between the derived closed form expression in (2.10) for residual SI power and the numerical simulations. The PN 3-dB bandwidth and the IRR are varied to highlight the effect of ICI on the residual SI power. Increasing β and the IRR result in a higher floor even when the digital-domain cancellation error is

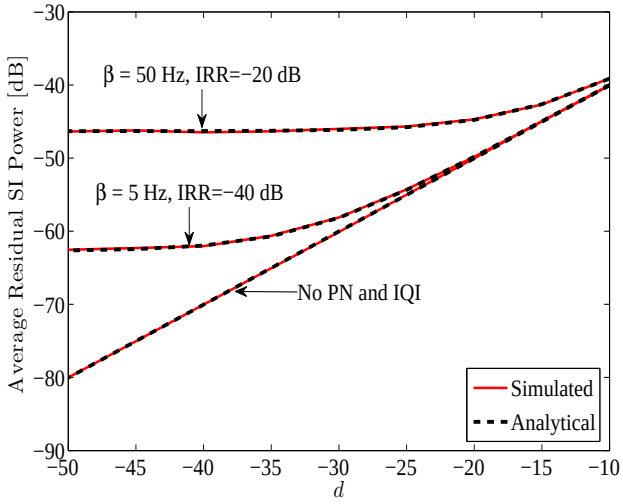

Figure 2.1: Analytical (dashed black) and simulated (solid red) average residual SI power versus the amount of digital-domain cancellation d.

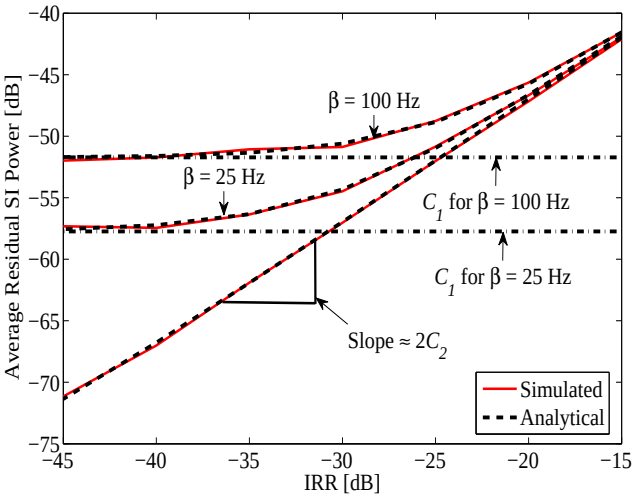

Figure 2.2: Analytical (dashed black) and simulated (solid red) average residual SI power versus the oscillators' IRR. The dash-dotted lines represent C_1.

relatively small. This occurs because the ICI caused by the PN and IQI is not suppressed at any of the SI cancellation stages.

In Fig. 2.2, the average residual SI power is plotted versus the IRR parameter for different PN levels. When the IRR is small, the residual SI power is constant, and the average residual SI power level is determined by the constant C_1 in (2.16)

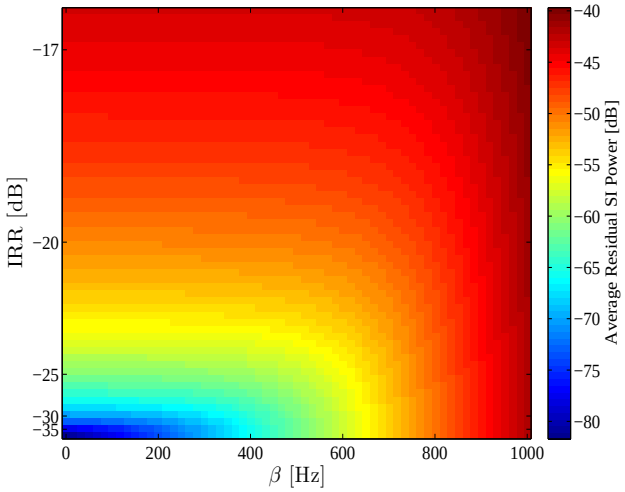

Figure 2.3: Heat-map plot depicting the average residual SI power as a function of β and the IRR.

which is plotted using a dash-dotted line for different values of β. Interestingly, the approximation of the constant C_1 in (2.16) is still accurate even for high PN level of $\beta = 100$ Hz because of high sampling rate. Increasing IQI level, the average residual SI power increases linearly with a constant rate which is proportional to C_2 as shown in (2.12).

To illustrate the joint effects of IQI and PN on the residual SI power, Fig. 2.3 shows a heat-map plot where the y-axis represents the IRR and the x-axis represents β. As both β and the IRR increase, the residual SI power increases. This figure conveys the same message as Fig. 2 but for a wider range of PN and IQI levels by varying β and $\frac{|\nu|^2}{|\mu|^2}$, respectively.

2.2. Residual Self-interference Analysis in Cooperative Networks

Section 2.1 discussed the joint effects of PN and IQI on a FD transceiver operating in a bidirectional communication scheme. Now, this chapter discusses the effect of IQI on a relay with a FD transceiver adopting an AF relaying protocol, which has a different nature (see e.g. [27] and the references therein). The contribution here focuses

on the instability of the performance of the relay caused by the cumulative SI which arises due to the IQ mismatch.

2.2.1. System Model

The system model consists of a source S, a destination D, and a relay R mediating between the two while operating in a FD mode. Furthermore, the direct link between S and D is assumed to be missing due to severe fading of the $S \rightarrow D$ link. Moreover, the relay transceiver circuit is assumed to suffer from IQI, while the IQI of the source and destination are neglected to focus on the effects of IQI at the relay. The received signal by the relay R at time k before the effect of IQI is given by

$$r_R[k] = h_{SR}x[k] + v_R[k] + i_R[k], \tag{2.17}$$

where $x[k]$ is the data symbol transmitted from S to R at time k, h_{SR} represents the channel coefficient between S and R where it is modeled as circularly symmetric complex Gaussian random variable with zero mean and variance σ^2_{SR} ($h_{SR} \sim \mathcal{N}(0, \sigma^2_{SR})$). In the analysis, it is assumed that h_{SR} is constant for the whole sampled time interval, i.e. the channel $S \rightarrow R$ is slowly varying. Furthermore, $v_R[k]$ is the additive white Gaussian noise (AWGN) at the relay R at time instant k, i.e. $v_R \sim \mathcal{N}(0, \sigma^2_{v_R})$. Finally, $i_R[k]$ represents the residual SI at the relay since it is operating in a FD mode. The received signal $r_R[k]$ at the relay after experiencing the effects of IQI can be written as

$$\bar{r}_R[k] = \mu_{Rx} r_R[k] + \nu_{Rx}\Big(r_R[k]\Big)^*, \tag{2.18}$$

where the operator $(.)^*$ yields the conjugate of a complex number, $\mu_{Rx/Tx} = \cos(\frac{\theta_{Rx/Tx}}{2}) + j\alpha_{Rx/Tx}\sin(\frac{\theta_{Rx/Tx}}{2})$ and $\nu_{Rx/Tx} = \alpha_{Rx/Tx}\cos(\frac{\theta_{Rx/Tx}}{2}) - j\sin(\frac{\theta_{Rx/Tx}}{2})$, where $\alpha_{Rx/Tx}$ represent the gain imbalance at the relay's receiver/transmitter, which is writen in dBs by applying $\tilde{\alpha}_{Rx/Tx} = 10\log_{10}(1 + \alpha_{Rx/Tx})$ and $\theta_{Rx/Tx}$ is the phase imbalance at the relay's receiver/transmitter in degrees. IQI is also present at the relay's transmission front-end. Hence, the transmitted signal by the relay at time k after

experiencing transmit IQI is given by

$$y_R[k] = \mu_{Tx}\bar{r}_R[k] + \nu_{Tx}\left(\bar{r}_R[k]\right)^*. \tag{2.19}$$

In AF relaying protocol, the received signal $r_R[k]$ is forwarded to the destination by simply amplifying it by a factor which is designated as a. Hence, the transmitted signal by the relay at time k after amplification and before the effect of transmit IQI is

$$\bar{y}_R[k] = a \times y_R[k]. \tag{2.20}$$

Next, the signal is multiplied by the coefficient representing the SI channel. The channel coefficient possesses the same statistical properties and characteristics that of the $S \rightarrow R$ link, but with a much higher variance. In other words, if the SI channel variance is denoted by σ_R^2, then $\sigma_R^2 \gg \sigma_{SR}^2$. Hence, the interference at the k^{th} time slot can be written as

$$\bar{i}_R[k] = h_R \times \bar{y}_R[k]. \tag{2.21}$$

The received signal experiences again receive IQI, and therefore the interference at time $k+1$ can be written as

$$\breve{i}_R[k+1] = \mu_{Rx}\bar{i}_R[k] + \nu_{Rx}\left(\bar{i}_R[k]\right)^*. \tag{2.22}$$

Devices that operate in FD mode must have a SI cancellation scheme. In the analysis, the relay is assumed to have passive and active SI cancellation capabilities. The passive cancellation strategy allows the suppression of the received SI signal by tens of dBs, while the active SI cancellation strategy aims at the total suppression of the SI signal, which relies on the knowledge of the transmitted signal and having an estimate of the SI channel coefficient h_R, which is denoted by $\hat{h}_R$. In the modeling of $\hat{h}_R$, the well-known model of representing the estimate of a CSI quantity is adopted which is $\hat{h}_R = h_R + \tilde{h}_R$, where $\tilde{h}_R \sim \mathcal{N}(0, \sigma_{\tilde{h}_R}^2)$ [64]. Therefore, the interference at time $k+1$ received after SI

cancellation can be expressed as

$$i_R[k+1] = \breve{i}_R[k+1] - \hat{h}_R \times \bar{y}_R[k]. \tag{2.23}$$

Expanding (2.23) yields

$$i_R[k+1] = \left(\mu_{Rx} h_R - \hat{h}_R\right) \bar{y}_R[k] + \nu_{Rx} \left(h_R \bar{y}_R[k]\right)^* . \tag{2.24}$$

Using a range of IQI parameters that correspond to a practical scenario, it can be assumed that $\mu_{Rx/Tx} \approx 1$. Also, the assumption that $|\tilde{h}_R|^2 \ll |h_R|^2$ is used. Hence,

$$i_R[k+1] \approx \nu_{Rx} \left(h_R y_R[k]\right)^* . \tag{2.25}$$

Next, the following approximations are applied

$$\begin{aligned} i_R[k+1] &= \nu_{Rx} h_R^* a \left(y_R[k]\right)^* , \\ &\overset{(I)}{\approx} \nu_{Rx} \mu_{Tx}^* h_R^* a \left(\bar{r}_R[k]\right)^* , \\ &= \nu_{Rx} \mu_{Tx}^* h_R^* a \left(\mu_{Rx} r_R[k] + \nu_{Rx} \Big(r_R[k]\Big)^*\right)^* , \\ &\overset{(II)}{\approx} = \nu_{Rx} \mu_{Tx}^* \mu_{Rx}^* h_R^* a \left((c[k])^* + (i_R[k])^*\right), \end{aligned} \tag{2.26}$$

where $c[k] = h_{SR} x[k] + v_R[k]$, and the approximations in (I) and (II) are applied based on the assumptions that $\nu_{Rx} \nu_{Tx}^* \ll \nu_{Rx} \mu_{Tx}^*$ and $|\nu_{Rx}|^2 \ll \nu_{Rx} \mu_{Rx}^*$, respectively [65]. Since, by now, the relationship between $i_R[k+1]$ and $i_R[k]$ has been established, a general expression that represents the recursive relation presented in (2.26) is written as follows

$$\begin{aligned} i_R[k+1] \approx \sum_{n=1}^{k+1} & f_1(\nu_{Rx} \mu_{Tx}^* \mu_{Rx}^* (h_R)^* a, n) \\ & \times f_2(c[k+1-n], n-1), \end{aligned} \tag{2.27}$$

where the functions $f_1(.,.)$ and $f_2(.,.)$ are described in Algorithms 1 and 2, respectively.

Algorithm 1: The f_1 function

Input: $C \in \mathbb{C},\ n \in \mathbb{N}$

Output: $R \in \mathbb{C}$

$R \leftarrow 1$

For $(p = 1..n)$

if $p \mod 2 == 0$

$R \leftarrow R \times C^*$**,**

else

$R \leftarrow R \times C$**,**

end

end

Return R**;**

Algorithm 2: The f_2 function

Input: $C \in \mathbb{C},\ n \in \mathbb{N}$

Output: $R\, q \in \mathbb{C}$

$R \leftarrow 1$

if n **mod** $2 == 0$

$q \leftarrow C^*$**,**

else

$q \leftarrow C$**,**

end

Return R**;**

2.2.2. *Amplification Restrictions*

Since R is operating in a FD mode, amplifying the received signal form S to D is now restricted not only by the additive noise, but by the residual SI. Hence, in this section, the effect of the residual SI on determining the amplification factor that stabilizes the performance of the relay is investigated. The amplified up-converted signal at the relay is modeled in the base-band by writing

$$\begin{aligned} t_R[k] \approx \mu_{Tx} \Bigg(& a\Big(\mu_{Rx}\left(h_{SR}x[k] + v_R[k] + i_R[k]\right) \\ & + \nu_{Rx}\left(h_{SR}x[k] + v_R[k] + i_R[k]\right)^* \Big)\Bigg) \\ & + \nu_{Tx} \Bigg(a\Big(\mu_{Rx}\left(h_{SR}x[k] + v_R[k] + i_R[k]\right)\Big)\Bigg)^*, \end{aligned} \tag{2.28}$$

where the approximation is again attributed to low IQI levels. To calculate the power of $t_R[k]$, the following is applied

$$\mathbb{E}\{|t_R[k]|^2\} = \gamma_1 a \left(|h_{SR}|^2\sigma_x^2 + \sigma_{v_R}^2 + \mathbb{E}\{|i_R[k]|^2\}\right), \tag{2.29}$$

where $\mathbb{E}\{.\}$ represents the expectation operator, and $\gamma_1 = |\mu_{Tx}|^2|\mu_{Rx}|^2 + |\nu_{Rx}|^2|\mu_{Tx}|^2 + |\nu_{Tx}|^2|\mu_{Rx}|^2$. Since $c[m] \perp c[n]\ \forall n \neq m$ (the symbol $\perp$ denotes statistical independence), the term $\mathbb{E}\{|i_R[k]|^2\}$ can be shown to be equal to

$$\mathbb{E}\left\{|i_R[k]|^2\right\} = (|h_{SR}|^2\sigma_x^2 + \sigma_{v_R}^2)\sum_{n=1}^{\infty} |\nu_{Rx}\mu_{Tx}^*\mu_{Rx}^*(h_R)^* a|^{2n}. \tag{2.30}$$

Hence, the total power of the transmitted signal can be expressed as

$$\mathbb{E}\{|t_R[k]|^2\} = \gamma_1\gamma_2 a^2\Big(1 + \sum_{n=1}^{\infty} |\nu_{Rx}\mu_{Tx}^*\mu_{Rx}^*(h_R)^* a|^{2n}\Big). \tag{2.31}$$

where $\gamma_2 = |h_{SR}|^2\sigma_x^2 + \sigma_{v_R}^2$. Equation (2.31) implies that increasing the amplification factor a indefinitely can cause the system to oscillate and $t_R[k]$ to diverge ($t_R[k] \to \infty$ for a fixed large amplification factor a). Therefore, to prevent the oscillations and to

make sure that $t_R[k]$ does not diverge, the amplification factor a should always satisfy $a < a_{max}$, where a_{max} denotes the maximum amplification that can limit the transmission power, and is defined by

$$a_{max} = \frac{1}{|\nu_{Rx}||\mu_{Tx}||\mu_{Rx}||h_R|}. \tag{2.32}$$

It is worth mentioning that a_{max} depends on the transceiver's IQI levels and the power of the SI channel. Although (2.32) reveals some interesting properties and limitations of a, it is still interesting to determine the amplification factor that regulates the transmission power of R. Denoting $\mathbb{E}\{|t_R[k]|^2\} = p_r$, going back to (2.31) and using the property $\sum_{n=1}^{\infty} x^{2n} = \frac{x^2}{1-x^2}$ for $|x| < 1$, the result is

$$p_r = \gamma_1\gamma_2 a^2\Big(1 + \frac{|\nu_{Rx}\mu_{Tx}^*\mu_{Rx}^*(h_R)^* a|^2}{1 - |\nu_{Rx}\mu_{Tx}^*\mu_{Rx}^*(h_R)^* a|^2}\Big). \tag{2.33}$$

Solving for a, a new amplification parameter is defined, which is denoted by $a(p_R)$, that regulates the transmission power of the relay R to be p_R, and can be written as

$$a(p_R) = \sqrt{\frac{p_r}{\gamma_1\gamma_2 + p_r|\nu_{Rx}\mu_{Tx}^*\mu_{Rx}^*(h_R)^*|^2}}. \tag{2.34}$$

Interestingly, (2.34) reveals that increasing p_r indefinitely will make $a(p_R)$ converge to a_{max}. This can be shown by writing

$$\lim_{p_R\to\infty} a(p_R) = \frac{1}{|\nu_{Rx}||\mu_{Tx}||\mu_{Rx}||h_R|} = a_{max}. \tag{2.35}$$

As previously mentioned, residual errors may arise due to imperfect estimations of the IQI parameters. Hence, it is assumed that in practice, a_{max} and $a(p_R)$ can be obtained by using IQI parameters that were modeled to quantify the residual errors of their estimation. For example, the IQI parameters that were used to quantify the errors in their estimations could be an average or a worst-case quantity. The same can be said when considering h_R, where in practice, $\hat{h}_R$ is used instead of h_R. Further, (2.35) reveals that if the relay is asked to transmit with a high p_R, then the amplification factor risks

approaching a_{max}, and hence can cause the relay to oscillate. Especially with the availability of inaccurate IQI parameters and CSI quantities in practice, it is safer to assign an amplification factor $\tilde{a}(p_R) = \sqrt{a(p_R) - \delta}$, where $\sqrt{\delta} \neq 0$ is a very small positive quantity to ensure the stability of the relay's transmission power. Section 2.2.4 provides more insights on the discussed remarks.

2.2.3. Average Residual Self-interference Analysis

Although the residual SI power was calculated in the previous section, specifically in Equation (2.30), the averaging that was performed did not consider h_R as a random variable since it is considered to be constant for one coherence time slot. Hence, this section provides an approximation of the average residual SI power by considering the channel realizations h_{SR} and h_R as random variables, which change from one coherence time slot to another, and provide a general understanding of the relationship between the residual SI power and the IQI parameters. Starting from Equation (2.30), and taking the expectation of $P_{SI}[k+1] = \mathbb{E}\left\{|i_R[k+1]|^2\right\}$, which includes h_R this time, the result is

$$P_{SI}[k+1] = \left(\sigma^2_{h_{SR}}\sigma^2_x + \sigma^2_{v_R}\right) \sum_{n=1}^{k+1} \left|\nu_{Rx}\mu^*_{Tx}\mu^*_{Rx}a\right|^{2n} \mathbb{E}\left\{|h_R|^{2n}\right\}. \tag{2.36}$$

Since h_R is a circularly symmetric complex Gaussian random variable with zero mean and variance $\sigma^2_{h_R}$, $\mathbb{E}\{|h_R|^n\}$ can be rewritten as

$$\mathbb{E}\{|h_R|^n\} = \sigma^n_{h_R} \times \mathbb{E}\left\{\left(z^2_R + z^2_I\right)^{\frac{n}{2}}\right\}, \tag{2.37}$$

where z_R, z_I are complex Gaussian random variables with zero mean and a variance 1, and $z_R \perp z_I$. Hence, it is deduced that $w = z^2_R + z^2_I$ has a chi-squared distribution with 2 degrees of freedom and a probability density function $\frac{1}{2}e^{-\frac{x}{2}}$. Therefore, (2.37) can be solved by applying

$$\mathbb{E}\{|h_R|^n\} = \frac{\sigma^n_{h_R}}{2} \int_0^\infty w^{\frac{n}{2}} e^{-\frac{w}{2}} dw. \tag{2.38}$$

Table 2.1: Simulation Parameters

Parameter	Value
σ_x^2	30 [dBm]
$\sigma_{h_R}^2$	-20 [dB]
$\sigma_{h_R}^2/\sigma_{\tilde{h}_R}^2$	35 [dB]
$\sigma_{h_{SR}}^2$	-83 [dB]
p_R	30 [dBm]
δ	0.5 [dB]
$\sigma_{n_R}^2$	-100 [dB]

Making the substitutions $w = 2u$ and $dw = 2du$,

$$\mathbb{E}\{|h_R|^n\} = \sigma_{h_R}^n 2^{\frac{n}{2}} \int_0^\infty u^{\frac{n}{2}} e^{-u} du = \sigma_{h_R}^n 2^{\frac{n}{2}} \Gamma\left(\frac{n}{2}+1\right). \tag{2.39}$$

Hence, the average residual SI power can be written as

$$P_{SI}[k+1] = \left(\sigma_{h_{SR}}^2 \sigma_x^2 + \sigma_{v_R}^2\right) \times \sum_{n=1}^{k+1} \left\{ |\nu_{Rx}\mu_{Tx}^*\mu_{Rx}^* a|^{2n} \sigma_{h_R}^n 2^{\frac{n}{2}} \Gamma\left(\frac{n}{2}+1\right) \right\}, \tag{2.40}$$

where $\Gamma(u) = \int_0^\infty w^{u-1} e^w \, dw$ is the Gamma function. The result in (2.40) reveals that the average residual SI power is a sum of scaled Gamma functions, which means that the average residual SI power is monotonically increasing as a function of time.

2.2.4. Numerical Results

This section aims at confirming the following:

- The effectiveness of the theoretical configurations that are derived and designed to prevent the oscillations at the relay (see Fig. 2.4).
- The performance and the limitations of the designed power control model (see Fig. 2.5).
- The accuracy of the derived instantaneous and average lower bound of the residual SI power (see Fig. 2.4 and Fig. 2.6).

To confirm the findings of this section, the system model is simulated using the parameters listed in Table 2.1. Furthermore, in the sequel, it is assumed that $\alpha = \alpha_{Tx} = \alpha_{Rx}$ and $\theta = \theta_{Tx} = \theta_{Rx}$.

Fig. 2.4 shows the residual SI power as a function of the amplification factor a in dB for different IQI parameters. It is important to note that the residual SI power (magenta lines) are simulated without using any of the approximations used in this work. The figure also depicts $\tilde{a}_{max}$ which is defined as $\tilde{a}_{max} = \sqrt{a_{max}^2 - \delta}$. Choosing $\delta \neq 0$ in $\tilde{a}_{max}$ assures that, ideally, (2.30) will not diverge. In this setup, h_{SR} is set to be $-3.7968 \times 10^{-5} - j5.5546 \times 10^{-5}$ and $h_R = -0.0459 \times 10^{-5} - j0.0835 \times 10^{-5}$, and hence $10log_{10}(\frac{h_R}{h_{SR}}) \approx 63$ dB. The results show that $\tilde{a}_{max}$ captures the divergence point, and hence $\tilde{a}_{max}$ indeed represents a good indicator as to when the residual SI power starts diverging to high powers. Furthermore, as the IQI parameters become less severe, $\tilde{a}_{max}$ increases, indicating that there are less restrictions now on how much the amplification can be done at the relay.

Moreover, Fig. 2.5 depicts the power of the signal to be transmitted at the relay (p_R) with respect to k for fixed IQI parameters ($\alpha = 0.35$ dB, $\theta = 1.5^o$). In this setup, h_{SR} is set to be $8.7231 \times 10^{-5} - j6.4183 \times 10^{-5}$ and $h_R = -0.01 \times 10^{-5} + j0.2203 \times 10^{-5}$, and hence $10log_{10}(\frac{h_R}{h_{SR}}) \approx 73$ dB. The analytical (solid black) and simulation (dashed magenta) curves are plotted while using different values of $\tilde{a}(p_R)$, where $\tilde{a}(p_R) = \sqrt{a^2(p_R) - \delta}$. In particular, the parameter δ is used to reduce the divergence chances ($a_{max} \geq a(p_R)$) that might happen due to approximation errors. For low p_R

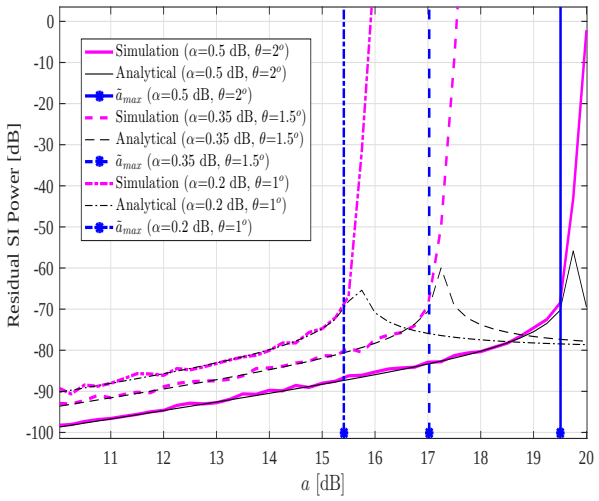

Figure 2.4: Residual SI power versus a.

values, i.e $p_R = \{-40, -50\}$ dB, the simulation results indeed converge to the desired p_R written in 2.33, while when the relay is asked to transmit with higher power, which is selected to be -30 dB, $a(p_R)$ approaches a_{max}. Since the analysis involved numerous approximations, requesting a transmit power of -30 dB forces p_R to diverge when δ is selected to be zero, while approximately converging to -30 dB when $\delta = 0.5$ dB as mentioned in Table 2.1. Although the results depict an error in the convergence when δ is used, the error in the convergence is relatively low anyway (around 2 dB) and it guarantees the convergence of p_R.

Fig. 2.6 shows the response of the average residual SI power $P_{SI}[k+1]$ as k varies while changing the IQI parameters $\alpha_{Rx/Tx}$ and $\theta_{Rx/Tx}$. As k progresses, $P_{SI}[k+1]$ increases with different rates, depending on the IQI parameters. It is important to stress on the fact that the results in Fig. 2.6, unlike what is shown in Fig. 2.4, reveal information about the residual SI at the IQI-affected relay when considering the statistics of the channel realizations, i.e. performance evaluation for different realizations of the channels. Although the lower bound is not precise in calculating the residual SI power, it is still useful in the sense that it describes and captures the effect of IQI on the residual SI power in terms of its overall behavior. The results reveal that

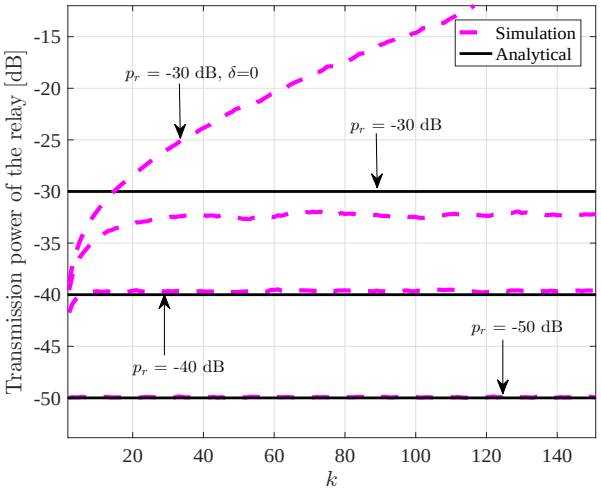

Figure 2.5: Simulated (dashed magenta) and analytical (solid black) p_R versus k.

$P_{SI}[k+1]$ quickly increases when $\alpha_{Rx/Tx} = 0.5$ dB and $\theta_{Rx/Tx} = 2^o$, while the rate of increasing drops $\alpha_{Rx/Tx} = 0.35$ dB and $\theta_{Rx/Tx} = 1.5^o$. Although $P_{SI}[k+1]$ is shown to be stable when $\alpha_{Rx/Tx} = 0.2$ and $\theta_{Rx/Tx} = 1^o$, it will surely diverge as for the other cases of the selected IQI parameters, but at a much larger value of k. This divergence occurs since there is no limit set on the amplification factor, and was arbitrarily chosen to be $a = 16.5$ dB. It is noted that this result is intended to highlight the effect of IQI, and not to emulate a practical scenario, where a relay has a limit on the transmit power. If the residual SI power's stability is to be insured on average, the minimum value of $a(p_R)$ over all possibilities of the channel realizations h_R should be used, which over a long period of time, can theoretically reach the value of zero. This is why $a(p_R)$ should be deduced for each realization of h_R to ensure stability.

2.3. Chapter Summary

This chapter presented a thorough analysis of the residual SI power jointly affected by PN and IQI. The analytical results were simplified to highlight the functional dependency of the residual SI power on the PN's 3-dB bandwidth and the IQI's IRR. The conducted simulations confirm the analysis. The analysis highlights the importance

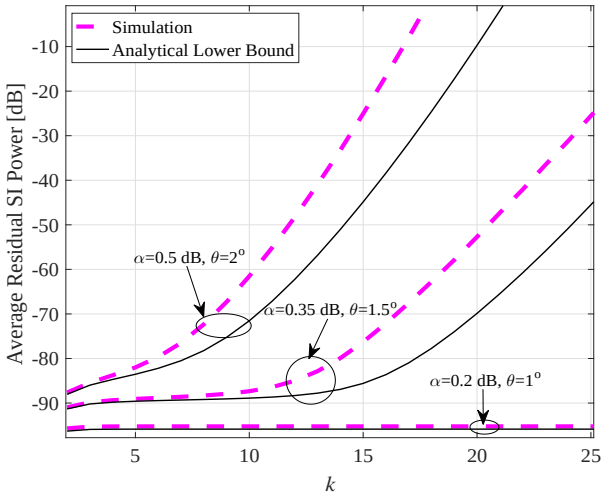

Figure 2.6: Average residual SI power versus k. $a^2 = 33$ dB.

of carefully devising further processing, possibly DSP, to reduce the residual SI power and hence enhancing the performance of FD communications.

Moreover, this chapter considered the effect of IQI on the process of SI cancellation in FD AF transceivers. The cumulative SI was modeled as a function of IQI, and the stability of the performance of the relay was thoroughly analyzed by evaluating the different transmission parameters and configurations that guarantee the stability of the system. The analysis further showed that the average SI power is bounded by a sum of scaled Gamma functions. The simulation results confirm the analysis of the residual SI power and the limits of the amplification factor.

Now that the performance of FD transceivers was quantified through the analysis of the residual SI power, the next chapter discusses several proposed DSP algorithms that perform multiple relay selection and beamforming when the relays adopt FD transceivers.

CHAPTER 3: ADAPTIVE RELAY SELECTION AND BEAMFORMING IN FULL-DUPLEX COOPERATIVE NETWORKS

Chapter 2 discussed the effects of RF impairments on the performance of FD transceivers. In Section 2.2, the effect of RF impairments on a FD AF relay was investigated. In this chapter, the effect of RF impairments is ignored and instead, the general behavior of the residual SI, which has a special effect in FD AF relays [24, 27], is emphasized upon. Moreover, the same network topology is adopted with the addition of the possibility of selecting multiple relays and beamforming the signals at each relay. The details of the contribution is detailed in the following sections.

3.1. System Model

The adopted dual-hop wireless network model consists of one source S transmitting data to one destination D with the assistance of N relays, where each relay is denoted by R_i ($i = 1 \dots N$).

The direct link between the source and the destination is assumed to be unavailable due to severe fading and path-loss. Consequently, the data can be transferred from S to D only through the relays [66, 67, 68, 69]. To enhance the communication quality

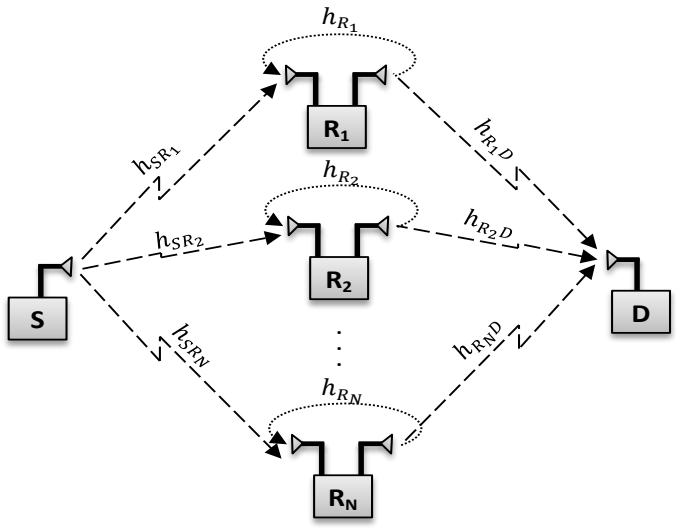

Figure 3.1: System Model.

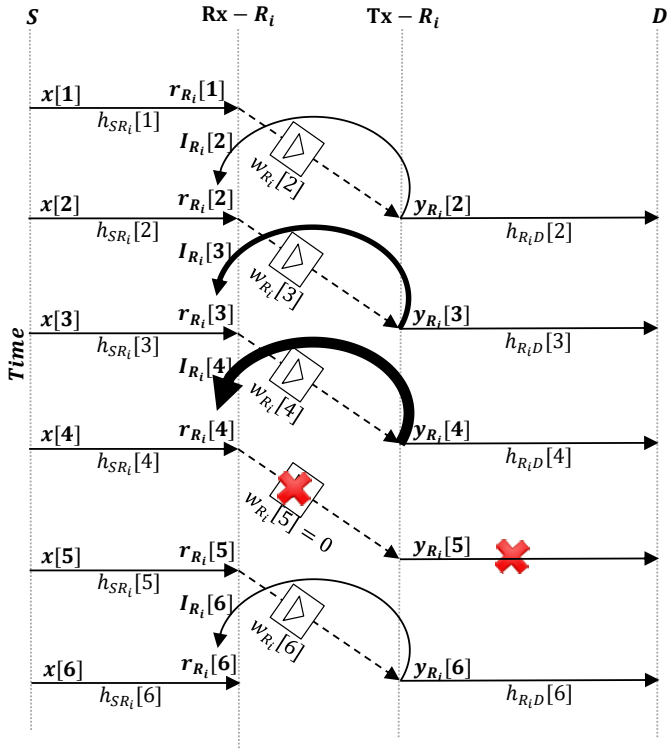

Figure 3.2: Schematic transmission model at the relay R_i.

between S and D, different techniques are proposed in this contribution to select a set of 'best' relays out of the N available relays, based on different selection criteria.

All the relays are assumed to operate in FD mode [27, 25], i.e. each selected relay simultaneously transmits and receives information on the same frequency band, creating SI due to leaking from the previous relay's transmission(s). The channel coefficients for the links $S \rightarrow R_i$ and $R_i \rightarrow D$ are denoted by h_{SR_i} and h_{R_iD}, respectively. The coefficients h_{SR_i} and h_{R_iD} are modeled as complex circularly-symmetric zero-mean Gaussian random variables with variances $\sigma^2_{SR_i}$ and $\sigma^2_{R_iD}$, respectively. Fig. 3.1 depicts the adopted system model.

In the half-duplex case, the selection is dependent on the CSIs between the source and the relay ($S \rightarrow R_i$) and from the relay to the destination ($R_i \rightarrow D$) [70], or only their second order statics [33]. However, to guarantee maximum diversity, the selection in FD cooperative networks has to take into consideration the residual SI at each relay, while assuming that each relay is able to cancel some of its SI [27, 25].

Fig. 3.2 represents a detailed schematic drawing of the adopted transmission scheme that a single relay could potentially follow in the network. In particular, during the n^{th} time slot, the source broadcasts the transmitted data $x[n]$ to all the relays. If a relay R_i is selected to forward the data, the received signal $r_{R_i}[n]$ at the i^{th} relay is multiplied by a corresponding beamforming and amplification coefficient $w_{R_i}[n+1]$. The resulting signal $y_{R_i}[n+1]$ is then forwarded in the next time slot to the destination. However, due to the transmission leakage between the Rx and Tx antennas of the relays, SI loops back to the relay's receiver (where the thickness of the SI line represents the severity of the SI). As the SI has a cumulative behavior [27, 24], after some transmission slots (5 transmission slots in Fig. 2), the SI might becomes so high that the diversity brought by that particular relay is low compared to other relays. In this case, it might be better to stop using the relay R_i for at least one time slot to null out the cumulative SI before including it again in the selection set in the next time slot.

In particular, at time slot n, the relay R_i receives the symbol $x[n]$ from the source S, and simultaneously transmits information to the destination D. Therefore, the received signal at the i^{th} relay can be written as

$$r_{R_i}[n] = h_{SR_i}[n]x[n] + v_{R_i}[n] + I_{R_i}[n], \tag{3.1}$$

where $v_{R_i}[n]$ is AWGN with variance $\sigma^2_{v_{R_i}}$ at the relay R_i in the n^{th} time slot, and $I_{R_i}[n]$ represents the residual SI at the relay R_i in the n^{th} time slot. Furthermore, the residual SI $I_{R_i}[n]$ at time n can be expressed by (See the proof in Appendix B)

$$\begin{aligned} I_{R_i}[n] = \sum_{m=1}^{n-1} \Big(\prod_{p=n-m+1}^{n} \tilde{h}_{R_i}[p] w_{R_i}[p] \Big) \times \\ \Big(h_{SR_i}[n-m]x[n-m] + v_{R_i}[n-m] \Big), \end{aligned} \tag{3.2}$$

where $\tilde{h}_{R_i}[n]$ represents the residual SI channel [24] modeled as a zero-mean Gaussian random variable with a variance $\sigma^2_{R_i}$ [64]. Note that $\sigma^2_{R_i}$ approaching zero implies that the SI cancellation capability of the relay is high. From (3.2), it is deduced that the

residual SI depends of the SI cancellation capability for each relay and the beamforming coefficients at all the previous time slots. Next, if the relay R_i is selected, a beamforming coefficient $w_{R_i}[n]$ is applied, and the transmitted signal $y_{R_i}[n]$ is then expressed by writing

$$\begin{aligned} y_{R_i}[n] &= w_{R_i}[n]h_{SR_i}[n-1]x[n-1] + w_{R_i}[n]v_{R_i}[n-1] \\ &\quad + w_{R_i}[n]I_{R_i}[n-1]. \end{aligned} \tag{3.3}$$

Therefore, the received signal $y_D[n]$ at the destination can be written as

$$y_D[n] = (\mathbf{w}[n])^H \mathbf{a}[n] + v_D[n], \tag{3.4}$$

where $v_D[n]$ is the AWGN in the n^{th} time slot at the destination with variance $\mathbb{E}\{v_D[n]v_D^*[n]\} = \sigma_{v_D}^2$, and

$$\mathbf{w}[n] \triangleq \Big[w_{R_1}[n], \ldots, w_{R_N}[n]\Big]^H,$$

$$\mathbf{a}[n] \triangleq \Big[a_{R_1}[n], \ldots, a_{R_N}[n]\Big]^H, \tag{3.5}$$

$$\mathbf{b}[n] \triangleq \Big[b_{R_1}[n], \ldots, b_{R_N}[n]\Big]^H, \tag{3.6}$$

where $a_{R_i}[n]$ and $b_{R_i}[n]$ are defined by writing

$$\begin{aligned} a_{R_i}[n] &\triangleq h_{R_i,D}[n]h_{S,R_i}[n-1]x[n-1] + h_{R_i,D}[n]v_{R_i}[n-1] \\ &\quad + h_{R_i,D}[n]I_{R_i}[n-1], \\ &= h_{S,R_i,D}[n]x[n-1] + b_{R_i}[n], \end{aligned} \tag{3.7}$$

and

$$b_{R_i}[n] \triangleq h_{R_iD}[n]v_{R_i}[n-1] + h_{R_iD}[n]I_{R_i}[n-1],$$

where

$$h_{S,R_i,D}[n] \triangleq h_{S,R_i}[n-1] \times h_{R_i,D}[n].$$

From (3.4), it can be seen that the received signal at the destination depends on the new realizations of $\mathbf{a}$ (h_{SR_i}, h_{R_iD}, $\tilde{h}_{R_i} \mid i = 1..N$) at the current time slot as well as all the previous ones. So, unlike the work in [27, 23] and to enhance the diversity at the destination, the amplification and beamforming coefficients for each relay should be adapted at each time slot depending on the new realizations.

3.2. Cost Function Analysis

In this section, the cost function that will be the performance metric on which the proposed multiple relay selection and beamforming solutions will be based on is formulated.

In this work, the cost function is selected to be the MSE as it has been shown for example in [71, 72] that MSE minimization based selection techniques enhance the BER performance. Therefore, the MSE of the received signal $\epsilon[n]$ is next calculated, which can be computed by applying

$$\epsilon[n] \triangleq \mathbb{E}\left\{|x[n-1] - y_D[n]|^2\right\}. \tag{3.8}$$

Assuming statistical independence between x, v_{R_i} and v_D, the result is

$$\begin{aligned}
\epsilon[n] &= (\mathbf{w}[n])^H \underbrace{\mathbf{h}_{S,R,D}[n]\mathbf{h}_{S,R,D}^H[n]}_{\triangleq \mathbf{A}[n]}(\mathbf{w}[n])\sigma_x^2 \\
&+ (\mathbf{w}[n])^H \underbrace{\mathbb{E}\left\{\mathbf{b}[n](\mathbf{b}[n])^H\right\}}_{\triangleq \mathbf{B}[n]}(\mathbf{w}[n]) + \sigma_D^2 + \sigma_x^2 \\
&- (\mathbf{w}[n])^H \mathbf{h}_{S,R,D}[n]\sigma_x^2 - \mathbf{h}_{S,R,D}^H[n](\mathbf{w}[n])\sigma_x^2. \\
&= (\mathbf{w}[n])^H(\mathbf{A}[n]\sigma_x^2 + \mathbf{B}[n])\mathbf{w}[n] + \sigma_D^2 + \sigma_x^2 \\
&- (\mathbf{w}[n])^H \mathbf{h}_{S,R,D}[n]\sigma_x^2 - \mathbf{h}_{S,R,D}^H[n](\mathbf{w}[n])\sigma_x^2, \qquad (3.9)
\end{aligned}$$

where

$$\mathbf{A}[n] \triangleq \mathbf{h}_{S,R,D}[n]\mathbf{h}_{S,R,D}^H[n],$$

and

$$B_{i,j}[n] \triangleq \mathbb{E}\left\{b_{R_i}[n]^* b_{R_j}[n]\right\}, \qquad (3.10)$$

$$= \begin{cases} 0, & \text{if } i \neq j, \\ |h_{R_i,D}[n]|^2 \left(\sigma_v^2 + \sum_{m=1}^{n-2}\left(\prod_{p=n-m}^{n-1}\sigma_{R_i}^2 |w_{R_i}[p]|^2\right)\right. & \\ \left. \times\left(|h_{SR_i}[n-1-m]|^2\sigma_x^2 + \sigma_v^2\right)\right), & otherwise. \end{cases}$$

The MSE expression in (3.9) can be further simplified to

$$\begin{aligned}
\epsilon[n] &= \mathbf{w}^H[n]\mathbf{R}[n]\ \mathbf{w}[n] - \mathbf{w}^H[n]\mathbf{h}_{S,R,D}[n]\sigma_x^2 \qquad (3.11) \\
&- \sigma_x^2\ \mathbf{h}_{S,R,D}^H[n]\mathbf{w}[n] + \sigma_D^2 + \sigma_x^2,
\end{aligned}$$

where

$$\mathbf{R}[n] \triangleq \sigma_x^2 \mathbf{A}[n] + \mathbf{B}[n]. \tag{3.12}$$

Using the Cholesky factorization $\mathbf{R}[n] = \mathbf{L}[n]\mathbf{L}^H[n]$, where $\mathbf{L}$ is a lower triangular matrix, $\epsilon[n]$ can be hence written as

$$\begin{aligned}\epsilon[n] = \sigma_x^2 + \sigma_D^2 - \mathbf{w}^H[n]\mathbf{L}^{-1}[n]\mathbf{L}[n]\tilde{\mathbf{h}}[n] \\ - \tilde{\mathbf{h}}^H[n]\mathbf{L}^{-H}[n]\mathbf{L}^H[n]\mathbf{w}[n] + \mathbf{w}^H[n]\mathbf{L}[n]\mathbf{L}^H[n]\mathbf{w}[n],\end{aligned} \tag{3.13}$$

where $\tilde{\mathbf{h}}[n] \triangleq \sigma_x^2 \mathbf{h}_{S,R,D}[n]$. Consequently, $\epsilon[n]$ can be written in the following form

$$\begin{aligned}\epsilon[n] = \underbrace{\sigma_x^2 - \tilde{\mathbf{h}}^H[n]\mathbf{L}^{-H}[n]\mathbf{L}^{-1}[n]\tilde{\mathbf{h}}[n] + \sigma_D^2}_{\epsilon_{min}[n]} \\ + \underbrace{||\mathbf{L}^H[n]\mathbf{w}[n] - \mathbf{L}^{-1}[n]\tilde{\mathbf{h}}[n]||_2^2}_{\epsilon_{excess}[n]}.\end{aligned} \tag{3.14}$$

From (3.14), it can be seen that ϵ_{min} does not depend on $\mathbf{w}[n]$. Consequently, the optimization of $\mathbf{w}[n]$ towards minimizing the MSE at the destination is equivalent to minimizing ϵ_{excess}.

3.3. Multiple Relay Selection and Beamforming Schemes

3.3.1. Problem Formulation

In this setup, it is assumed that each relay is capable of applying a beamforming coefficient before transmitting to the destination. Further, it has been shown that the problem of selecting k_{max} relays and computing their corresponding beamforming

coefficients under total power constraint is expressed by writing

$$\begin{aligned} \min_{\mathbf{w}} \quad & \left(||\mathbf{L}^H[n]\mathbf{w}[n] - \mathbf{L}^{-1}[n]\tilde{\mathbf{h}}[n]||_2^2 \right) \\ \text{s.t.} \quad & \text{card}(\mathbf{w}[n]) = k_{max} \\ & \sum_{i=1}^{N} P_{R_i}[n] = \sigma_x^2, \end{aligned} \tag{3.15}$$

where $k_{max} \in \{1, \ldots, N\}$ represents the number of selected relays, $P_{R_i}[n]$ denotes the transmission power of the relay R_i at the n^{th} time slot and card$(.)$ represents the cardinality function, i.e. the number of non-zero elements in $\mathbf{w}[n]$.

Note that the problem in (3.15) is an NP-hard problem and requires an exhaustive search over all the possible $\binom{N}{k_{max}}$ combinations, which might be computationally unaffordable [33]. Hence, computationally affordable algorithms are next implemented to solve the selection problem.

To simplify the optimization problem in (3.15), the problem of selecting the relays and their beamforming coefficients independently from the total transmission power constraint is first focused on, then -as it will be detailed in Section 3.3.4- the resulting selection vector is normalized to meet the requirements of the power constraint. Hence, after dropping the power constraint, the selection problem in (3.15) becomes

$$\begin{aligned} \min_{\mathbf{w}} \quad & \left(||\mathbf{L}^H[n]\mathbf{w}[n] - \mathbf{L}^{-1}[n]\tilde{\mathbf{h}}[n]||_2^2 \right) \\ \text{s.t.} \quad & \text{card}(\mathbf{w}[n]) = k_{max}. \end{aligned} \tag{3.16}$$

3.3.2. Unlimited Number of Selected Relays (UNSR)

In this part, to further reduce the complexity of the problem in (3.16), the non-convex cardinality constraint is first dropped. In this case, the selection problem can be written as

$$\min_{\mathbf{w}} \quad \left(||\mathbf{L}^H[n]\mathbf{w}[n] - \mathbf{L}^{-1}[n]\tilde{\mathbf{h}}[n]||_2^2 \right). \tag{3.17}$$

Unlimited Number of Selected Relays - Zero Forcing (UNSR-ZF)

One way to solve the problem (3.17) is by using the ZF solution given by

$$\mathbf{w}_{ZF}[n] = \mathbf{L}^{-H}[n]\mathbf{L}^{-1}[n]\tilde{\mathbf{h}}[n]. \tag{3.18}$$

Note that all the elements of the vector $\mathbf{w}_{ZF}[n]$ in (3.18) are non-zeros which is equivalent to selecting all the relays to forward the data. However, due to the SI cumulative effect, some relays that suffer from high levels of SI might be requested to transmit with a very small power to null out the cumulative SI before including it again in the selection set in the next time slots, i.e., $\max\Big(\mathbf{w}_{ZF}[n]\Big) \gg \min\Big(\mathbf{w}_{ZF}[n]\Big)$. To solve this issue, excluding the relays that are requested to transmit with a very small power compared to the maximum relay transmission power from the selection set is proposed, i.e. $\mathbf{w}_{\textit{UNSR-ZF}}[n]$ is obtained by nulling the coefficients of $\mathbf{w}_{ZF}[n]$ that satisfy the condition $|\mathbf{w}_{\textit{UNSR-ZF}}[n]| < \frac{\max(|\mathbf{w}_{\textit{UNSR-ZF}}[n]|)}{10}$.

Unlimited Number of Selected Relays - ℓ_1-norm (UNSR-ℓ_1)

Although UNSR-ZF reduces the number of unnecessary relays by excluding the ones that have a very low transmission power, the resulting total number of selected relays might still be more than necessary, i.e. some of the selected relays are using the network resources without providing a significant improvement on the BER performance at the destination. To solve this issue, the ℓ_1-norm sparsifying operator [33] is exploited to force the selection of the least possible number of relays by reformulating

the selection to the following optimization problem

$$\begin{aligned} \min_{\mathbf{w}} \quad & \left(||\mathbf{L}^H[n]\mathbf{w}[n] - \mathbf{L}^{-1}[n]\tilde{\mathbf{h}}[n]||_1^2 \right) \\ \text{s.t.} \quad & ||\mathbf{L}^H[n]\mathbf{w}[n] - \mathbf{L}^{-1}[n]\tilde{\mathbf{h}}[n]||_2^2 \leq \delta, \end{aligned} \tag{3.19}$$

where δ is a threshold predefined by the network administrators corresponding to the minimum acceptable error in ϵ_{excess}. Note that UNSR-ℓ_1 selection technique reduces the number of selected relays compared with UNSR-ZF at the price of higher complexity (optimization problem solving compared to a direct analytical solution). Also, choosing very small values of δ forces the network to use a big number of relays while a bigger δ would require less relays for communications. Consequently, the choice of δ creates a compromise between the MSE performance and the number of selected relays.

3.3.3. Limited Number of Selected Relays (LNSR)

Both UNSR-ZF and UNSR-ℓ_1 techniques aim to minimize the MSE at the destination with a limited number of relays. However, none of them can force the selection of a certain number of active relays in the network which might be impractical in some scenarios. Henceforth, the following presented techniques will guarantee the selection of at most k_{max} relays.

Limited Number of Selected Relays - Zero Forcing (LNSR-ZF)

In this part that, due to synchronization and implementation challenges, the total number of active relays can not exceed a predefined integer k_{max}, i.e.

$$\begin{aligned} \min_{\mathbf{w}} \quad & \left(||\mathbf{L}^H[n]\mathbf{w}[n] - \mathbf{L}^{-1}[n]\tilde{\mathbf{h}}[n]||_2^2 \right) \\ \text{s.t.} \quad & \text{card}(\mathbf{w}[n]) \leq k_{max}. \end{aligned} \tag{3.20}$$

To satisfy this condition, the same selection steps of UNSR-ZF are followed. Then, only the k_{max} relays that have the largest $|\mathbf{w}_{\textit{LNSR-ZF}}[n]|$ are kept active, i.e. the selection

set of LNSR-ZF is given by

$$S_{\textit{LNSR-ZF}} = \underset{i\in 1\ldots N}{\overset{k_{max}}{\operatorname{argmax}}}\Big(|\mathbf{w}_{\textit{LNSR-ZF}}[n]|\Big). \tag{3.21}$$

Then, the same computed beamforming coefficients for UNSR-ZF are kept for LNSR-ZF in the updated selection set, i.e.

$$\mathbf{w}_{\textit{LNSR-ZF}}[n] = \begin{cases} \mathbf{w}_{\textit{UNSR-ZF}}[n] & \text{if } i \in S_{\textit{LNSR-ZF}}[n] \\ 0 & otherwise. \end{cases} \tag{3.22}$$

Limited Number of Selected Relays - ℓ_1-norm (LNSR-ℓ_1)

Similar to the UNSR-ℓ_1 technique, the total number of active relays is minimized using ℓ_1-norm squared, then thresholding is performed according to a predefined integer k_{max}, i.e.

$$\begin{aligned} \min_{\mathbf{w}} \quad & \left(||\mathbf{L}^H[n]\mathbf{w}[n] - \mathbf{L}^{-1}[n]\tilde{\mathbf{h}}[n]||_1^2\right) \\ \text{s.t.} \quad & ||\mathbf{L}^H[n]\mathbf{w}[n] - \mathbf{L}^{-1}[n]\tilde{\mathbf{h}}[n]||_2^2 \leq \delta \\ & \text{card}(\mathbf{w}[n]) \leq k_{max}. \end{aligned} \tag{3.23}$$

Thus, the only selected relays are the k_{max} relays that have the largest $|\mathbf{w}_{R_i}^{\textit{UNSR-}\ell_1}[n]|$, i.e.

$$S_{\textit{LNSR-}\ell_1} = \underset{i\in 1\ldots N}{\overset{k_{max}}{\operatorname{argmax}}}\Big(|\mathbf{w}^{\textit{UNSR-}\ell_1}[n]|\Big). \tag{3.24}$$

The computed beamforming coefficients for UNSR-ℓ_1 are kept for LNSR-ℓ_1 in the updated selection set, i.e.

$$w_{R_i}^{\textit{LNSR-}\ell_1}[n] = \begin{cases} w_{R_i}^{\textit{UNSR-}\ell_1}[n] & \text{if } i \in S_{\textit{UNSR-}\ell_1} \\ 0 & otherwise. \end{cases} \tag{3.25}$$

3.3.4. *Power Constraint*

The power of the signal transmitted from the i^{th} relay $P_{R_{r_i}}$ can be written as

$$\begin{aligned} P_{R_i}[n] &= \mathbb{E}\left\{|y_{R_i}[n]|^2\right\} \\ &= |w_{R_i}[n]|^2\sigma_{S,R}^2\sigma_x^2 + |w_{R_i}[n]|^2\sigma_v^2 + |w_{R_i}[n]|^2 \\ &\times \Big(\sigma_{S,R}^2\sigma_x^2 + \sigma_v^2\Big)\sum_{m=1}^{n-1}(\sigma_{R_i}^2)^m\Big(\prod_{p=n-m}^{n-1}|w_{R_i}[p]|^2\Big), \end{aligned} \tag{3.26}$$

where $\sigma_{S,R}^2 = \mathbb{E}\{h_{S,R_i}h_{S,R_i}^*\}$, and $\sigma_R^2 = \mathbb{E}\{h_{R_i}h_{R_i}^*\}$ for $i \in \{1,\ldots,N\}$. Hence, to satisfy the power constraint in (3.15), the computed beamforming coefficients are multiplied by the following constant

$$\alpha = \frac{\sigma_x^2}{\sum_{i=1}^{N} P_{R_i}[n]}. \tag{3.27}$$

In this way, the total transmit power from the relays will be equal to σ_x^2.

3.4. Numerical Results

In this section, the performance of the proposed techniques are simulated and compared with existing techniques in the literature. The performance of these techniques are first evaluated in terms of BER. For better comparison, the average number of selected relays and the relay re-usage percentage are also depicted as metrics to evaluate the performance of the investigated techniques. In particular, the relay re-usage percentage is defined as the average percentage of relays being reused in two consecutive time slots. This metric is used to show how often the network needs to apply switching for the relays that suffer from high residual SI to maintain the desired performance.

Table 3.1 summarizes the adopted simulation configuration parameters, unless stated otherwise in the sequel. In particular, the proposed multiple relay selection techniques are tested for $N = 20$ relays where binary phase-shift keying (BPSK) is used

Table 3.1: Simulation Parameters.

Parameter	Value	Description
N	20	Number of relays.
σ^2_{SR}	0 dB	Variance of $h_{SR_i} \mid i \in \{1, 2, \ldots, N\}$.
σ^2_{RD}	0 dB	Variance of $h_{R_iD} \mid i \in \{1, 2, \ldots, N\}$.
σ^2_x	0 dB	Variance of $x[n] \mid n \in \{1, 2, \ldots, \infty\}$.
n_c	100	Sampled time length at which the CSI is constant.
δ	-15 dB	Minimum acceptable error in ϵ_{excess}.

to modulate the data. The BER performance is evaluated for different configurations of the residual SI channel variance ($\sigma^2_{R_i}$), the relay transmit power (σ^2_x) and the maximum number of selected relays (k_{max}). It is assumed that the channel coefficients h_{SR_i} and h_{R_iD} $\forall i \in \{1, \ldots, N\}$ are fixed for a certain period of time n_c[1]. Furthermore, $\sigma^2_{SR} = \sigma^2_{RD} = 0$ dB.

To highlight the gains of the proposed multiple relay selection and beamforming techniques, the proposed approaches are comapred with the below techniques:

- Optimal Single Relay Selection (OSRS) adopted from [25]: A single relay is selected based on maximizing the SINR at the destination.
- Optimal Single Relay Selection adopted from [25] with beamforming (OSRS-BF): A single relay is selected based on maximizing the SINR at the destination with beamforming applied at the selected relay.

[1]Note that assuming that the channel coefficients are varying at each time slot and that their realizations are perfectly known by the source might not be practical in some networks. That's why the channel coefficients h_{SR_i} and h_{R_iD} are assumed to be slowly varying and change after n_c time slots.

Fig. 3.3 presents the effect of the residual SI power (by varying $\sigma^2_{R_i}$ $\forall i \in \{1, \ldots, N\}$ from -5 dB to 30 dB) on the performance of the different investigated techniques when the sinal-to-noise ratio (SNR) and k_{max} are set to be SNR=3 dB, $k_{max} = 15$.

First, it can be seen that the proposed techniques LNSR-ZF, UNSR-ZF, LNSR-ℓ_1 and UNSR-ℓ_1 outperform the OSRS technique presented in [25] even when beamforming is applied to it (OSRS-BF). This is, in part, due to the fact that the method in [25] selects only a single relay and that the proposed techniques in this contribution allow the network to switch between relays at each time slot, if necessary.

Note also that OSRS selection technique provides a high BER at these ranges of parameters compared to the remaining techniques because, in addition to selecting only a single relay, no beamforming is applied.

For low $\sigma^2_{R_i}$, the LNSR-ℓ_1 and UNSR-ℓ_1 perform the best with the lowest number of relays, especially for low values of δ, at the price of an increased complexity (optimizaion problem solving instead of direct ZF solution) compared to ZF techniques. However, the UNSR-ZF technique starts performing better than all other techniques as $\sigma^2_{R_i}$ increases. This is explained by looking at Fig. 3.3-b where the depicted results show the average number of selected relays as a function of $\sigma^2_{R_i}$. The results reveal that the UNSR-ZF method uses a larger number of selected relays as it focuses on minimizing the MSE more than reducing the number of selected relays. Note that, although up to 20 relays can be used by UNSR-ZF and UNSR-ℓ_1, and up to 15 relays can be used by LNSR-ZF and LNSR-ℓ_1, the average number of selected relays is much less than those used for very high values of SI. In particular, for high values of SI, no big difference can be seen between the BER of the different techniques (see Fig. 3.3-a) as the system performance is almost saturated. Hence, the proposed techniques automatically decide that using more relays will not be of great benefit to the MSE performance and therefore a smaller number of relays is used. On the other hand, the optimization in UNSR-ℓ_1 and LNSR-ℓ_1 have a target MSE to reach with the minimum possible number of relays. Hence, obviously, increasing the SI level will require from the system to use

more relays to reach this target until a value of SI (around 10 dB) where the target MSE is no longer reached anyway. At this point, the number of used relays by UNSR-ℓ_1 and LNSR-ℓ_1 techniques start to decrease by the effect of ℓ_1-norm minimization.

Furthermore, the relay re-usage percentage is depicted in Fig. 3.3-c as a function of $\sigma^2_{R_i}$. The LNSR-ZF technique has almost a fixed relay re-usage rate of about 67%. However, the other proposed UNSR-ZF and UNSR-ℓ_1 based methods are shown to be very responsive to $\sigma^2_{R_i}$. Note that the re-usage rate is fixed at 100% when $\sigma^2_{R_i}$ is low and could reach about 48% when $\sigma^2_{R_i}$ is high, i.e. when there is a very limited level of interference, there is no need to switch between the relays. Hence, it is noticed that when the level of SI is very high, reusing the same relays becomes more difficult because of the cumulative effect of the SI. Therefore, depending on the SI level, the proposed techniques dynamically decide whether there is a benefit or not from switching the transmission between the relays and how often this should be done given that switching might create few implementation and synchronization challenges and therefore should be avoided when not beneficial.

In Fig. 3.4-a, the BER performance is plotted against the source and the relay's transmit power ($P = \sigma^2_x = P_{R_i}[n]$), while the SNR is set to be 10 dB and $\sigma^2_{R_i} = 15$ dB.

Note that the UNSR-ZF technique shows the best BER performance compared to other techniques but while using the biggest number of selected relays as depicted in Fig. 3.4-b (20 relays are used and then the number drops after $P = 22$ dBm). Note that all the investigated techniques suffer from an error floor starting from some specific value of transmit power. In particular, increasing the transmit power enhances the SNR level but also increases the SI at the relays and deteriorates the performance. Hence, starting from 25 dBm, increasing the transmit power -almost- does not affect the BER performance.

It is observed that for the UNSR-ℓ_1 and LNSR-ℓ_1 techniques, the number of selected relays starts increasing as P increases, and then revert to decreasing when $P > 20$ dBm for the UNSR-ℓ_1 method and when $P > 24$ dBm for the LNSR-ℓ_1 method. This is due to the fact that increasing the transmit power at the relays increases

the SI, and the system decides to use less relays to mitigate the SI's detrimental effect on the overall BER performance. Moreover, the LNSR-ℓ_1 technique has the lowest number of selected relays as shown in Fig. 3.4-b. The OSRS method has a very high BER since beamforming is not applied, while the OSRS-BF performs better than the OSRS method, although it performs worse than the other proposed techniques due to only selecting one relay.

Fig. 3.4-c shows the re-usage percentage of the selected relays, and shows that the UNSR-ℓ_1 method is the most responsive to the variation of P, decreasing at a very fast rate when $P > 20$ dBm. The LNSR-ZF method has a re-usage percentage which is fixed at around 67%, and then starts decreasing when $P > 26$ dBm. Both the UNSR-ℓ_1 and the UNSR-ZF have higher re-usage percentages, while the UNSR-ℓ_1 technique starts becoming very responsive when $P > 20$ dBm after being constant at 100 $\%$ re-usage percentage. In particular, Fig. 3.4-c confirms that the proposed techniques and especially UNSR-ℓ_1 and LNSR-ℓ_1 can dynamically maximize the percentage of re-usage depending on the transmit power to keep the required performance whenever possible.

In Fig. 3.5-a, the BER performance is depicted against k_{max} for SNR=10 dB and $\sigma^2_{R_i} = 15$ dB. Without beamforming, the OSRS technique has high BER while with beamforming, the BER performance is enhanced and performs considerably better, although the rest of the proposed techniques outperform it as k_{max} increases. It can be seen also that increasing the maximum number of selected relays k_{max} increases the diversity level and reduces the BER of the limited number of selected relays techniques (LNSR-ZF and LNSR-ℓ_1). Further, both the LNSR-ℓ_1 and UNSR-ℓ_1 techniques reach a saturation level after around 13 relays are selected as increasing the number of relays would not enhance the performance. In particular, such kind of saturation is often seen in relay selection schemes as in e.g. [33]. Normally, by allowing UNSR-ℓ_1 to use up to 20 relays compared to LNSR-ℓ_1 which is allowed to use up to k_{max} relays with the same beamforming coefficients, UNSR-ℓ_1 should always perform better than LNSR-ℓ_1. However, it can be seen that LNSR-ℓ_1 has slightly higher BER performance compared

to UNSR-ℓ_1 technique from around $k_{max} = 8$ to $k_{max} = 12$ relays. This is due to the thresholding step at the end of UNSR-ℓ_1 and LNSR-ℓ_1 techniques intended to reduce the number of used relays which is indeed a low complexity but not optimal solution. From Fig. 3.5-b, both UNSR-ℓ_1 and LNSR-ℓ_1 use almost the same number of selected relays when k_{max} is around 13.

For the cases of the UNSR-ZF and LSNR-ZF, UNSR-ZF is always performing much better than its LNSR-ZF counterpart at the expense of always using more relays.

In Fig. 3.5-c, the re-usage percentage is plotted as a function of k_{max} for all the proposed techniques. It can be noticed that all the techniques that are designed to be a function of k_{max} are very responsive to the relay re-usage percentage and adaptively decide on how often the relays should switch based on the maximum allowed number of relays.

Lastly, concerning the effect of the constant δ that bounds the inequalities for the constraints in (3.19) and (3.23), the BER, the average number of selected relays and the average relay re-usage percentage are all plotted against δ in Fig. 3.6-a, Fig. 3.6-b and Fig. 3.6-c, respectively. The simulations were performed for an SNR of 2 dB, $\sigma^2_{R_i} = 12$ dB and for $k_{max} = 16$. The proposed selection techniques that are used to generate the results are UNSR-ℓ_1 and LNSR-ℓ_1, since both of the selection problems depend on the constant δ, which was varied between -18 dB and -4 dB. These results are provided to highlight the effect of δ besides the fact that it has an effect on the complexity of the proposed selection techniques. The results show that in general, the BER performances of both the UNSR-ℓ_1 and LNSR-ℓ_1 selection techniques depend on δ since both techniques show better performances when δ is small and the performance deteriorates as the value of δ increases. This behavior can be explained by the fact that tightening the bound in the constraints in (3.19) and (3.23) results in a better BER performance. Furthermore, the UNSR-ℓ_1 technique outperforms the performance of its LNSR-ℓ_1 counterpart in the interval that is around -18 dB $< \delta < -10$ dB since as depicted in Fig. 3.6-b, the average number of selected relays for the LNSR-ℓ_1 technique saturates at $k_{max} = 16$, while the average number of selected relays for the UNSR-

ℓ_1 selection technique keeps increasing, hence providing a better BER performance. In Fig. 3.6-c, the average relay re-usage percentage increases as δ gets smaller for the UNSR-ℓ_1 technique since the average number of selected relays is also increased, making the usage of the same relay inevitable. However, for the LNSR-ℓ_1 selection technique, the average relay re-usage percentage increases from 80% to around 93% when δ goes from -18 dB until -10 dB and then drops again to around 78% when δ reaches -6 dB. When δ is relatively high, the number of selected relays for both the UNSR-ℓ_1 LNSR-ℓ_1 techniques is low (as only a limited number of relays can satisfy the constraint in (3.19) and (3.23)). Hence, the UNSR-ℓ_1 and LNSR-ℓ_1 techniques provide almost the same solution and therefore the same number of relays and relay re-usage percentage. Note that the relay re-usage percentage decreases when δ goes from -10 dB until -6 dB as the number of selected relays for the UNSR-ℓ_1 and LNSR-ℓ_1 techniques also decreases. However, for small values of δ (form around -18 dB to -14 dB), the average number of selected relays for the LNSR-ℓ_1 technique saturates at $k_{max} = 16$, forcing the LNSR-ℓ_1 technique to drop the relay re-usage percentage to avoid the SI and maintain an acceptable BER performance.

3.5. Chapter Summary

This chapter presented a novel multiple relay selection and beamforming techniques by solving sparsity inducing optimization problems. The proposed multiple relay selection and beamforming approaches enhance the overall system performance in terms of BER when compared with single relay selection strategies. Results such as the average number of selected relays or the relay re-usage percentage gave more insights on the proposed techniques. Although the work did not consider the effects of IRI, the performance of such setups is of interest as it highlights the advantages of using such an approach at the special case of having no IRI. The next chapter presents novel DSP algorithms that perform efficient signal equalization at the receiver.

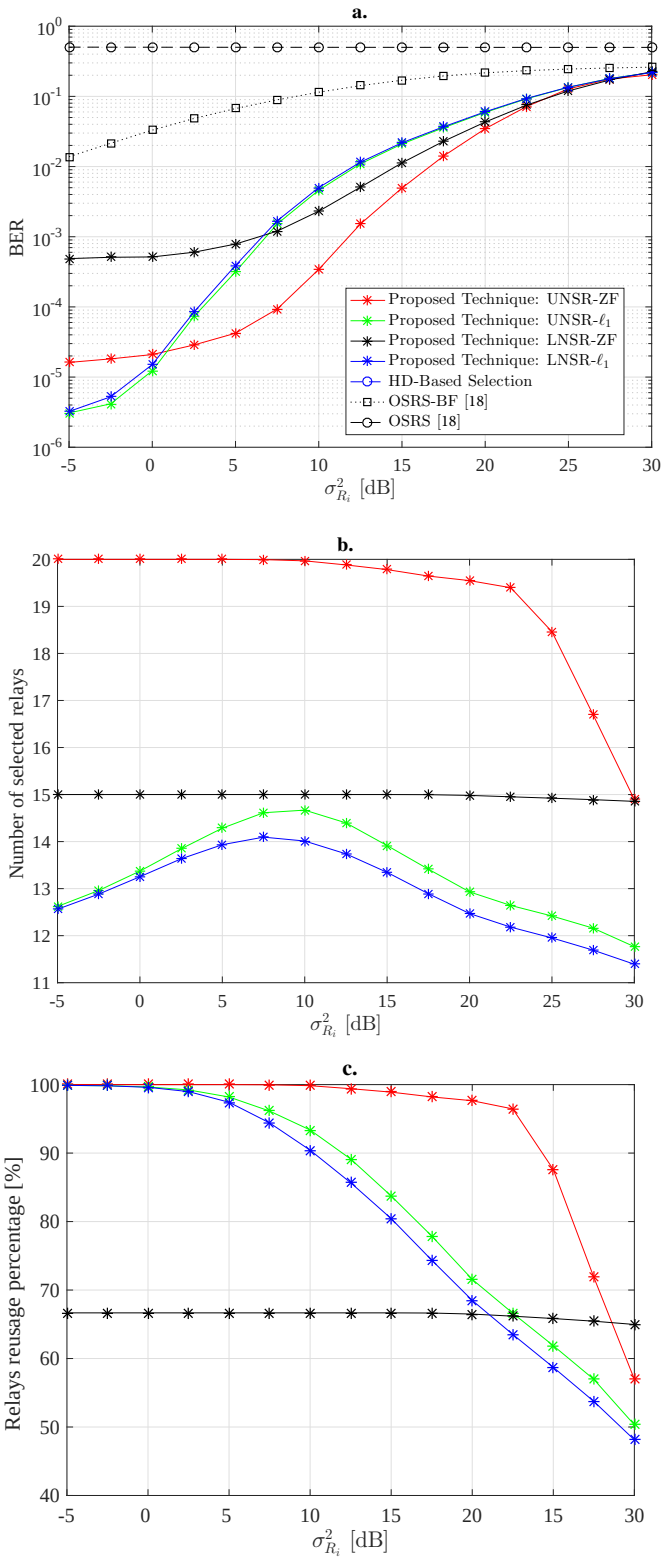

Figure 3.3: The behavior of different relaying strategies as a function of $\sigma^2_{R_i}$: **a**. Average BER vs. $\sigma^2_{R_i}$. **b**. Average number of selected relays vs. $\sigma^2_{R_i}$. **c**. Average relay re-usage percentage vs. $\sigma^2_{R_i}$.

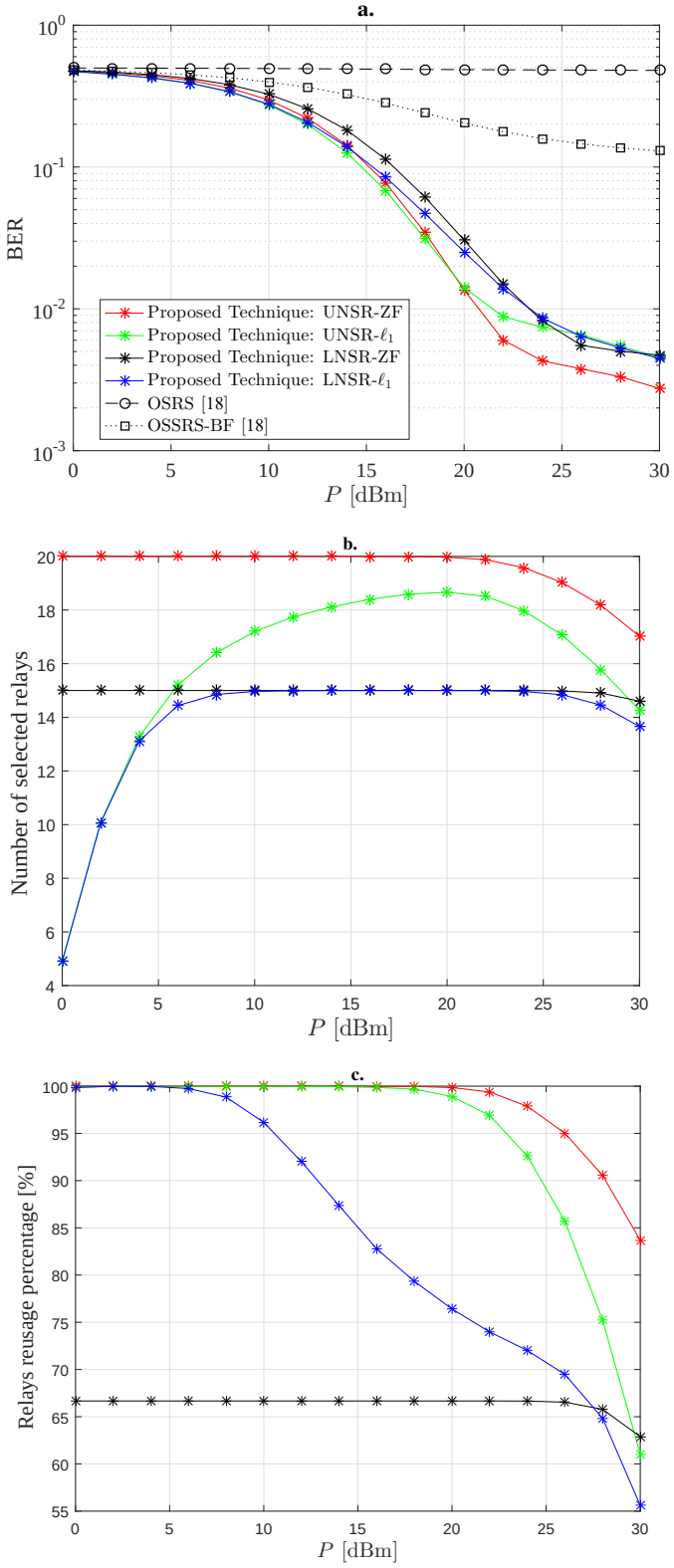

Figure 3.4: The behavior of different relaying strategies as a function of P: **a**. Average BER vs. P. **b**. Average number of selected relays vs. P. **c**. Average relay re-usage percentage vs. P.

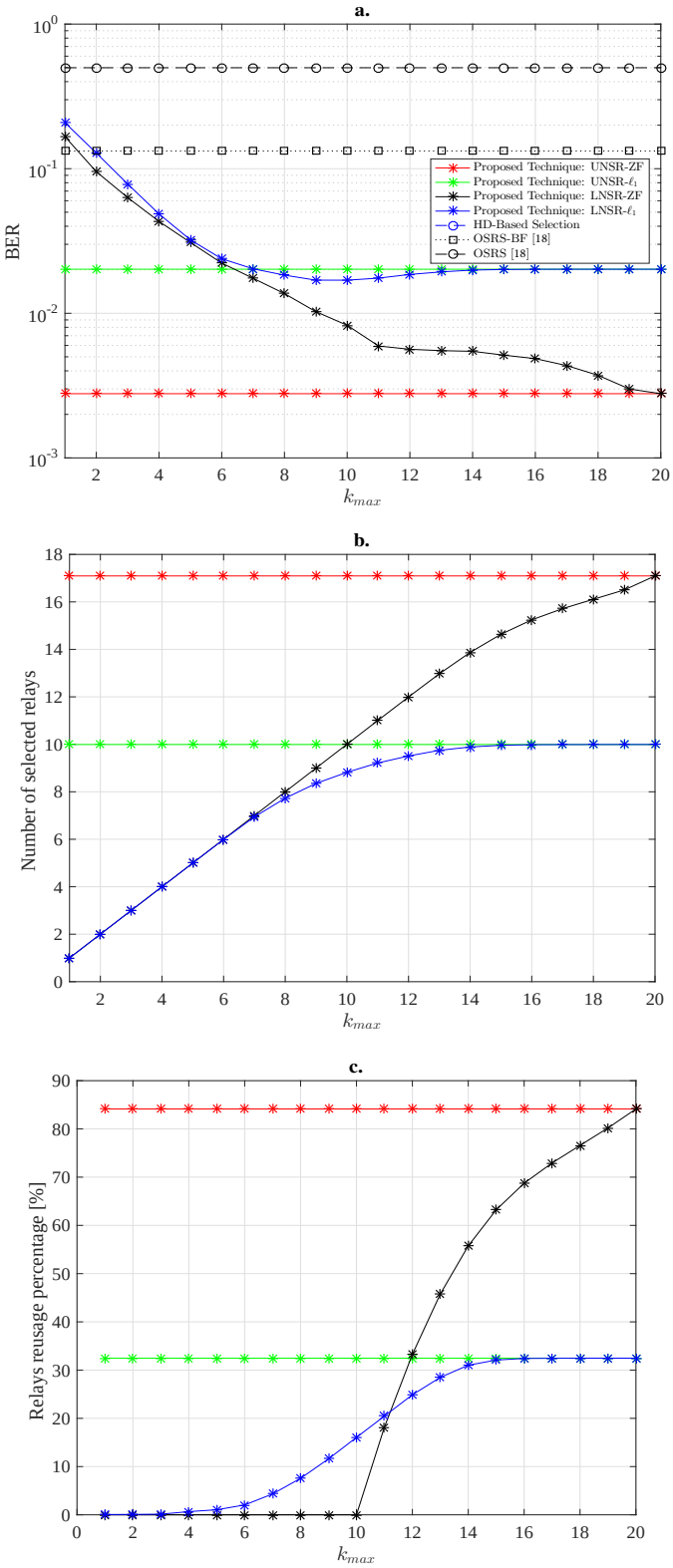

Figure 3.5: The behavior of different relaying strategies as a function of k_{max}: **a**. Average BER vs. k_{max}. **b**. Average number of selected relays vs. k_{max}. **c**. Average relay re-usage percentage vs. k_{max}.

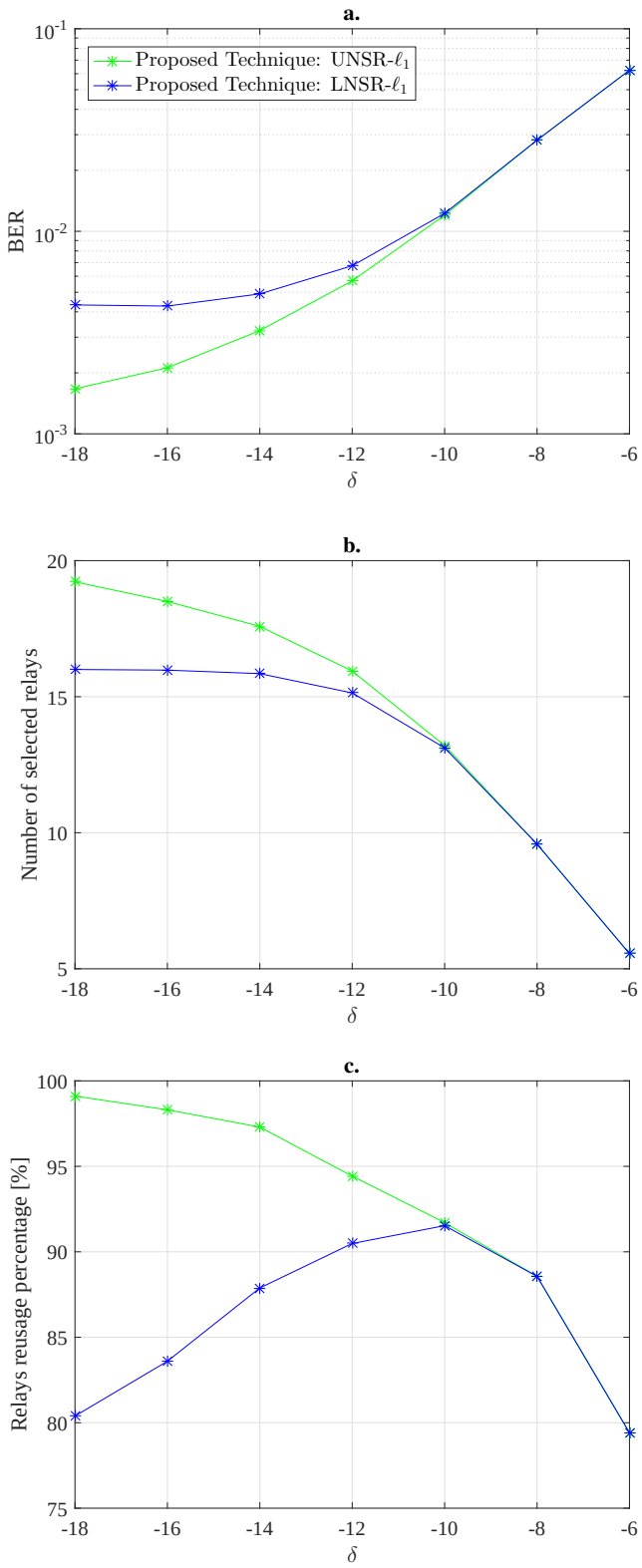

Figure 3.6: The behavior of the proposed UNSR-ℓ_1 and LNSR-ℓ_1 relay selection techniques as a function of δ: **a**. Average BER vs. δ. **b**. Average number of selected relays vs. δ. **c**. Average relay re-usage percentage vs. δ.

CHAPTER 4: SPARSE EQUALIZERS DESIGN FOR EFFICIENT OFDM DETECTION

The previous chapters discussed in details the possibility of using FD transceivers to improve the spectral efficiency of wireless systems at the physical layer, either by analysis (Chapter 2) or by designing methods and algorithms (Chapter 3) to exploit the FD technology as much as possible. Moreover, one of the goals of the designers of modern wireless communication standards and apparatus is energy efficiency [73]. As previously mentioned, OFDM presented and still presents an attractive choice for exchanging signals due its resilience with respect to the effects of wireless communication channels and the simplicity of its equalizer design. This simplicity is however jeopardized when other interferences are considered [51]. This chapter focuses on designing efficient signal equalizers when the multipath channel effect is no longer the main contributor to the OFDM signal's distortion. The efficiency is achieved by adopting sparse equalizers, which are realized by exploiting the sparsity of the overall interference and channel effects. The details of this contribution are presented below.

4.1. Sparse Equalization for OFDM Signals with Insufficient Cyclic Prefix

This section presents in details the design of adaptive sparse equalizers affected by the interferences induced by the use of an insufficient CP. The equalizers are shown to yield an acceptable performance even though a reduced number of taps are used in the equalization process. The sparse equalizers are realized by approximating the dense optimal equalizers with a sparse equalizer using well-known greedy algorithms. More details are discussed in the next section.

4.1.1. System Model

A single-input single-output OFDM system with N OFDM subcarriers is considered. The transmitted data symbols are assumed to be independent and the channel is assumed to be known and static at least over one OFDM symbol. Due to the insertion

of a short-lengthed (insufficient) CP, the received signal $\mathbf{y}_t \in \mathbb{C}^{N\times 1}$ at time t is impaired by ICI and ISI, and can be expressed by writing

$$\mathbf{y}_t = \mathbf{H}\mathbf{x}_t - \mathbf{A}\mathbf{x}_t + \mathbf{B}\mathbf{x}_{t-1} + \mathbf{n}_t, \tag{4.1}$$

where $\mathbf{x}_t \in \mathbb{C}^{N\times 1}$ is the data vector with $\mathbb{E}\{\mathbf{x}_t\mathbf{x}_t^H\} = \sigma_x^2\mathbf{I}_N$, and $\mathbf{x}_t \perp \mathbf{x}_{t-1}$. Further, $\mathbf{H} \in \mathbb{C}^{N\times N}$ is the time-domain circulant channel matrix where its first column is the zero-padded CIR, and L denotes the number of CIR taps. The matrices $\mathbf{A} \in \mathbb{C}^{N\times N}$ and $\mathbf{B} \in \mathbb{C}^{N\times N}$, respectively, represent the ICI and ISI effects [37]. The length of the CP is denoted by v, where the matrices $\mathbf{A}$ and $\mathbf{B}$ are non-zero matrices if and only if $v < L$, in which case they can be written as

$$\mathbf{A} = \begin{bmatrix} 0 & \cdots & h_{L-1} & \cdots & \cdots & h_{v+1} & 0 & \cdots & 0 \\ 0 & \cdots & 0 & h_{L-1} & \cdots & h_{v+2} & 0 & \cdots & 0 \\ \vdots & \ddots & \vdots & 0 & \ddots & \vdots & \vdots & \ddots & \vdots \\ 0 & \cdots & 0 & \cdots & 0 & h_{L-1} & 0 & \cdots & 0 \\ 0 & \cdots & 0 & \cdots & 0 & 0 & 0 & \cdots & 0 \\ \vdots & \ddots & \vdots & \ddots & \vdots & \vdots & \vdots & \ddots & \vdots \\ 0 & \cdots & 0 & \cdots & 0 & 0 & 0 & \cdots & 0 \end{bmatrix}, \tag{4.2}$$

and

$$\mathbf{B} = \begin{bmatrix} 0 & \cdots & 0 & h_{L-1} & \cdots & \cdots & h_{v+1} \\ 0 & \cdots & 0 & 0 & h_{L-1} & \cdots & h_{v+2} \\ \vdots & \ddots & \vdots & \ddots & 0 & \ddots & \vdots \\ 0 & \cdots & 0 & \cdots & 0 & 0 & h_{L-1} \\ 0 & \cdots & 0 & \cdots & \cdots & 0 & 0 \\ \vdots & \ddots & \vdots & \ddots & \vdots & \ddots & \vdots \\ 0 & \cdots & 0 & \cdots & \cdots & 0 & 0 \end{bmatrix}. \tag{4.3}$$

It is worth noting that the first term of the right hand side in (4.1) represents the desired signals, while the second and third terms capture the effect of both ICI and ISI, respectively. If $v \geq L$, $\mathbf{A}$ and $\mathbf{B}$ are zero matrices, and hence neither ICI nor ISI exist. However, if the CP length is insufficient, the residual ISI of length equal to $(L - v)$ induces ICI within the current symbol and ISI from the previous symbol and hence, the orthogonality between the different OFDM subcarriers will be lost. Since ISI and ICI may severely downgrade the OFDM performance, an equalization process is needed to counteract these interference effects when the CP is insufficient. Last but not least, $\mathbf{n}_t$ represents the receiver's zero-mean AWGN with $\mathbb{E}[\mathbf{n}_t \mathbf{n}_t^H] = \sigma_n^2 \mathbf{I}_N$ and $\mathbf{n}_t \perp \mathbf{x}_t \perp \mathbf{x}_{t-1}$.

4.1.2. Problem Formulation

In this section, various techniques of reduced-complexity equalizer designs to mitigate the effects of ISI and ICI at the OFDM receiver are presented. The optimization problems that are used in the design of the proposed reduced-complexity sparse linear MMSE and DFE equalizers are first formulated. Further, the complexity of the introduced approach is compared with well-known conventional equalizer designs and it is shown that the proposed equalizer can be designed with a lower complexity when compared to them. Finally, a method to verify the reliability of the proposed equalizers is introduced.

4.1.3. Linear Equalizer Design

To combat the effects of ICI and ISI, the received signal is passed through an $N \times N$ linear MMSE equalizer matrix denoted by $\mathbf{E}_{LE}$. Thus, the compensated received signal can be written as follows

$$\begin{aligned} \hat{\mathbf{x}}_t^{LE} &= \mathbf{E}_{LE}\, \mathbf{y}_t^{LE}, \\ &= \mathbf{E}_{LE} \underbrace{(\mathbf{H} - \mathbf{A})}_{\stackrel{def}{=}\mathbf{G}} \mathbf{x}_t + \mathbf{E}_{LE}\mathbf{B}\mathbf{x}_{t-1} + \mathbf{E}_{LE}\mathbf{n}_t. \end{aligned} \tag{4.4}$$

Defining the error vector as $\mathbf{v}_{LE} = \hat{\mathbf{x}}_t^{LE} - \mathbf{x}_t$, the MSE is computed by evaluating $\mathbb{E}_{LE}\{\mathbf{v}_{LE}\mathbf{v}_{LE}^H\}$. By exploiting the linearity of the trace and the expectation operators, the MSE can be expressed as

$$\begin{aligned}\text{MSE}_{LE} \overset{def}{=} \sigma_{e,LE}^2 = \sigma_x^2 \text{Tr}\Big(&\mathbf{E}_{LE}\mathbf{G}\mathbf{G}^H\mathbf{E}_{LE}^H - \mathbf{G}^H\mathbf{E}_{LE}^H \\ &- \mathbf{E}_{LE}\mathbf{G} + \mathbf{E}_{LE}\mathbf{B}\mathbf{B}^H\mathbf{E}_{LE}^H + \gamma^{-1}\mathbf{E}_{LE}\mathbf{E}_{LE}^H + \mathbf{I}_N\Big),\end{aligned} \tag{4.5}$$

where $\gamma \overset{def}{=} \frac{\sigma_x^2}{\sigma_n^2}$. Using the property $\text{Tr}(\mathbf{XY}) = \text{vec}(\mathbf{X}^H)^H\text{vec}(\mathbf{Y})$, (4.5) can be written as follows

$$\begin{aligned}\sigma_{e,LE}^2 &= \sigma_x^2 \text{Tr}\Big(\mathbf{E}_{LE}\underbrace{(\mathbf{G}\mathbf{G}^H + \mathbf{B}\mathbf{B}^H + \gamma^{-1}\mathbf{I}_N)}_{\overset{def}{=}\mathbf{R}_{LE}}\mathbf{E}_{LE}^H \\ &\quad - \mathbf{E}_{LE}\mathbf{G} - \mathbf{G}^H\mathbf{E}_{LE}^H + \mathbf{I}_N\Big), \\ &= \sigma_x^2\left(\mathbf{e}_{LE}^H\mathbb{R}_{LE}\mathbf{e}_{LE} - \mathbf{g}^H\mathbf{e}_{LE} - \mathbf{e}_{LE}^H\mathbf{g} + \mathbf{i}_{N^2}^H\mathbf{i}_{N^2}\right),\end{aligned} \tag{4.6}$$

where $\mathbf{g} = \text{vec}(\mathbf{G})$, $\mathbf{i} = \text{vec}(\mathbf{I}_N)$, $\mathbf{e}_{LE} = \text{vec}(\mathbf{E}_{LE}^H)$, $\mathbb{R}_{LE} = \mathbf{R}_{LE} \otimes \mathbf{I}_N$, and $\otimes$ denotes the Kroenecker product. Using the well know Cholesky's matrix factorization, which is applied by writing $\mathbb{R}_{LE} = \mathbb{L}\mathbb{L}_{LE}^H$, where $\mathbb{L}_{LE}$ is a lower triangular matrix. Hence,

$$\begin{aligned}\sigma_{e,LE}^2 = \sigma_x^2\Big(&\mathbf{e}_{LE}^H\mathbb{L}\mathbb{L}_{LE}^H\mathbf{e}_{LE} - \mathbf{g}^H\mathbb{L}_{LE}^{-H}\mathbb{L}_{LE}^H\mathbf{e}_{LE} - \\ &\mathbf{e}_{LE}^H\mathbb{L}_{LE}\mathbb{L}_{LE}^{-1}\mathbf{g} + \mathbf{i}_{N^2}^H\mathbf{i}_{N^2}\Big).\end{aligned} \tag{4.7}$$

By completing the square, the result is

$$\sigma_{e,LE}^2 = \underbrace{\sigma_x^2\left(N + \mathbf{g}^H\mathbb{L}_{LE}^{-H}\mathbb{L}_{LE}^{-1}\mathbf{g}\right)}_{\overset{def}{=}\sigma_{e,LE,min}^2} + \underbrace{\sigma_x^2\left(||\mathbb{L}_{LE}^H\mathbf{e}_{LE} - \mathbb{L}_{LE}^{-1}\mathbf{g}||_2^2\right)}_{\overset{def}{=}\sigma_{e,LE,exc}^2}. \tag{4.8}$$

Here, $\sigma_{e,LE,exc}^2$ is the only term in (4.8) that depends on $\mathbf{e}_{LE}$ and thus can be used to compute the sparse equalizer coefficients. In particular, $\sigma_{e,LE,exc}^2$ is used to control the sparsity level of the designed equalizer. For example, if $\sigma_{e,LE,exc}^2 = 0$, the excess error

(the second term in the right-hand side of (4.8)) will be zero and thus the equalizer is optimal yet not sparse (dense) and its design complexity is computationally demanding. On the other hand, allowing for some tolerable excess error will help reduce the implementation complexity at the cost of a performance loss. To achieve a desirable performance-complexity tradeoff, the following problem for the design of sparse linear equalizers is formulated

$$\hat{\mathbf{e}}_{LE} = \underset{\mathbf{e}_{LE}\in\mathbb{C}_{N^2\times 1}}{\operatorname{argmin}} \|\mathbf{e}_{LE}\|_0 \text{ s.t. } \sigma^2_{e,LE,exc} \leq \epsilon_{LE}, \tag{4.9}$$

where $\|\mathbf{e}_{LE}\|_0$ is the number of nonzero elements in its argument and ϵ_{LE} can be chosen as a function of the noise variance. To solve (4.9), a general approach presented in the sequel to sparsely design the linear equalizer such that the performance loss does not exceed a pre-specified tolerable limit is proposed.

4.1.4. Decision-Feedback Equalizer Design

To better combat the ISI and ICI effects, a weighted sum of past decisions are fed back to help cancel out the interferences they cause in the present signaling interval. Fig. 4.1 depicts a block diagram of the proposed sparse DFE equalizer. In the DFE model, the received signal for one OFDM symbol at time t can be modeled as [37]

$$\begin{aligned}\hat{\mathbf{x}}_t^{DFE} &= \mathbf{E}_{DFE}\left(\mathbf{y}_t^{DFE} - \mathbf{B}\mathbf{x}_{t-1}\right), \\ &= \mathbf{E}_{DFE}\mathbf{G}\mathbf{x}_t + \mathbf{E}_{DFE}\mathbf{n}_t.\end{aligned} \tag{4.10}$$

Note that in the above equation, the error which may be incurred from the previous symbol is subtracted first from the current symbol before the equalization process. The error vector is defined as $\mathbf{v}_{DFE} = \hat{\mathbf{x}}_t^{DFE} - \mathbf{x}_t$, and hence the MSE is computed by applying $\mathbb{E}\{\mathbf{v}_{DFE}\mathbf{v}_{DFE}^H\}$. To avoid cumbersome notations, the time index is dropped and

the MSE is further simplified to get

$$\begin{aligned}\text{MSE}_{DFE} \overset{def}{=} \sigma^2_{e,DFE} = \mathbb{E}_{DFE}\Big[\text{Tr}\Big(&\mathbf{E}_{DFE}\mathbf{G}\mathbf{x}\mathbf{x}^H\mathbf{G}^H{\mathbf{E}_{DFE}}^H \\ &- \mathbf{E}_{DFE}\mathbf{G}\mathbf{x}\mathbf{x}^H + \mathbf{E}_{DFE}\mathbf{n}\mathbf{n}^H{\mathbf{E}_{DFE}}^H \\ &- \mathbf{x}\mathbf{x}^H\mathbf{G}^H{\mathbf{E}_{DFE}}^H + \mathbf{x}\mathbf{x}^H\Big)\Big]. \end{aligned} \tag{4.11}$$

Exploiting the linearity of the expectation operator,

$$\begin{aligned}\sigma^2_{e,DFE} = \sigma^2_x\text{Tr}\Big(&\mathbf{E}_{DFE}\mathbf{G}\mathbf{G}^H{\mathbf{E}_{DFE}}^H - \\ &\mathbf{G}^H{\mathbf{E}_{DFE}}^H - \mathbf{E}_{DFE}\mathbf{G} + \gamma^{-1}\mathbf{E}_{DFE}{\mathbf{E}_{DFE}}^H + \mathbf{I}_N\Big). \end{aligned} \tag{4.12}$$

Following the same steps for the case of the LE, and setting $\mathbf{R}_{DFE} \overset{def}{=} \mathbf{G}\mathbf{G}^H + \gamma^{-1}\mathbf{I}_N = \mathbf{L}_{DFE}\mathbf{L}^H_{DFE}$, the MSE for the case of the DFE can be written as

$$\begin{aligned}\sigma^2_{e,DFE} = &\underbrace{\sigma^2_x\left(N + \mathbf{g}^H\mathbb{L}^{-H}_{DFE}\mathbb{L}^{-1}_{DFE}\mathbf{g}\right)}_{\overset{def}{=}\sigma^2_{e,DFE,min}} \\ &+ \underbrace{\sigma^2_x\left(||\mathbb{L}^H_{DFE}\mathbf{e}_{DFE} - \mathbb{L}^{-1}_{DFE}\mathbf{g}||^2_2\right)}_{\overset{def}{=}\sigma^2_{e,DFE,exc}}, \end{aligned} \tag{4.13}$$

where $\mathbb{R}_{DFE} = \mathbf{R}_{DFE} \otimes \mathbf{I}_N$ and $\mathbb{L}_{DFE} = \mathbf{L}_{DFE} \otimes \mathbf{I}_N$. $\sigma^2_{e,DFE,exc}$ is the only term in (4.13) that depends on $\mathbf{e}_{DFE}$ and thus can be used to compute the sparse equalizer coefficients. Specifically, the use of $\sigma^2_{e,DFE,exc}$ is suggessted to control how sparse is the designed DFE equalizer. Thus, for example, if $\sigma^2_{e,DFE,exc} = 0$, the excess error will be zero and thus the equalizer is optimal. However, the DFE is not sparse and its design complexity is computationally expensive. On the other hand, when allowing for some negligible excess error, the implementation complexity can be reduced at the cost of a tolerable loss in the system performance. To handle such performance-complexity tradeoff, an optimization problem for the design of sparse DFE equalizers is formulated as follows

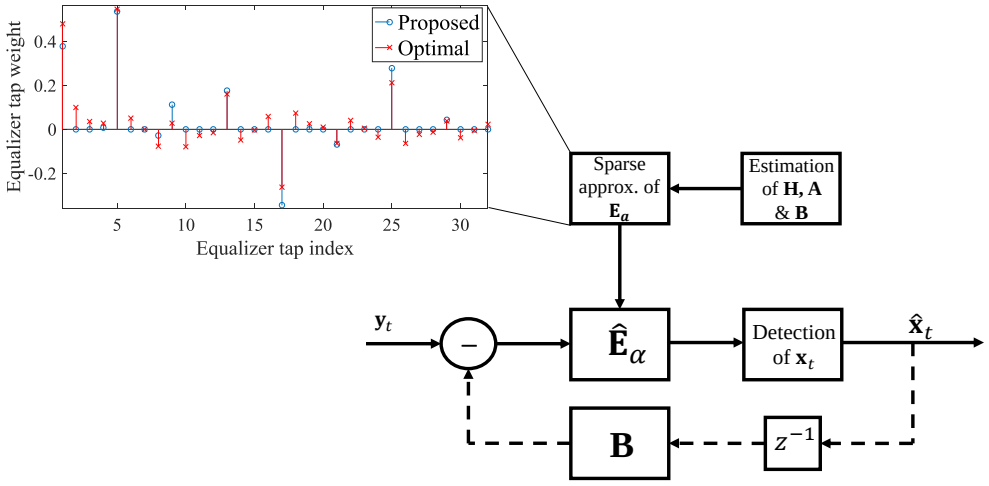

Figure 4.1: A schematic diagram illustrating the proposed system. The dashed line represents the feedback present in the case of using a DFE and absent in the case of using an LE approach.

$$\hat{\mathbf{e}}_{DFE} = \underset{\mathbf{e}_{DFE}\in\mathbb{C}_{N^2\times 1}}{\operatorname{argmin}} \|\mathbf{e}_{DFE}\|_0 \text{ s.t. } \sigma^2_{e,DFE,exc} \leq \epsilon_{DFE}, \tag{4.14}$$

where $\|\mathbf{e}_{DFE}\|_0$ is the number of nonzero elements in its argument and ϵ_{LE} can be chosen as a function of the noise variance. Next, a generalized approach to design a sparse DFE equalizer is presented.

4.1.5. Proposed Design Approach

The proposed sparse equalizer design approach is presented for both LEs and DFEs. The proposed design allows the flexibility of controlling the sparsity level of these equalizers, which can be controlled based on different criteria, namely the number of active entries of the equalizer and tolerable losses in the SINR or the data rate. The choice of the number of active entries in the equalizer matrix represents a performance-complexity tradeoff and further, under the formulation, the designer has a direct control on the desired number of the nonzero entries. The second choice is to design the equalizer such that the loss in the performance is upper bounded by a certain value. The

bound on the performance loss can be on either the data rate or the SINR. Thus, the following optimization problem is formulated

$$\hat{\mathbf{e}}_\alpha = \underset{\mathbf{e}_\alpha \in \mathbb{C}_{N^2\times 1}}{\operatorname{argmin}} \|\mathbf{e}_\alpha\|_0 \text{ s.t. } \sigma^2_{e,\alpha,exc} \leq \epsilon, \tag{4.15}$$

where $\alpha \in \{\textit{LE,DFE}\}$ and ϵ is a design parameter used to control the sparsity level of the equalizer. Clearly, this problem is not convex, and a relaxation can be performed to make it convex by substituting the ℓ_0-norm in (4.15) with the ℓ_1-norm. Under this relaxation, the above problem can be solved using any convex optimization solvers. However, besides its complexity, the resulting solution does not exactly yield zero entries in $\hat{\mathbf{e}}_\alpha$. Another approach is to use some of the available greedy algorithms, as for example the orthogonal-matching pursuit (OMP) algorithm [74], which is denoted by the function OMP(dictionary matrix, data vector, c), where c is a stopping criterion that can be set as the number of active entries in the equalizer matrix or a bound on the performance loss. This allows us to have a flexible stopping criterion depending on the constraints faced by the designer. Next, the decision-point average SINR for both linear and decision-feedback equalizers is defined. The decision-point SINR ζ_α can be written as

$$\begin{aligned}
\zeta_\alpha(\mathbf{e}_\alpha) &\overset{def}{=} \frac{\mathbb{E}[\text{Tr}(\mathbf{H}\mathbf{x}\mathbf{x}^H\mathbf{H}^H])}{\mathbb{E}[\mathbf{v}_\alpha^H\mathbf{v}_\alpha]}, \\
&= \frac{\mathbb{E}[\text{Tr}(\mathbf{x}\mathbf{x}^H])\mathbb{E}[\text{Tr}(\mathbf{H}^H\mathbf{H})]}{\mathbb{E}[\mathbf{v}_\alpha^H\mathbf{v}_\alpha]}, \\
&= \frac{||\mathbf{h}||_2^2\sigma_x^2}{\sigma^2_{e,\alpha,min} + \sigma^2_{e,\alpha exc}}, \\
&\overset{(a)}{\geq} \frac{||\mathbf{h}||_2^2\sigma_x^2}{\sigma^2_{e,\alpha,min} + \epsilon_{\text{SINR},\alpha}}, \\
&= \frac{\zeta_\alpha^{\max}(\mathbf{e}_\alpha)}{1 + \frac{\epsilon_{\text{SINR},\alpha}}{\sigma^2_{e,\alpha,min}}},
\end{aligned} \tag{4.16}$$

where $\epsilon_{\text{SINR},\alpha}$ is a design parameter, and $\sigma^2_{e,\alpha,exc} \leq \epsilon_{\text{SINR},\alpha}$, which is the reason behind the inequality in (a). In other words, $\epsilon_{\text{SINR},\alpha}$ is a performance penalty a designer is willing to afford for designing a reduced-complexity equalizer. The parameter $\epsilon_{\text{SINR},\alpha}$

will be used as an input to the OMP algorithm to determine the desired sparsity level of the equalizer. Further, $\psi_{\text{SINR},\alpha} \overset{def}{=} \frac{\zeta^{\max}_{max,\alpha}(\mathbf{e}_\alpha)}{\zeta_\alpha}$, where $\zeta_{max,\alpha}(\mathbf{e}_\alpha) \overset{def}{=} \frac{||\mathbf{h}||_2^2\sigma_x^2}{\sigma^2_{e,min,\alpha}}$. Then, the performance loss is quantified by $\psi_{\text{SINR},\alpha}$ (in dB), i.e.,

$$\begin{aligned}\psi_{\text{SINR},\alpha} &= 10\log_{10}\left(\frac{\zeta^{\max}_{\alpha}(\mathbf{e}_{opt})}{\zeta_\alpha(\mathbf{e}_\alpha)}\right), \\ &\leq 10\log_{10}\left(1+\frac{\epsilon_{\text{SINR},\alpha}}{\sigma^2_{e,\alpha,min}}\right) \overset{def}{=} \psi^{\max}_{\text{SINR},\alpha}. \end{aligned} \tag{4.17}$$

Then, $\epsilon_{\text{SINR},\alpha}$ is computed based on an acceptable value for $\psi^{\max}_{\text{SINR},\alpha}$ and compute the sparse solution $\mathbf{e}_\alpha$ accordingly from equation (4.15).

Now, the losses in the data rate resulting from the sparse approximation of the optimal equalizer solution is quantified. As previously discussed, the insertion of a CP results in a loss of the bandwidth efficiency. To overcome this problem, one can use a CP of insufficient length and rectify the effects of the ISI and ICI by employing an equalizer at the receiver side, which could be an LE or a DFE. Therefore, the rate gains resulting from reducing the CP length after the sparse approximation of the optimal equalizer are analyzed.

The average data rate of one OFDM symbol is defined by R_α, after equalization, as follows

$$\begin{aligned} R_\alpha &= \delta\mathbb{E}\left\{\log_2\left(1+\frac{\text{Tr}(\mathbf{H}\mathbf{x}\mathbf{x}^H\mathbf{H}^H])}{\mathbf{v}_\alpha^H\mathbf{v}_\alpha}\right)\right\}, \\ &\overset{(b)}{\leq} \delta\log_2\left(1+\zeta_\alpha\right), \\ &\overset{(c)}{\approx} \underbrace{\delta\log_2\left(\frac{||\mathbf{h}||_2^2\sigma_x^2}{\sigma^2_{e,\alpha,min}}\right)}_{R_{max,\alpha}} - \delta\log_2\left(1+\frac{\sigma^2_{e,\alpha,exc}}{\sigma^2_{e,\alpha,min}}\right), \end{aligned} \tag{4.18}$$

where the inequality in (b) follows from Jensen's inequality and the approximation in (c) is valid under the assumption that the system operates in the high SNR regime, $\delta = \Delta f\frac{N}{N+v}$, where Δf denotes the subcarrier spacing. In (4.17), a design control parameter is defined, which is a function of $\psi_{\text{SINR},\alpha}$ that controls the amount of SINR loss. Another design parameter is now defined, which is denoted by $\epsilon_{\text{Rate},\alpha}$. This control

parameter is a function of the rate loss, i.e., $\psi_{\text{Rate},\alpha}$. Next, after some straight-forward manipulations, $\epsilon_{\text{Rate},\alpha}$ can be written as

$$\epsilon_{\text{Rate},\alpha} \geq \left(2^{\frac{\psi_{\text{Rate},\alpha}}{\delta}} - 1\right) \sigma^2_{e,\alpha,min}, \tag{4.19}$$

where $\psi_{\text{Rate},\alpha} \stackrel{def}{=} R_{max,\alpha} - R_\alpha$.

To this end, it was shown that the problem of designing sparse LEs and DFEs matrix entries can be cast into a sparse approximation of a vector by a fixed matrix. The general form of this problem is given by (4.15). In order to solve this problem, any greedy algorithm can be used to determine the locations and weights of the equalizer matrix entries. Here, for simplicity, the well-known OMP greedy algorithm [74] is used, which estimates $\mathbf{e}_\alpha$ by iteratively selecting a set, e.g., S, of the dictionary matrix columns that are most correlated with the data vector and then solving a restricted least-squares problem using the selected columns. Then, after properly selecting the equalizer design constraint, $\mathbf{e}_\alpha$ can be relaized by applying any one of the following functions

$$\mathbf{e}_\alpha = \text{OMP}\left(\mathbb{L}_\alpha^H, \mathbb{L}_\alpha^{-1}\mathbf{g}, \lceil p \times N^2 \rceil\right), \tag{4.20}$$

$$\mathbf{e}_\alpha = \text{OMP}\left(\mathbb{L}_\alpha^H, \mathbb{L}_\alpha^{-1}\mathbf{g}, \epsilon_{\text{SINR},\alpha}\right), \tag{4.21}$$

or

$$\mathbf{e}_\alpha = \text{OMP}\left(\mathbb{L}_\alpha^H, \mathbb{L}_\alpha^{-1}\mathbf{g}, \epsilon_{\text{Rate},\alpha}\right), \tag{4.22}$$

where p is a parameter that defines the desired percentage of active entries in $\mathbf{e}_\alpha$. Recall that $\mathbb{L}_\alpha^H$ is the dictionary matrix, $\mathbb{L}_\alpha^{-1}\mathbf{g}$ is the data vector that is used to estimate $\mathbf{e}_\alpha$, and the final argument c can be a condition on the number of active entries in the equalizer matrix ($\lceil p \times N^2 \rceil$), an upper-bound of the SINR losses ($\epsilon_{\text{SINR},\alpha}$), or a predefined limit on the data rate ($\epsilon_{\text{Rate},\alpha}$). Algorithm 3 presents the steps of the OMP algorithm required to provide the sparse equalizer matrix $\mathbf{e}_\alpha$ when the design is restricted by the number of active entries. This algorithm was described in details in [74]. In line number 3,

Algorithm 3: OMP Algorithm

Input: Matrix $\mathbb{L}_{\alpha}^{H}$, vector $\mathbb{L}_{\alpha}^{-1}\mathbf{g}$, scalar $\beta = \lceil p \times N^2 \rceil$

Output: Vector $\mathbf{e}_{\alpha}$

Initialize: $S = [\,]$; $j = 1$; $I \in \{1, \ldots, N^2\}$; $\hat{\mathbf{e}}_{\alpha}^{H} = \mathbf{0}_{N^2 \times 1}$; $\mathbf{t} = [\,]$**;**

while ($j \leq \beta$)

  $\bar{S} = S \triangle I$**;**

  $k =$ **argmax**$(|\mathbb{L}_{\alpha}^{H}(:, \bar{S})\mathbb{L}_{\alpha}^{-1}\mathbf{g}|)$;

  $S = S \cup k$**;**

  $\mathbf{t} = \mathbb{L}_{\alpha}^{-H}(:, S)\mathbb{L}_{\alpha}^{-1}\mathbf{g}$**;**

  $j = j + 1$**;**

end

$\mathbf{e}_{\alpha}(S) = \mathbf{t}$**;**

$\triangle$ represents the disjunctive union symbol. Extending Algorithm 1 to encompass the performance loss restrictions presented above is straight-forward.

It is worth noting that the analysis of the MSE described above that will be used in the realization of the proposed sparse equalizer can be done in a different way. It has been shown in [37] that, while satisfying the orthogonality principle that results in the realization of the optimal equalizer, the following is written

$$\mathbf{G} - \mathbf{R}_{\alpha}\mathbf{E}_{\alpha}^{H} = \mathbf{0}_{N \times N}, \tag{4.23}$$

or

$$\mathbf{g} - \mathbb{R}_{\alpha} \otimes \mathbf{e}_{\alpha}^{H} = \mathbf{0}_{N^2 \times 1}. \tag{4.24}$$

Therefore, the sparsifying dictionary matrix is no more a decomposed lower-triangular matrix constructed by the Cholesky factorization technique. Furthermore, it has been

shown in [46] that the Cholesky factorization written in e.g. (4.7) outperforms the approach in (4.24). Therefore, the study focuses on the Cholesky factorization based technique.

This section is concluded by noting that several equalization structures follow as special cases of the general design approach presented here including:

- The one-tap frequency-domain equalizer where a sufficient CP is considered. The equalizer is realized by taking the FFT of the time domain channel response while setting the sparsity level to zero, i.e., $p = 0$, then scaling each OFDM subcarrier by a single tap.
- For any v, the optimal equalizer in the MMSE sense can be considered as a special case of the proposed design by fully equalizing the effects of the ISI and ICI.
- In the DFE setup, the ZF equalizer can also be generated as a special case of the proposed approach when the SNR tends to infinity.

4.1.6. Computational Complexity

Here, the orders of the complexities of some conventional equalizers are compared with the proposed equalizer design approach. For both cases of linear and decision-feedback equalizers, it has been shown in [37] that a ZF equalizer can be constructed by applying

$$\mathbf{E}_{ZF} = \mathbf{G}^{-1} = (\mathbf{H} - \mathbf{A})^{-1}. \tag{4.25}$$

To invert the matrix in (4.25), the computational complexity is of the order of $\mathcal{O}(N^3)$ [75]. The channel matrix $\mathbf{H}$ can be inverted by applying $\mathbf{H}^{-1} = \mathbf{F}^H \bar{\mathbf{H}}^{-1} \mathbf{F}$, where $\mathbf{F}$ is the unitary FFT matrix and $\bar{\mathbf{H}}$ is a diagonal matrix where its diagonal entries represent the frequency response of the wireless channel. However, $\mathbf{A}$ is singular and inverting it is not possible. However, inverting $\mathbf{G}$ without inverting $\mathbf{A}$ is possible using a modified version of the Woodbury formula reported in [76], where it shows that it is possible to

write

$$(\mathbf{H}-\mathbf{A})^{-1}=\mathbf{H}^{-1}+\underbrace{(\mathbf{I}_N-\mathbf{H}^{-1}\mathbf{A})^{-1}}_{\mathbf{\Lambda}}\mathbf{H}^{-1}\mathbf{A}\mathbf{H}^{-1}, \tag{4.26}$$

and to compute $\mathbf{\Lambda}$, the Newman series approximation is used, which states that [77]

$$\mathbf{\Lambda}=\sum_{n=0}^{\infty}(\mathbf{H}^{-1}\mathbf{A})^n, \text{ iff } \rho(\mathbf{H}^{-1}\mathbf{A})<1, \tag{4.27}$$

where $\rho(.)$ denotes the spectral norm function, i.e. the maximum eigenvalue of the matrix $\mathbf{H}^{-1}\mathbf{A}$. Hence, $\mathbf{G}$ can be inverted while just having to invert $\mathbf{H}$, which involves the eigen-decomposition of $\mathbf{H}$ requiring the computation complexity of $\mathcal{O}(Nlog(N))$. However, the condition in (4.27) cannot be guaranteed since the application involves dealing with random matrices that result in random values of the spectral norm. Further, even if the condition $\rho(\mathbf{H}^{-1}\mathbf{A})<1$ is satisfied, using Woodbury's formula will actually increase the complexity of realizing $\mathbf{E}_{ZF}$ since n in (4.27) might be large to give satisfactory results.

With respect to the optimal MMSE equalizer design, it requires the inversion of $\mathbf{R}_\alpha$, which also costs an order of $\mathcal{O}(N^3)$ operations. However, the proposed sparse equalizer can be realized through the OMP algorithm with a complexity of $\mathcal{O}\left(N^2W\right)$, where $1\leq W\leq N$, depending on how sparse is the proposed equalizer. For the sake of comparison, the proposed sparse equalizer is compared with another sparse equalizer which is refered to as the *"significant entries"* equalizer. The significant entries equalizer is constructed by thresholding the optimal equalizer (in the MMSE sense) in terms of the maximum absolute values of the equalizer entries. The number of entries depends on how many of the active entries are needed (which determines the sparsity level of the equalizer accordingly). However, the optimal MMSE equalizer needs to be computed first to estimate the significant entries of the equalizer. Hence, to design an equalizer based on the significant entries approach, $\mathcal{O}(N^3)$ computations are needed. The complexity comparisons for the proposed method and some other approaches are summarized in Table 4.1.

Table 4.1: Comparison Between The Order of The Complexities of The Proposed Equalizer Designs to Some Other Selected Equalizers.

Equalizer Type	Design Complexity
Conventional MMSE Equalizer	$\mathcal{O}(N^3)$
Significant-entries Equalizer	$\mathcal{O}(N^3)$
ZF Equalizer	$\mathcal{O}(N^3)$
Proposed Equalizer	$\mathcal{O}(N^2W)$

4.1.7. Worst-case Coherence Analysis

A useful metric to evaluate the performance of the proposed equalizer is the WCC metric. The WCC operator, which is denoted by $\mu(.)$, can be written as [46, 47]

$$\mu(\mathbf{R}_\alpha) = \max_{i \neq j} \frac{|\langle \mathbf{R}_\alpha(i), \mathbf{R}_\alpha(j) \rangle|}{||\mathbf{R}_\alpha(i)||_2 ||\mathbf{R}_\alpha(j)||_2}. \tag{4.28}$$

where $\langle ., . \rangle$ denotes the inner product operator. The normalization in (4.28) sets $\mu(\mathbf{R}_\alpha)$ to be in the range [0,1]. A lower $\mu(\mathbf{R}_\alpha)$ implies that the OMP algorithm will likely recover the equalizer entries. More discussion about the WCC metric can be found in e.g. [46, 47]. Further, it is worth noting that other metrics, which are similar to the WCC metric, have been studied in the literature as in e.g. [78]. The metric that has been studied there was the MEC metric since it is easier to analyze. However, the WCC presents the worst-case-scenario performance of the dictionary matrix's coherence, and thus was selected to be included in the simulation studies instead of the MEC. In the sequel, the results of the WCC simulations are discussed for the cases of LE and DFE equalizers, and will show that a Cholesky factorization approach to design the dictio-

Table 4.2: Values of The Parameters Used in The Simulations.

Parameter	Value
Number of Subcarriers	128
Subcarrier Spacing	10.94 KHz
CP Length	16
Subcarrier Modulation	16-QAM
OFDM Symbol Time	102.83 μs
OFDM Symbol Time (Useful)	91.41 μs

nary matrix will yield better results when compared with selecting $\mathbf{R}_\alpha$ as the dictionary matrix. Next, the results of the numerical experiments are presented to evaluate the performance of the proposed designs considering both LE and DFE equalizers.

4.1.8. Numerical Results

In the simulations, the OFDM-based IEEE 802.16 Mobile WiMax standard described in [79] is used where the key IEEE 802.16 standard parameters are shown in Table 4.2. Furthermore, an equal tap channel (ETC) model [80] is used where the channel is composed of 4 taps with normalized delays of $(0, 4, 8, 12)$ samples and an average gain of 0.25 for each tap, where each tap is generated as a complex independent Gaussian random variable. Further, coded OFDM using a convolutional encoder $[133, 171]$ with a rate of $1/2$ and a constraint length of 7 is adopted. At the receiver, a Viterbi decoder is used with hard decision decoding. In the simulation settings, the vector $\mathbb{L}_\alpha^{-1}\mathbf{g}$ is segmented into N vectors, and then the OMP algorithm is applied in a parallel fashion. This was performed to further reduce the computational time since N in the simulations is set to 128, which will make the data vector's size to be 16384.

This increase in dimension (from N to N^2) consumes larger memory and increases the simulation time. Thus, parallelization helps reduce the simulation time.

Throughout the simulations, the proposed OMP-based equalizer designs are compared with the significant-entries (Sig. entries) equalizer, Sufficient CP based design and ZF equalizer. The proposed equalizer design approach is further compared with the optimal MMSE equalizer defined as $\mathbf{E}_{MMSE} = \mathbf{G}^H\mathbf{R}^{-H}$[37]. Note that the optimal equalizer follows as a special case of the approach by setting the excess losses to zero, i.e., full equalization with 100% active taps. The Sufficient CP equalizer (when $L \leq v$) and the optimal MMSE equalizer can be considered as benchmarks for the comparative study. The OMP algorithm is applied to the MMSE-DFE case since, as it will be shown in the results, the MMSE-DFE equalizer performs the closest to the Sufficient CP based design, and generally it is aimed at performing as close as possible to the Sufficient CP based design while reducing the complexity of realizing the equalizer.

First, the effect of the sparse equalizer designs on the performance is studied, where the percentage of the active entries (i.e, entries with nonzero weights) of the total equalizer length N^2 is ploted versus the maximum SINR loss. In Fig. 4.2, it is clear that the proposed approach requires far less active entries when compared with the Sig. entries based design for different received SNR values, and far less active entries are required when more performance loss is tolerated. As expected, the higher the received SNR, a higher number of active entries is needed in order to cancel the effects of the ISI and ICI.

In Fig. 4.3, the coded BER is plotted for a varying received SNR and a CP of length 2, i.e., $v = 2$. The best performance of all tested methods in terms of coded BER is the OFDM system deploying sufficient CP, followed by the optimal MMSE equalizer (full equalization with 100%). Thresholding based techniques such as the Sig. entries approach does not perform well as it fails to choose the best entries that cancel-out the effects of ISI and ICI. This means that relying only on the largest magnitudes to select the equalizer entries and ignoring its phase components deteriorates the performance

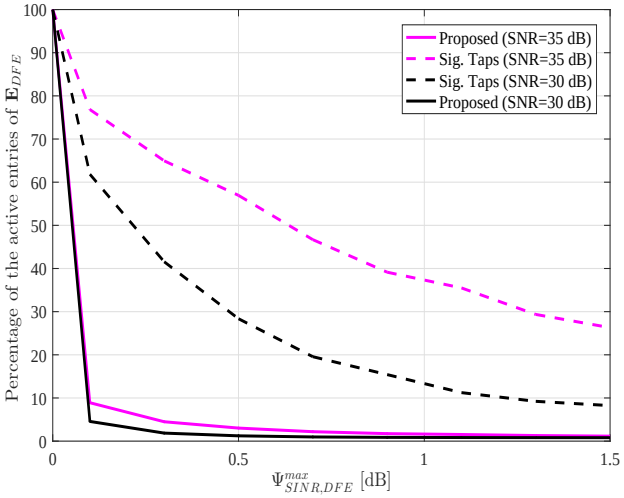

Figure 4.2: Percentage of the active entries of the equalizer matrix (p) vs. the loss in SNR in dB for different received SNR. In this case, v=8.

of the equalizer when the receiver AWGN is negligible. Also, both ZF and MMSE LEs perform much worse than the ZF and MMSE DFEs. In Fig. 4.4, the coded BER is plotted against the percentage of the active number of entries of the Sig. entries and the proposed equalizers. As it can be seen from the figure, the proposed equalizer converges fast to the optimal equalizer's BER as p increases, where it almost performs as well as the optimal equalizer with only 40% of its taps being active.

In Fig. 4.5, the average WCC is plotted for different values of the received SNR when $v = 8$. The WCC of $\mathbb{L}_{LE}$, $\mathbb{L}_{DFE}$, $\mathbb{R}_{LE}$ and $\mathbb{R}_{DFE}$ are investigated. It is noted that $\mu(\mathbf{L}_{DFE}) = \mu(\mathbf{I}_N \otimes \mathbf{L}_{DFE})$. Furthermore, $\mu(\mathbb{R}_\alpha)$ and $\mu(\mathbb{L}_\alpha)$ are below 1 which reflects the high likelihood of the proposed approach to estimate the non-zero entries perfectly. It is noticed that the WCC of all selected dictionary matrices saturate at high SNR as the coherence becomes independent of the SNR. On the other hand, at low SNR, the noise dominates over the channel taps and therefore the dictionary matrices become close to identity matrices which, hence, have almost zero WCC. Furthermore, interestingly, the WCC for the LE and the DFE are almost identical.

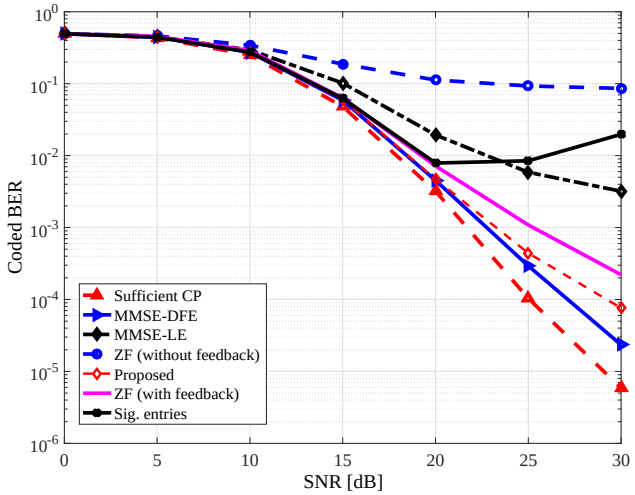

Figure 4.3: Coded BER vs. the received SNR for $v = 2$ when different types of equalizers are implemented.

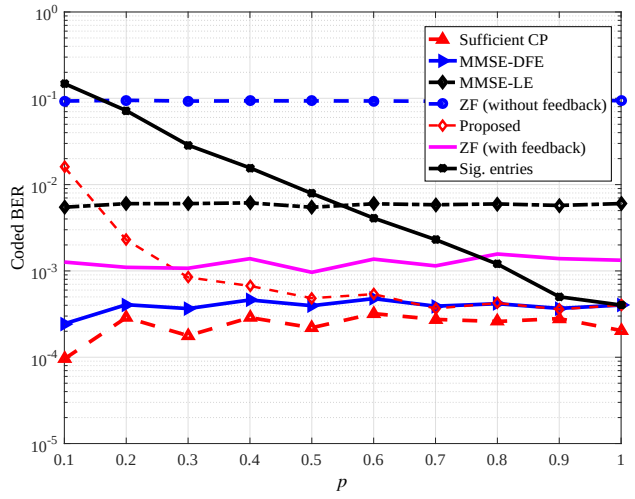

Figure 4.4: Coded BER vs p with $v = 2$ and a received SNR of 25 dB for different types of equalizers.

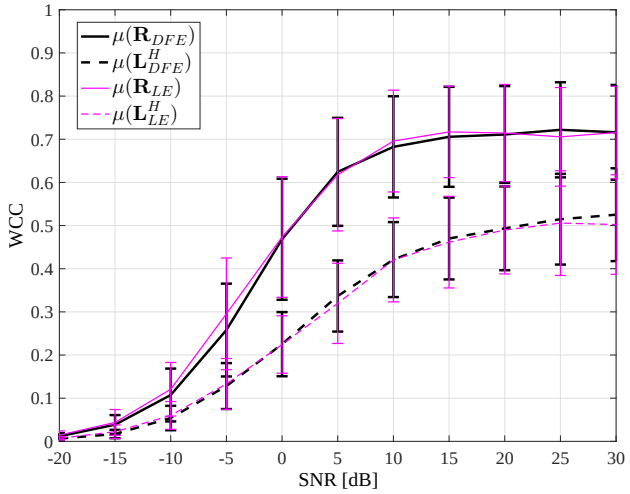

Figure 4.5: WCC vs the received SNR with $v = 8$.

Moreover, to shed some light on the behavior of the WCC when v is varied, Fig. 4.6 depicts the effect of decreasing v on $\mu(\mathbb{R}_{DFE})$, $\mu(\mathbb{L}_{DFE})$, $\mu(\mathbb{R}_{LE})$ and $\mu(\mathbb{L}_{LE})$. It is furhter noticed that $\mu(\mathbb{R}_{DFE})$ significantly depends on v, although inserting a CP with length 1 is similar to inserting a CP with length 4, and inserting a CP with length 5 will have a similar effect as inserting a CP with length 8, etc. This is due to the structure of the sparse ETC channel model that is used in the simulations. However, for the cases of $\mu(\mathbb{L}_{DFE})$ and $\mu(\mathbb{L}_{LE})$, it can be deduced that the WCC does not change with decreasing the CP length. That makes the proposed design approach more attracting and adds a value for considering it in the practical applications to improve the bandwidth efficiency. Since the coherence of $\mu(\mathbb{L}_{DFE})$ and $\mu(\mathbb{L}_{LE})$ is still low for even small values of v, a good performance with a high likelihood of well estimating the locations and weights of the non-zero entries can still be obtained. Due to this independence of v, the proposed approach is considered as a robust method.

Figs. 4.7 and 4.8 depict the data rate of an OFDM symbol when the percentage of the active entries and the CP length in samples are varied, respectively. Clearly, reducing the length of the CP length will increase the data rate as more useful data is transmitted. For both figures, the CP length for the Sufficient CP case is set to be equal to 16, totally eliminating the ISI effect. In Fig. 4.7, our proposed equalizer performs

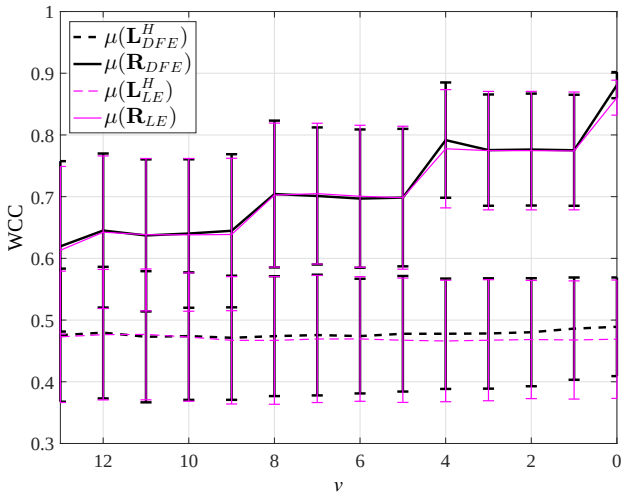

Figure 4.6: WCC vs v when the received SNR is set to 15 dB.

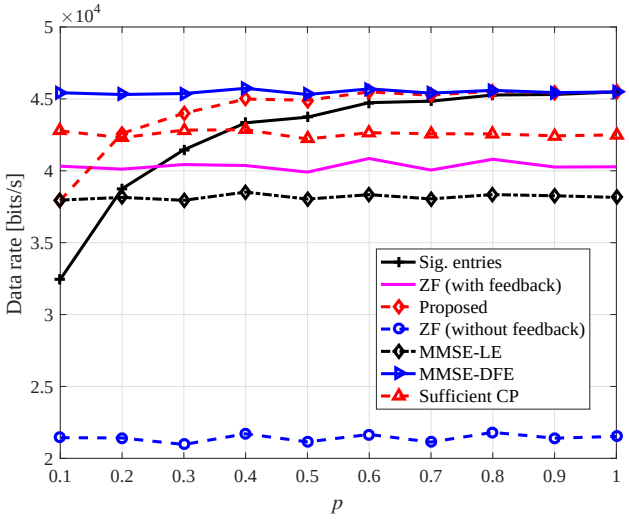

Figure 4.7: Data rate vs. p for different equalizer designs when the received SNR is equal to 20 dB and $v = 2$.

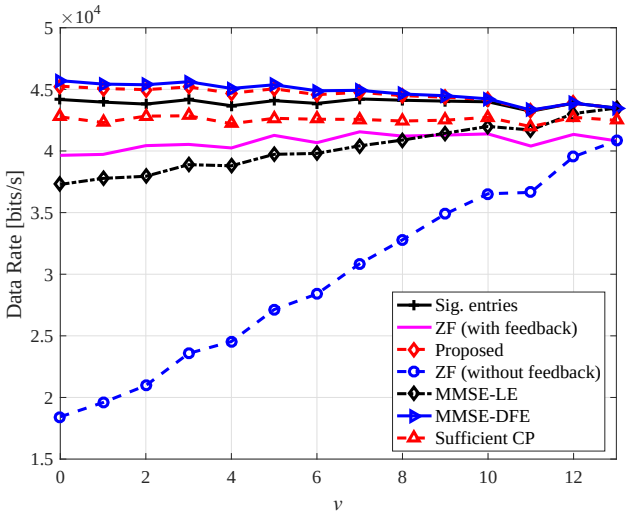

Figure 4.8: Data rate vs. v for different equalizer designs when the received SNR is equal to 20 dB and $p = 50\%$.

better than the significant entries equalizer for all p's and performs very close to the optimal equalizer when $p = 40\%$. Most importantly, our proposed equalizer results in a higher rate than the Sufficient CP case after using only 20% of the equalizer's entries, and the Sig. entries equalizer starts yielding better rate results after 40% of its entries are activated. The proposed equalizer not only outperforms the significant entries equalizer in terms of performance, but is less complex to design as the Sig. entries equalizer requires first to get the dense and complex optimal equalizer result before thresholding it. In Fig. 4.8, since the CP length for the Sufficient CP case is set to 16 samples, our proposed equalizer always results in a higher data rate even when only 50% of its entries are being active.

4.2. Sparse Equalization for OFDM Impaired by Phase Noise

The contribution discussed in section 4.1 yielded the development of a sparse equalizer when the OFDM signal is impaired by interferences due to the insertion of an insufficient CP. In this section, a similar sparse equalizer is designed, although in this case, the interference is due to RF impairments, specifically PN. PN requires the design of a complex equalizer to be mitigated [81, 82], thus, this section aims at using an

approximation of the optimal equalizer while still performing close to it. More details are in what follows.

4.2.1. System Model

The PN impaired OFDM symbol at the receiver is modeled as follows [1]

$$\tilde{\mathbf{x}} = \mathbf{EHx} + \mathbf{n}, \tag{4.29}$$

where $\mathbf{x}$ is the $N \times 1$ transmitted OFDM data symbol with $\mathbb{E}[\mathbf{x}\mathbf{x}^H] = \sigma_x^2 \mathbf{I}_N$, and N denotes the number of OFDM subcarriers. Further, $\mathbf{n}$ is the $N \times 1$ AWGN vector where $\mathbb{E}[\mathbf{n}\mathbf{n}^H] = \sigma_n^2 \mathbf{I}_N$. Moreover, $\mathbf{H}$ is the $N \times N$ frequency-domain channel matrix where its diagonal elements, which is denoted by the $N \times 1$ vector $\mathbf{h}$, represents the channel's frequency response. Furthermore, $\mathbb{E}[\mathbf{H}_{k,k}\mathbf{H}^*_{k',k'}] = \rho_{k,k'}$, where [83], [84]

$$\rho_{k,k'} = \sum_{l=0}^{L-1} \sigma_h^2 \exp(-j2\pi(k-k')l/N), \tag{4.30}$$

and L denotes the number of channel impulse response (CIR) taps. In addition, $\mathbf{E}$ is the receiver PN column-wise circulant matrix where the k-th element of its first column is given by

$$e_k = \frac{1}{N} \sum_{n=0}^{N-1} \exp(j(\phi_n - (2\pi kn/N))), \tag{4.31}$$

where ϕ_n represents the PN sample which perturbs the received signal. The receiver's PN, which is generated using the FRO model, has the statistical property $\phi_{n+n'} - \phi_n \sim \mathcal{N}(0, 4\pi\beta T_s|n'|)$ [85], where β denotes the PN 3-dB bandwidth and T_s is the sampling time.

As previously discussed, the PN affecting the received signal destroys the orthogonality between the OFDM subcarriers. Hence, equalization at the receiver is

[1] In a downlink communication scenario, it is reasonable to ignore PN at the base station transceiver since the oscillator of its transceiver is typically of much higher quality when compared with that of the user terminal.

a necessity to correctly recover the OFDM data symbols and enhance the system's performance. In the next section, the proposed reduced-complexity sparse PN mitigation and channel equalization framework is presented along with an analysis of its performance and complexity.

In the equalization task, the matrices $\mathbf{H}$ and $\mathbf{E}$ are constructed by estimating the frequency-domain channel response and the PN contributions to the received signal. Throughout the derivation of the optimal equalizer in the next section, the equalizer is generalized to include the effects of imperfect PN and channel estimates. Since the joint estimation of the PN and the multipath channel effects are beyond the scope of this contribution, the interested reader may refer to e.g. [56, 57] for more details about the joint estimation of the PN and channel effects in an OFDM system.

4.2.2. Problem Statement and Formulation

An $N \times N$ equalizer matrix $\mathbf{P}$ is applied to the received signal $\tilde{\mathbf{x}}$ to compensate for the effects of the channel and the receiver PN. Denoting the equalized received vector by $\hat{\mathbf{x}} = \mathbf{P}\tilde{\mathbf{x}}$ and the $N \times 1$ error vector by $\mathbf{v} = \mathbf{x} - \hat{\mathbf{x}}$, the MSE can be minimized by satisfying the orthogonality principle

$$\mathbb{E}\left[\mathrm{Tr}\left(\mathbf{v}^H \hat{\mathbf{x}}\right)\right] = 0, \tag{4.32}$$

where Tr(.) denotes the trace operator. Expanding Equation (4.32) yields

$$
\begin{aligned}
&\mathbb{E}_{\mathbf{x},\mathbf{n}}\left[(\mathbf{x}-\widehat{\mathbf{x}})^H\widehat{\mathbf{x}}\right] \\
&= \mathbb{E}_{\mathbf{x},\mathbf{n}}\left[\mathbf{x}^H\mathbf{P}\left(\mathbf{EHx}+\mathbf{n}\right)-\left(\mathbf{EHx}+\mathbf{n}\right)^H\mathbf{P}^H\mathbf{P}\left(\mathbf{EHx}+\mathbf{n}\right)\right], \\
&= \mathbb{E}_{\mathbf{x},\mathbf{n}}\left[\mathbf{x}^H\mathbf{PEHx}+\mathbf{x}^H\mathbf{Pn}-\mathbf{x}^H\mathbf{H}^H\mathbf{E}^H\mathbf{P}^H\mathbf{PEHx}+\right. \\
&\qquad\left.\mathbf{x}^H\mathbf{H}^H\mathbf{E}^H\mathbf{P}^H\mathbf{Pn}-\mathbf{n}^H\mathbf{P}^H\mathbf{PEHx}-\mathbf{n}^H\mathbf{P}^H\mathbf{Pn}\right], \\
&\overset{(a)}{=} \mathbb{E}_{\mathbf{x},\mathbf{n}}\left[\mathbf{x}^H\mathbf{PEHx}\right]+\mathbb{E}_{\mathbf{x},\mathbf{n}}\left[\mathbf{x}^H\mathbf{Pn}\right] \\
&- \mathbb{E}_{\mathbf{x},\mathbf{n}}\left[\mathbf{x}^H\mathbf{H}^H\mathbf{E}^H\mathbf{P}^H\mathbf{PEHx}\right] \quad +\mathbb{E}_{\mathbf{x},\mathbf{n}}\left[\mathbf{x}^H\mathbf{H}^H\mathbf{E}^H\mathbf{P}^H\mathbf{Pn}\right] \\
&- \mathbb{E}_{\mathbf{x},\mathbf{n}}\left[\mathbf{n}^H\mathbf{P}^H\mathbf{PEHx}\right]-\mathbb{E}_{\mathbf{x},\mathbf{n}}\left[\mathbf{n}^H\mathbf{P}^H\mathbf{Pn}\right], \\
&\overset{(b)}{=} \mathbb{E}_{\mathbf{x},\mathbf{n}}\left[\mathbf{x}^H\mathbf{PEHx}\right]-\mathbb{E}_{\mathbf{x},\mathbf{n}}\left[\mathbf{x}^H\mathbf{H}^H\mathbf{E}^H\mathbf{P}^H\mathbf{PEHx}\right] \\
&- \mathbb{E}_{\mathbf{x},\mathbf{n}}\left[\mathbf{n}^H\mathbf{P}^H\mathbf{Pn}\right],
\end{aligned}
\tag{4.33}
$$

where (a) follows from the linearity of the expectation operator and (b) follows from the independency between the data and noise, i.e. the second, fourth and fifth terms in (a) will cancel out due to data and noise independency. Using the properties $\mathbf{w}^H\mathbf{Xw} = \mathrm{Tr}(\mathbf{Xw}^H\mathbf{w})$, $\mathrm{Tr}(\mathbf{X}+\mathbf{Y}) = \mathrm{Tr}(\mathbf{X})+\mathrm{Tr}(\mathbf{Y})$ and $\mathrm{Tr}(\mathbf{XYZ}) = \mathrm{Tr}(\mathbf{YZX}) = \mathrm{Tr}(\mathbf{ZXY})$, where $\mathbf{w}$ is an arbitrary $N\times 1$ vector, $\mathbf{X}$, $\mathbf{Y}$ and $\mathbf{Z}$ are arbitrary $N\times N$ matrices, $\mathbb{E}_{\mathbf{x},\mathbf{n}}\left[\mathrm{Tr}\left(\mathbf{v}^H\hat{\mathbf{x}}\right)\right]$ can be written as follows

$$
\begin{aligned}
\mathbb{E}_{\mathbf{x},\mathbf{n}}\left[\mathrm{Tr}\left(\mathbf{v}^H\hat{\mathbf{x}}\right)\right] &= \mathrm{Tr}\Big(\mathbf{H}^H\mathbf{E}^H\mathbf{P}^H\mathbf{PEH}\Big)+\left(\mathrm{SNR}^{-1}\right)\mathrm{Tr}\Big(\mathbf{P}^H\mathbf{P}\Big) \\
&\quad -\mathrm{Tr}\Big(\mathbf{PEH}\Big),
\end{aligned}
\tag{4.34}
$$

where $\mathrm{SNR} = \frac{\sigma_x^2}{\sigma_n^2}$. Satisfying the orthogonality principle defined in (4.32), the result is

$$
\mathrm{Tr}\Big(\mathbf{EHH}^H\mathbf{E}^H\mathbf{P}^H\mathbf{P}\Big)+\left(\mathrm{SNR}^{-1}\right)\mathrm{Tr}\Big(\mathbf{P}^H\mathbf{P}\Big)-\mathrm{Tr}\Big(\mathbf{EHP}\Big)=0. \tag{4.35}
$$

Let $\mathbf{0}_N$ be an $N \times N$ all-zeros matrix, then

$$\begin{aligned}\text{Tr}\left(\left[\mathbf{E}\mathbf{H}\mathbf{H}^H\mathbf{E}^H\mathbf{P}^H + \text{SNR}^{-1}\mathbf{P}^H - \mathbf{E}\mathbf{H}\right]\mathbf{P}\right) &= 0,\\ \left(\mathbf{E}\mathbf{H}\mathbf{H}^H\mathbf{E}^H\mathbf{P}^H + \text{SNR}^{-1}\mathbf{P}^H - \mathbf{E}\mathbf{H}\right)\mathbf{P} &= \mathbf{0}_N.\end{aligned}$$

By excluding the trivial solution of $\mathbf{P} = \mathbf{0}_N$, and defining $\mathbf{D} = \mathbf{E}\mathbf{H}\mathbf{H}^H\mathbf{E}^H + \text{SNR}^{-1}\mathbf{I}_N$, it can be shown that

$$\mathbf{P}_{\text{opt}} = \mathbf{H}^H\mathbf{E}^H\mathbf{D}^{-H}. \tag{4.36}$$

The above equalizer is modeled assuming perfect knowledge of the multipath channel and PN effects. However, a more practical assumption would be to consider imperfect estimates of $\mathbf{H}$ and $\mathbf{E}$, which are denoted by $\hat{\mathbf{H}}$ and $\hat{\mathbf{E}}$. Thus, we define $\hat{\mathbf{E}}_{i,j} = \mathbf{E}_{i,j}\left(1 + \Xi_{\mathbf{E}_{i,j}}\right)$ and $\hat{\mathbf{H}}_{i,j} = \mathbf{H}_{i,j}\left(1 + \Xi_{\mathbf{H}_{i,j}}\right)$, where $\Xi_{\mathbf{E}}$ and $\Xi_{\mathbf{H}}$ are $N \times N$ matrices that model the PN and channel estimation errors, respectively. In addition, the entries of both matrices follow a normal distribution with zero-mean and variances $\sigma^2_{\Xi_{\mathbf{E}}}$ and $\sigma^2_{\Xi_{\mathbf{H}}}$, respectively. Hence, the derivation of the optimal equalizer using imperfect estimates of $\mathbf{H}$ and $\mathbf{E}$ can be carried out in a similar fashion, and the optimal equalizer $\underline{\mathbf{P}}_{\text{opt}}$ which is a function of the imperfect PN and channel estimates can thus be written as

$$\underline{\mathbf{P}}_{\text{opt}} = \hat{\mathbf{H}}^H\hat{\mathbf{E}}^H\hat{\mathbf{D}}^{-H}. \tag{4.37}$$

where $\hat{\mathbf{D}} = \hat{\mathbf{E}}\hat{\mathbf{H}}\hat{\mathbf{H}}^H\hat{\mathbf{E}}^H + \text{SNR}^{-1}\mathbf{I}_N$.

Equations (4.36) and (4.37) refer to the optimal equalizer solutions in the MMSE sense. However, $\underline{\mathbf{P}}_{\text{opt}}$ and $\mathbf{P}_{\text{opt}}$ are not sparse and their implementation complexity increase proportionally to N^3 which can be computationally expensive. On the other hand, choosing $\mathbf{P}$ different from $\underline{\mathbf{P}}_{\text{opt}}$ (or equivalently $\mathbf{P}_{\text{opt}}$) leads to a performance loss. Thus, to achieve a desirable performance-complexity trade-off, the following sparse approximation design problem is formulated

$$\text{vec}(\hat{\mathbf{P}}) = \underset{\text{vec}(\mathbf{P})\in\mathbb{C}_{N^2\times 1}}{\text{argmin}} \|\text{vec}(\mathbf{P})\|_0 \text{ such that } \nu_{\text{excess}} \leq \epsilon, \tag{4.38}$$

where $\|\text{vec}(\mathbf{P})\|_0$ represents the number of non-zero elements of $\text{vec}(\mathbf{P})$, $\text{vec}(.)$ denotes the matrix vectorization operator, ϵ is the stopping criterion, and ν_{excess} is the excess MSE after applying the sparse equalizer, where it can be shown that

$$\begin{aligned}
&\text{MSE} \triangleq \nu \\
&= \mathbb{E}\left[\mathbf{v}^H\mathbf{v}\right] = \underbrace{\text{Tr}\left[\sigma_x^2\mathbf{I}_N\right]}_{\nu_{\text{min}}} \\
&+ \underbrace{\text{Tr}\left[\sigma_x^2\mathbf{H}^H\mathbf{E}^H\mathbf{P}^H\mathbf{P}\mathbf{E}\mathbf{H} - 2\sigma_x^2\mathbf{P}\mathbf{E}\mathbf{H} + \sigma_n^2\mathbf{P}^H\mathbf{P}\right]}_{\nu_{\text{excess}}}.
\end{aligned} \tag{4.39}$$

While one can attempt to use convex-optimization-based approaches by approximating the ℓ_0-norm with the squared ℓ_1-norm to reduce the search space [33], various low-complexity greedy algorithms exist in the literature, and can be employed to solve our problem in an efficient manner. Next, the proposed framework for designing a sparse equalizer such that the performance loss does not exceed a predefined limit is discussed.

4.2.3. Sparse Equalizer Design Framework

In this subsection, a quantification of the error resulting from the sparse approximation of the MMSE equalizer is performed using the received signal's SINR. The matrix $\mathbf{E}$ is defined as

$$\mathbf{E} = \begin{bmatrix} e_0 & e_{N-1} & \cdots & e_1 \\ e_1 & e_0 & \cdots & e_2 \\ \vdots & \vdots & \ddots & \vdots \\ e_{N-1} & e_{N-2} & \cdots & e_0 \end{bmatrix}. \tag{4.40}$$

Furthermore, **E** can be decomposed as follows

$$\mathbf{E} = e_0\mathbf{I}_N + \underbrace{\begin{bmatrix} 0 & e_{N-1} & \cdots & e_1 \\ e_1 & 0 & \dots & e_2 \\ \vdots & \vdots & \ddots & \vdots \\ e_{N-1} & e_{N-2} & \cdots & 0 \end{bmatrix}}_{\mathbf{E}_{ICI}}, \tag{4.41}$$

where e_0 represents the PN CPE effect and the $N \times N$ matrix $\mathbf{E}_{ICI}$ represents the ICI effect caused by the oscillator PN. Applying the decomposition in (4.41) to (4.29) yields

$$\begin{aligned} \tilde{\mathbf{x}} &= \mathbf{EHx} + \mathbf{n}, \\ &= e_0\mathbf{Hx} + \mathbf{E}_{ICI}\mathbf{Hx} + \mathbf{n}. \end{aligned} \tag{4.42}$$

Moreover, equation (4.42) can be written as follows

$$\tilde{x}_k = e_0 h_k x_k + \sum_{l\neq k, l=0}^{N-1} h_k x_k e_{ICI,l-k} + n_k. \tag{4.43}$$

Denoting the instantaneous SINR of the received signal by $\dot{\zeta}_k^{max}$, then

$$\dot{\zeta}_k^{max} = \frac{|e_0|^2|h_k|^2|x_k|^2}{\sum\limits_{\substack{l=0 \\ l\neq k}}^{N-1} |h_k|^2|x_k|^2|E_{ICI,l-k}|^2 + |n_k|^2}. \tag{4.44}$$

Assuming that the data, PN and the AWGN terms are mutually independent and stationary random processes, the k^{th} subcarrier's average SINR is defined, which is denoted by ζ_k^{max}, by writing

$$\begin{aligned} \zeta_k^{max} &= \frac{\mathbb{E}\left[|e_0|^2\right]\mathbb{E}\left[|h_k|^2\right]\mathbb{E}\left[|x_k|^2\right]}{\sum\limits_{\substack{l=0 \\ l\neq k}}^{N-1} \mathbb{E}[|h_k|^2]\mathbb{E}[|x_k|^2]\mathbb{E}\left[|E_{ICI,l-k}|^2\right] + \mathbb{E}\left[|n_k|^2\right]} \\ &= \frac{J_0\sigma_{h,k}^2\sigma_{x,k}^2}{\sum_{l=0,l\neq k}^{N-1} J_{l-k}\sigma_{h,l}^2\sigma_{x,l}^2 + \sigma_{n,k}^2}, \end{aligned} \tag{4.45}$$

where $J_{l-k} = \mathbb{E}\left[|E_{ICI,l-k}|^2\right]$ is derived in [85]. Furthermore, another interference parameter is added in the denominator of ζ_k^{max} that accounts for the error resulting from the sparse approximation of the equalizer matrix which will be denoted by ϵ_k. Hence, Equation (4.45) can be re-written as

$$\zeta_k = \frac{\overbrace{J_0\sigma_{h,k}^2\sigma_{x,k}^2}^{\triangleq\alpha_d}}{\underbrace{\sum_{l=0,l\neq k}^{N-1} J_{l-k}\sigma_{h,l}^2\sigma_{x,l}^2 + \sigma_{n,k}^2 + \epsilon_k}_{\triangleq\alpha_I}}. \tag{4.46}$$

After some straight-forward mathematical manipulations, the following can be written

$$\begin{aligned} \frac{\zeta_k^{max} - \zeta_k}{\zeta_k\zeta_k^{max}} &= \frac{\epsilon_k}{\alpha_d}, \\ \frac{\gamma_k - 1}{\zeta_k^{max}} &= \frac{\epsilon_k}{\alpha_d}, \end{aligned} \tag{4.47}$$

where $\gamma_k = \frac{\zeta_k^{max}}{\zeta_k}$. Solving for ϵ_k, the result is

$$\begin{aligned} \epsilon_k &= (\gamma_k - 1)\,\alpha_I, \\ \therefore \epsilon_k &= (\gamma_k - 1)\left(\sum_{l=0,l\neq k}^{N-1} J_{l-k}\sigma_{h,l}^2\sigma_{x,l}^2 + \sigma_{n,k}^2\right). \end{aligned} \tag{4.48}$$

Next, the sparse approximation problem of the equalizer matrix is formulated as follows

$$\begin{aligned} \text{vec}(\hat{\mathbf{P}}^H) = \underset{\text{vec}(\mathbf{P}^H)\in\mathbb{C}_{N^2\times 1}}{\text{argmin}} \quad & \|\text{vec}(\mathbf{P}^H)\|_0 \\ \text{s.t.} \quad & \|\text{vec}(\mathbf{EH}) - \underbrace{(\mathbf{D}\otimes\mathbf{I}_N)}_{\triangleq\bar{\mathbf{D}}}\text{vec}(\mathbf{P}^H)\|_2^2 \leq \epsilon, \end{aligned} \tag{4.49}$$

where $\|.\|_2$ is the ℓ_2-norm operator and $\otimes$ denotes the Kronecker product operator. These parameters are used as input arguments to the orthogonal matching pursuit (OMP) greedy algorithm [74] to estimate $\text{vec}(\hat{\mathbf{P}}^H)$. In the analysis, the stopping

criterion is defined as either a predefined number of non-zero entries or as the residual error from the sparse approximation of vec($\mathbf{P}$) which can be controlled by the designer. More details on the OMP algorithm's functionality are widely available in the literature as in e.g. [74]. The MMSE equalizer matrix $\hat{\mathbf{P}}^H$ is then reshaped from vec($\hat{\mathbf{P}}^H$) and used in the equalization of the received data vector.

4.2.4. Reduced-Complexity Equalizer Design

In this section, a reduced-complexity design is proposed for the MMSE equalizer matrix $\hat{\mathbf{P}}^H$ discussed above. The proposed design in Section 4.2.3 involves the inversion of the matrix $\mathbf{D}$ with $\mathcal{O}(N^3)$, where N is the length of the OFDM symbol whose computational cost grows larger as the number of subcarriers in an OFDM symbol increases. In contrast, the matrix inversion can be computed efficiently by exploiting the inherent structure of the underlying matrices that form the equalizer matrix $\mathbf{P}^H$ along with a few matrix manipulations. The reduction in the complexity of inverting the matrix $\mathbf{D}$ can be achieved by inverting diagonal matrices, which are relatively simple to invert.

To calculate $\mathbf{P}^H$, an inversion of $\mathbf{D}$ is needed. To achieve this, the following matrix identities are applied [76]:

$$\begin{aligned}(\mathbf{X}+\mathbf{XYX}) &= \mathbf{X}(\mathbf{I}_N+\mathbf{YX}) = (\mathbf{I}_N+\mathbf{XY})\mathbf{X},\\ (\mathbf{I}_N+\mathbf{XY})^{-1}\mathbf{X} &= \mathbf{X}(\mathbf{I}_N+\mathbf{YX})^{-1}, \qquad (4.50a)\\ (\mathbf{I}_N+\mathbf{X})^{-1} &= (\mathbf{I}_N+\mathbf{X})^{-1}(\mathbf{I}_N+\mathbf{X}-\mathbf{X}),\\ &= \mathbf{I}_N-(\mathbf{I}_N+\mathbf{X})^{-1}\mathbf{X}, \qquad (4.50b)\end{aligned}$$

where $\mathbf{X}$ and $\mathbf{Y}$ are arbitrary $N \times N$ matrices. Let $\boldsymbol{\mathcal{H}} = \mathbf{H}\mathbf{H}^H$, and $\boldsymbol{\Lambda} = \text{SNR}^{-1}\mathbf{I}_N$. Then using these identities, the inverse of $\mathbf{D}$ is computed as follows

$$\begin{aligned}
\mathbf{D}^{-1} &= (\boldsymbol{\Lambda} + \mathbf{E}\boldsymbol{\mathcal{H}}\mathbf{E}^H)^{-1}, \\
&= (\boldsymbol{\Lambda}[\boldsymbol{\Lambda}^{-1}\mathbf{E}\boldsymbol{\mathcal{H}}\mathbf{E}^H + \mathbf{I}_N])^{-1}, \\
&= (\boldsymbol{\Lambda}^{-1}\mathbf{E}\boldsymbol{\mathcal{H}}\mathbf{E}^H + \mathbf{I}_N)^{-1}\boldsymbol{\Lambda}^{-1}, \\
&= \left[\mathbf{I}_N - (\mathbf{I}_N + \boldsymbol{\Lambda}^{-1}\mathbf{E}\boldsymbol{\mathcal{H}}\mathbf{E}^H)^{-1}\boldsymbol{\Lambda}^{-1}\mathbf{E}\boldsymbol{\mathcal{H}}\mathbf{E}^H\right]\boldsymbol{\Lambda}^{-1}, && \text{(4.51a)} \\
&= \left[\mathbf{I}_N - \boldsymbol{\Lambda}^{-1}\mathbf{E}(\mathbf{I}_N + \boldsymbol{\mathcal{H}}\mathbf{E}^H\boldsymbol{\Lambda}^{-1}\mathbf{E})^{-1}\boldsymbol{\mathcal{H}}\mathbf{E}^H\right]\boldsymbol{\Lambda}^{-1}, && \text{(4.51b)} \\
&= \boldsymbol{\Lambda}^{-1} - \left(\frac{\sigma_x^2}{\sigma_n^2}\right)^2 \mathbf{E}\boldsymbol{\Psi}\mathbf{E}^H, && \text{(4.51c)}
\end{aligned}$$

where $\boldsymbol{\Psi} = \text{diag}\left(\mathbf{a} \oslash (\mathbf{b} + \mathbf{1}_N)\right)$, $\mathbf{a} = \mathbf{h} \odot \mathbf{h}^*$ with the size of $N \times 1$, $\mathbf{b} = \mathbf{h} \odot \mathbf{h}^* \times \left(\frac{\sigma_x^2}{\sigma_n^2}\right)$ with the size of $N \times 1$, and $\mathbf{1}_N$ is the $N \times 1$ all ones vector. Furthermore, $\odot$ and $\oslash$ denote the element-wise multiplication and division operations, respectively. The identities in (4.50b) and (4.50a) are used in the steps (4.51a) and (4.51b), respectively. Thus, inverting the matrix $\mathbf{D}$ can be realized with a significantly reduced complexity.

The number of CM/A of the OMP algorithm is $\mathcal{O}\left(N^2 S\right)$ [74], where S is the number of non-zero entries of $\hat{\mathbf{P}}$ [74], which is less than the complexity of implementing the well-known Gauss-Jordan algorithm for inverting matrices with a complexity of $\mathcal{O}\left(N^3\right)$ [75]. Nonetheless, the complexity of inverting the matrix $\mathbf{D}$ cab still be reduced by applying some algebraic manipulations.

As it was shown, inverting the matrix $\mathbf{D}$ using our approach was shown to have a complexity of $\mathcal{O}\left(N\right)$. Given this low complexity, the One-Step Thresholding (OST) algorithm is proposed, which is used in e.g. [86], [87] and [88], to determine the non-zero coefficients of any given vector. The description of this algorithm is shown in Algorithm 4. This algorithm simply selects the set $\widehat{\kappa}$ of the matrix columns (i.e., atoms) of $\bar{\mathbf{D}}$ that are most correlated with the data vector $\text{vec}(\mathbf{P}^H)$ to estimate the locations of the non-zero entries. Once the non-zero locations are estimated, the proposed low complexity method to determine the values of all non-zero entries of the equalizer is

used, where the values are acquired from $\mathbf{P}_{\text{opt}}$. By doing so, directly inverting $\mathbf{D}$ can be avoided, and the equalizer is designed by only inverting diagonal matrices. Table 4.3 presents a comparison between the orders of the complexities of each of the discussed design approaches.

In the next section, the proposed PN mitigation and channel equalization design method is compared with a significant entries equalization approach. The significant entries equalizer is computed by thresholding the absolute value of the optimal MMSE equalizer to include its largest entries based on the value of ϵ that is used in our proposed equalizer. Furthermore, our equalization method is compared with the channel equalization and PN mitigation equalizer proposed in [1]. Although the equalizer in [1] has a complexity of $\mathcal{O}(N)$, the results in the next section will demonstrate the superiority of the performance of our proposed equalizer. The novelty of our design can be summarized as follows:

1. It significantly reduces the complexity of computing the equalizer coefficients by using the proposed reduced complexity approach.

2. It reduces the implementation complexity since only a few nonzero filter coefficients need to be implemented. Hence, it reduces the implementation cost and power consumption accordingly.

3. It results in a better performance-complexity tradeoff for PN-impaired OFDM receivers.

4.2.5. Maximum Expected Coherence Analysis

In this section, the proposed joint channel and PN equalization scheme is analyzed. The analysis is based on the sparsifying matrix, which is the matrix $\mathbf{D}$ in our case, where the correlations between its normalized columns are computed. Specifically, an MEC analysis is carried out as performed in [78], where it is denoted by $\mu_{max}(\mathbf{D})$. Furthermore, a small $\mu_{max}(\mathbf{D})$ cannot ensure that the OMP will be suitable for our proposed

Algorithm 4: The One-Step Thresholding (OST) Algorithm

Input: Unit-norm matrix $\bar{\mathbf{D}}$, vector vec$(\mathbf{P}^H)$, and a threshold $\epsilon > 0$

Output: Estimate of the non-zero locations $\widehat{\kappa} \subset \{0, \ldots, N-1\}$

1. $\mathbf{z} = \bar{\mathbf{D}}^H \text{vec}(\mathbf{P}^H)$

2. $\widehat{\kappa} \leftarrow \{0, \ldots, N-1 : |z_i| > \epsilon\}$

Table 4.3: Computational Complexity of Various Joint PN Mitigation and Channel Equalization Design Approaches.

Equalizer Type	Design Complexity
Conventional Optimal Equalizer	$\mathcal{O}(N^3)$
Significant-Entries Equalizer	$\mathcal{O}(N^3)$
Sparse OMP-Based Equalizer	$\mathcal{O}(N^2 S)$
Equalizer in [1]	$\mathcal{O}(N)$
Proposed Approach	$\mathcal{O}(N)$

equalization scheme, while a large $\mu_{max}(\mathbf{D})$ implies that our sparsifying matrix is not suitable for our proposed model [78]. The MEC is defined as follows

$$\mu_{max}(\mathbf{D}) = \max_{i,j:i\neq j} \left[\mathbb{E}\left[\frac{|\mathbf{D}^H(:,j)\mathbf{D}(:,i)|}{\|\mathbf{D}(:,i)\|_2 \|\mathbf{D}(:,j)\|_2} \right] \right]. \tag{4.52}$$

The norms in the denominator can be excluded from the maximization since, on average, the norms of the columns of $\mathbf{D}$ can be shown to be equal, which is easy to see from the underlying structure of the matrix $\mathbf{D}$. Therefore,

$$\mathbb{E}\left[\mathbf{D}^H(:,j)\mathbf{D}(:,i)\right] = \mathbf{u}_j^H \mathbb{E}[\mathbf{D}^H\mathbf{D}]\mathbf{u}_i, \tag{4.53}$$

where $\mathbf{u}_i$ is an $N \times 1$ unit vector whose i^{th} entry is equal to 1 and its other entries are zeros. Furthermore, the maximization function was omitted since, by inspecting the structure of the matrix $\mathbf{D}$, the maximum value of the inner product of the i^{th} and j^{th} columns occurs when $j = \text{mod}(\frac{i+N\pm1}{N})$, where mod denotes the modulo function. All the possibilities of the mean of the column-wise inner products of the matrix $\mathbf{D}$ are depicted in Fig. 4.9. Last but not least, our simulations suggest that, for a small β, the column-wise inner product of $\mathbf{D}$ can be approximated by the product of only the first two elements of the i^{th} and j^{th} columns, which can be written as

$$\begin{aligned}
\mu_{max}(\mathbf{D}) &\approx \mathbb{E}\Bigg[\Big||e_0|^2|h_0|^2\Big(\sum_{i=0}^{N-1} e_i e_{i-(N-1)}^* |h_{N-i}|^2\Big) \\
&\quad + |e_0|^2|h_1|^2\Big(\sum_{i=0}^{N-1} e_i^* e_{i-(N+1)} |h_{N-(i-1)}|^2\Big)\Big|\Bigg], \\
&\approx \mathbb{E}\left[|h_0|^2\Big|\sum_{i=0}^{N-1} e_i e_{i-(N-1)}^* |h_{N-i}|^2\Big|\right] \\
&\quad + \mathbb{E}\left[|h_1|^2\Big|\sum_{i=0}^{N-1} e_i^* e_{i-(N+1)} |h_{N-(i-1)}|^2\Big|\right]. \qquad (4.54)
\end{aligned}$$

From the above expression, a larger number of channel taps and a more severe PN effect will increase the possibility that any two consecutive columns of the sparsifying matrix will be highly correlated. In the next section, a numerical evaluation of the MEC (both exact and approximated MECs) for different values of β is carried out.

4.2.6. Numerical Results

In this section, the performance of the proposed design approach is investigated. In the simulations, a 64 OFDM subcarrier with a sampling frequency of 2 MHz and a subcarrier spacing of 31.25 kHz is assumed. A multipath channel with uniform power delay profile is adopted where the number of taps is selected to be 6.

Fig. 4.10 depicts the percentage of the active entries of $\hat{\mathbf{P}}$ as a function of γ_k for different values of β. The figure also shows the percentage of the active entries of $\hat{\mathbf{P}}$

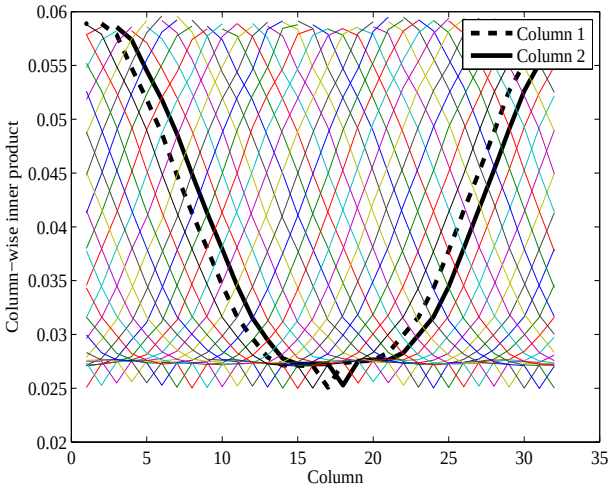

Figure 4.9: Mean of all column-wise coherence possibilities of the matrix **D** for $N = 32$ and $\beta = 500$ Hz. The highlighted two columns (solid and dashed black lines) are the first and second columns of the matrix **D**. Note that the same trend will be obtained for any two consecutive columns.

when its most significant entries in terms of the absolute value are considered, which is refered to as the "significant-entries" approach. In this setup, the worst case SINR is used by maximizing its denominator. In other words, instead of taking the expectation $\sum_{\substack{l=0 \\ l\neq k}}^{N-1} \mathbb{E}[|h_k|^2]\mathbb{E}[|x_k|^2]\mathbb{E}\left[|E_{ICI,l-k}|^2\right] + \mathbb{E}\left[|n_k|^2\right]$, the maximum of the denominator of the SINR in (4.44) is taken to emulate a worst-case scenario for ϵ_k. This parameter is denoted by ϵ_k^{sim}, and is modeled by applying

$$\epsilon_k^{sim} = (\gamma_k - 1) \times \mathbb{E}\left[\max_k \left(\sum_{\substack{l=0 \\ l\neq k}}^{N-1} |h_k|^2|x_k|^2|E_{ICI,(l-k)}|^2 + |n_k|^2\right)\right]. \tag{4.55}$$

Therefore, $\epsilon_k^{sim} \geq \epsilon_k$.

Interestingly, when the OMP is used, the percentage of the active entries of $\hat{\mathbf{P}}$ is less than the significant entries equalizer for both $\beta = 300,\ 1000$ Hz. As γ_k increases, the percentage of the active elements in $\hat{\mathbf{P}}$ decreases. This is expected since an increas-

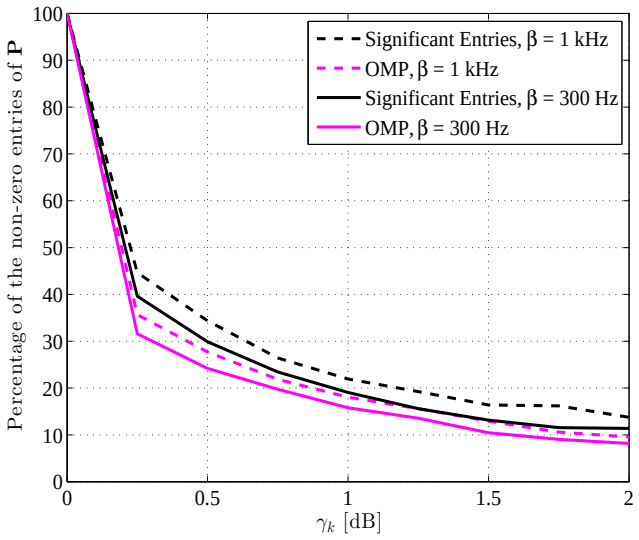

Figure 4.10: Percentage of active entries in $\hat{\mathbf{P}}$ versus γ_k for different values of β and an SNR of 20dB. Solid lines represent the case of $\beta = 300$Hz while the dashed-lines represent the case of $\beta = 1$KHz

ing γ_k implies a higher tolerance to the error resulting from the sparse approximation of the optimal equalizer matrix $\mathbf{P}$, and a higher tolerance for error allows a sparser approximation of $\mathbf{P}$. If β is increased, more elements of $\hat{\mathbf{P}}$ are needed to achieve the same performance when compared to the case of having a smaller β, therefore, an increased PN level leads to a less efficient sparse approximation of $\mathbf{P}$. Furthermore, decreasing the number of active entries reduces the OFDM transceiver design complexity and, hence, power consumption since a smaller number of CM/A operations are needed.

Fig. 4.11 shows the coded BER versus SNR performance when the optimal equalizer, our proposed sparse equalizer, significant entries equalizer and the equalizer in [1] are used where perfect knowledge of the PN and channel quantities are assumed. The coding rate was set to be 1/2 with the convolutional encoder [133, 171] and a constraint length of 7. At the receiver, a Viterbi decoder is used with hard decision decoding. For the case of the significant entries and our proposed sparse equalizers, around 23% of the equalizer's entries are active. The results in Fig. 4.11 show that the performance of our proposed sparse equalizer outperforms the significant entries

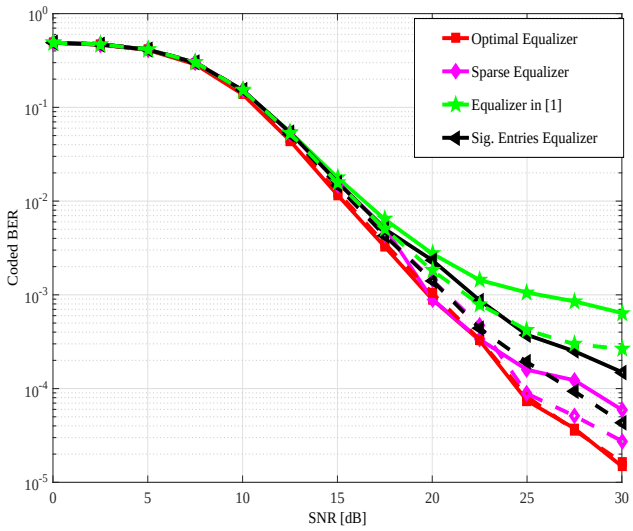

Figure 4.11: Coded BER versus the SNR for the optimal equalizer, sparse equalizer, significant-entries equalizer and the equalizer in [1]. A sparsity level (active entries) of 23% is selected and $\sigma_e^2 = 0$. The solid lines represent the results for $\beta = 1$ kHz while the dashed-lines represent the results for $\beta = 500$ Hz.

equalizer and the equalizer proposed in [1], and the performance of our proposed sparse equalizer gets closer to the optimal one as β is decreased. However, by incorporating more active entries, the performance gap will be significantly reduced, especially at high SNR.

Fig. 4.12 depicts the BER versus SNR for a fixed $\beta = 1$ kHz and for different channel and PN estimation error variances, where $\sigma^2_{\Xi_\mathbf{H}}, \sigma^2_{\Xi_\mathbf{E}} \in \{0.025,\ 0.075\}$ *for all considered equalizers*. Both estimation error variances of the PN and the channel are assumed to be equal and are quantified by the parameter σ_e^2, i.e. $\sigma_e^2 = \sigma^2_{\Xi_\mathbf{H}} = \sigma^2_{\Xi_\mathbf{E}}$. Fig. 4.12 shows that the proposed sparse equalizer still performs the best followed by the significant-entries equalizer. Furthermore, the equalizer in [1] performs the worst. This figure demonstrates that exploiting the correlations between the columns of the sparsifying matrix and the received data (as in our proposed design) results in a better performance than the significant entries equalizer and the equalizer in [1].

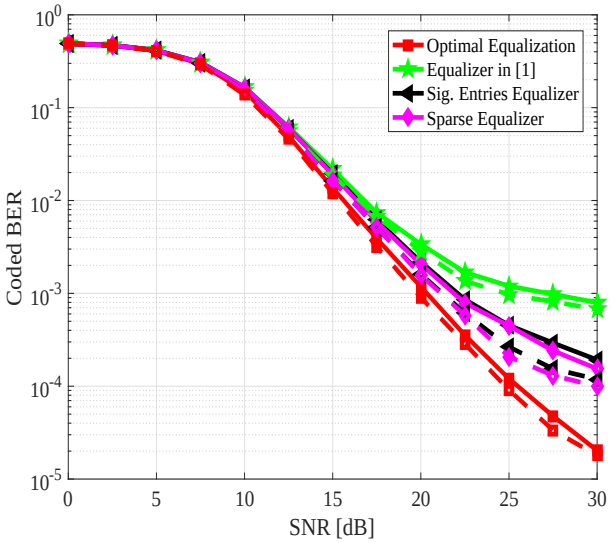

Figure 4.12: Coded BER versus the SNR for the optimal equalizer, sparse equalizer, significant-entries equalizer and the equalizer in [1]. A sparsity level (active entries) of 23% is used and $\beta = 1$ kHz. The solid lines represent the results for $\sigma_e^2 = 0.075$ while the dashed-lines represent the results for $\sigma_e^2 = 0.025$.

Another useful metric to assess the performance of our sparse approximation technique is the worst-case coherence (WCC) metric, which is applied and extensively analyzed in e.g., [46]. Fig. 4.13 shows the WCC versus the SNR for different values of β. The simulations show that increasing β increases the WCC metric, but for a moderately high β, the mean of the WCC is still considerably less than one which points to the likely success of OMP and/or OST in approximating the equalizers' coefficients [47]. Furthermore, at high SNR levels, the noise effect is negligible and, hence, the sparsifying matrix (e.g., $\mathbf{D} = \mathbf{E}\mathbf{H}\mathbf{H}^H\mathbf{E}^H$) does not depend on the SNR. As a result, the coherence converges to a constant value. On the other hand, at low SNR, the noise effect dominates over the channel effect. Hence, the channel can be approximated as a single-tap channel. Then, the sparsifying matrix (e.g., $\text{SNR}^{-1}\mathbf{I}_N$) can be approximated as a scaled identity matrix, i.e., WCC approaches zero.

Fig. 4.14 depicts the WCC versus the SNR for $\beta = 500$ Hz where $\hat{\mathbf{D}}$ is used as the dictionary matrix. The estimation error variance values which are used to generate

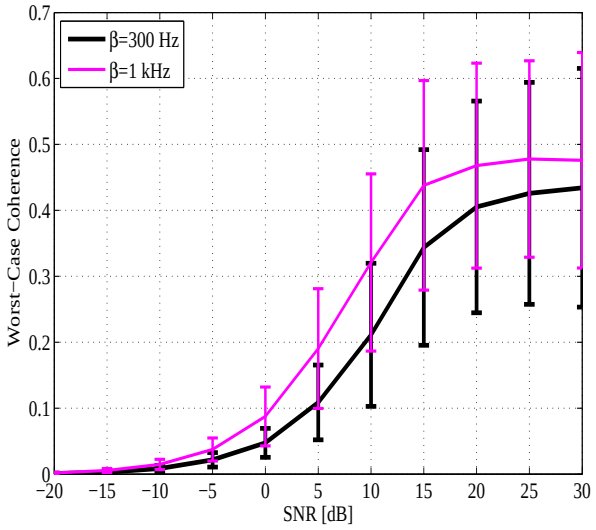

Figure 4.13: Worst-case coherence versus the SNR for for $\sigma_e^2 = 0$, $\beta = 300$Hz and $\beta = 1$KHz.

the results are $\sigma^2_{\Xi_\mathbf{H}}, \sigma^2_{\Xi_\mathbf{E}} \in \{0,\ 0.1\}$, and $\sigma_e^2 = \sigma^2_{\Xi_\mathbf{H}} = \sigma^2_{\Xi_\mathbf{E}}$, i.e., it is also assumed that the estimation error variances are equal for both the estimates of PN and the multipath channel's frequency responses. The results reveal that as the estimation error variance increases, the WCC metric also increases for all SNR levels. This increase is due to additional error terms added to the columns of the sparsifying matrix since the correlation between them is increased accordingly. Hence, the larger the value of the estimation error variance is, the larger the coherence metric will be. Moreover, even when the estimation error variance is large (0.1 or equivalently 10%), the coherence metric still converges to a constant value, which is considerably less than one, at high SNR.

In Fig. 4.15, the MEC metric is plotted versus the SNR for different values of β. The figure shows that the MEC metric in (4.52) converges to a value close to the approximation in (4.54) as the SNR increases for all β. While the approximation in (4.54) is shown to perform better for small β and the approximation becomes less accurate as β increases, it still captures the same behavior as that of the WCC, i.e., saturates at high SNR and increases as β increases. Thus, this approximation turns out

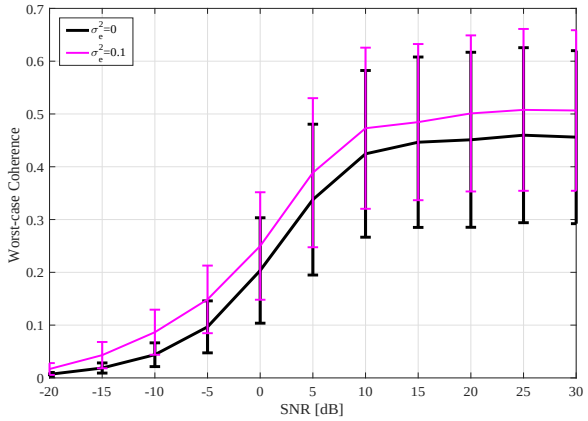

Figure 4.14: Worst-case Coherence versus SNR for different values of σ_e^2, where $\beta = 500$ Hz.

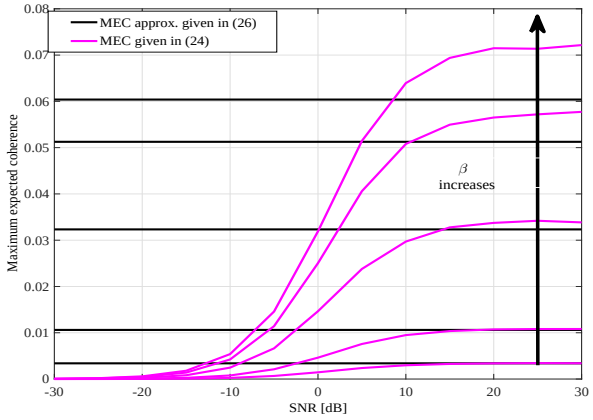

Figure 4.15: Maximum expected coherence for $\beta \in \{1,\ 10,\ ,100,\ 300,\ 500\}$ Hz.

to be quite accurate for small values of β and gives insights on the behavior of the MEC for large values of β.

4.3. Chapter Summary

This chapter presented a novel sparse equalizer for OFDM signals with insufficient CP. The approach is based on trading-off the complexity and the performance of the equalizer realization by formulating several optimization problems. The optimization problem was solved using the well-known OMP algorithm which has a low realization complexity. Such an approach is expected to also increase the efficiency of OFDM signals as the CP can be shortened while relaxing the equalization process at the receiver.

Furthermore, a novel low-complexity equalization of the effects of PN and the channel was proposed. The results demonstrate a considerable gain in terms of BER when the proposed approach was adopted while having a negligible performance loss, especially for low values of the PN's 3-dB bandwidth. The MEC metric was also analyzed for the sparsifying matrix that is used in the proposed approach which provided some insights into the performance of the adopted equalization scheme.

CHAPTER 5: CONCLUSIONS AND FUTURE WORK

5.1. Conclusions

This dissertation covered various wireless communication techniques that are expected to be deployed in future wireless communication standards which require higher network capacity figures, higher communication reliability and efficient data processing using state-of-the-art DSP.

In particular, the topic of performance analysis of radio signals that are operated by FD transceivers was presented in Chapter 2, where the effects of RF impairments on the signals was thoroughly analyzed. Closed-form expressions were derived for the average residual SI power in FD OFDM transceivers in the presence of both PN and IQI. Moreover, it was demonstrated that for small PN and IQI levels, their effects on the average residual SI power can be decoupled. In addition, the average residual SI power was shown to be linearly proportional to both IQI's IRR and the PN 3-dB bandwidth. The analysis showed the importance of implementing more sophisticated digital-domain SI cancellation techniques due to IQI and PN to avoid severe performance degradation.

Moreover, in Chapter 2, Section 2.2, the relationship between IQI and the residual SI in a FD AF relaying network was studied. After simplifying the modeling of the residual SI power, an approximate maximum amplification factor that prevents the relay from being saturated with residual SI was derived, which in turn permits the relay to have a stable performance. Furthermore, an appropriate amplification factor was derived to control the transmission power of the relay. Moreover, a lower bound presenting the relationship between the residual SI power and IQI was derived, where it was shown that the residual SI is bounded by a sum of scaled Gamma functions. The analysis has shown that, even for low values of IQI parameters, the residual SI power can be a major obstacle that prevents the FD AF relay from achieving a satisfactory performance.

Furthermore, Chapter 3 discussed novel multiple relay selection schemes for AF FD dual-hop relay networks that utilizes sparsity inducing optimization problems to-

wards minimizing the MSE level were presented. Based on the accurate modeling of the cumulative SI at each relaying node, the proposed algorithms adopt a hybrid strategy involving FD and switching approaches to avoid the high SI interference at each relay node, and hereby improve the overall system performance in terms of BER. A compromise between BER performance, number of used relays and selection complexity is created between the different proposed techniques. The level of hybridity of our proposed algorithm was captured by simulating the relay re-usage rate as a function of the SI level, transmit power and number of selected relays. The proposed techniques showed their high efficiency and demonstrated that they can dynamically decide when and how often the transmission should be switched from one relay to another to keep the desired performance.

Efficient signal equalization techniques were also tackled in this dissertation, where the equalization of OFDM signals suffering from ICI and ISI due to the insertion of an insufficient CP was studied. As discussed in Chapter 4, Section 4.1, the equalizer design problem was formulated as a convex optimization problem, and then, using the OMP algorithm, the level of sparsity of the proposed equalizer was controlled by either a predefined number of the non-zero entries or by bounding the amount of losses that can be tolerated. Using only 40% of the equalizer entries, the proposed reduced-complexity sparse equalizer performs as good as that of the optimal MMSE equalizer (full dense equalization) in terms of coded BER and data rate. The compatibility of our proposed equalizer was tested through investigating the WCC metric and the dictionary matrices were shown to have low coherences which makes our approach a robust method.

Finally, as detailed in Chapter 4, Section 4.2, the problem of joint equalization of the channel and PN effects in direct-conversion OFDM receivers was formulated as a sparse approximation problem of the equalizer matrix. The results demonstrated that a significant reduction in the percentage of the active entries of the equalizer matrix can be obtained with negligible performance losses, while still performing better compared with the existing approaches. The sparsifying matrix was analyzed to shed some light

on the performance of the OMP and OST algorithms for the sparse approximation of the equalizer matrix, where it was shown that our sparsifying matrix is suitable for our proposed joint channel and PN equalization scheme.

5.2. Future Work

In light of the above contributions, several ideas are still worth investigating. As previously mentioned, the insertion of insufficient CP has been thoroughly studied, but the modeling of the system and thus the equalization schemes ignore practical considerations such as the RF impairments in transceivers.

Furthermore, detection methods in wireless communication systems can be performed by exploiting the current capabilities of using big data and relatively high computational power. For instance, deep neural networks have been used to detect wireless signals by training the neural network using simulated data [89, 90]. The problem of residual SI when RF impairments were considered was investigated in this dissertation, and the study concluded that more sophisticated algorithms must be developed to suppress the residual SI to power levels where the receiver can decode the useful received signal. A study has been recently published in which the problem of SI cancellation using neural networks was investigated [91]. The study assumed that IQI and power amplifier non-linearities are the dominating RF impairments, while the rest of the transceiver electronics are assumed to be ideal. A testbed is then created to verify the proposed cancellation approach. Testing in a laboratory environment when most of the used components operate almost ideally is not practical [21]. For instance, in [92], the authors had to manually inject IQI to the used hardware to be able to verify the performance of their proposed IQI mitigation scheme. As previously mentioned, PN varies from one sample to another, and the tracking and compensation for its detrimental effects could deteriorate the system performance. Hence, the problem of SI cancellation/directly detecting the intended received signal when FD transceivers are deployed using neural networks is an interesting topic to consider.

Recently, a decision tree algorithm was proposed to perform relay selection in a relay network where the second-order statistics of the CSI was used to perform multiple relay selection [93]. Therefore, using deep neural networks can be also implemented in relay selection applications, especially in the case when the relays use FD transceivers in which handling the resulting interferences can become a tedious task.

REFERNCES

[1] P. Rabiei, W. Namgoong, and N. Al-Dhahir, "A Non-iterative Technique for Phase Noise ICI mitigation in Packet-based OFDM Systems," *IEEE Transactions on Signal Processing*, vol. 58, no. 11, pp. 5945–5950, 2010.

[2] J. Zhu, W. Ser, and A. Nehorai, "Channel Equalization for DMT with Insufficient Cyclic Prefix," in *Asilomar Conference on Signals, Systems and Computers*. IEEE, 2000, vol. 2, pp. 951–955.

[3] E. Everett, M. Duarte, C. Dick, and A. Sabharwal, "Empowering full-duplex wireless communication by exploiting directional diversity," in *Asilomar Conference on Signals, Systems and Computers*. IEEE, 2011, pp. 2002–2006.

[4] X. Huang and Y. J. Guo, "Radio frequency self-interference cancellation with analog least mean-square loop," *IEEE Transactions on Microwave Theory and Techniques*, vol. 65, no. 9, pp. 3336–3350, 2017.

[5] E. Ahmed and A. Eltawil, "All-digital self-interference cancellation technique for full-duplex systems," *IEEE Transactions on Wireless Communications*, vol. 14, no. 7, pp. 3519–3532, 2015.

[6] D. Korpi, M. Heino, C. Icheln, K. Haneda, and M. Valkama, "Compact inband full-duplex relays with beyond 100 db self-interference suppression: Enabling techniques and field measurements," *IEEE Transactions on Antennas and Propagation*, vol. 65, no. 2, pp. 960–965, 2017.

[7] R. Chang, "High-speed multichannel data transmission with bandlimited orthogonal signals," *Bell Sys. Tech. J*, vol. 45, no. 10, pp. 1775–1796, 1966.

[8] J. G. Andrews, S. Buzzi, W. Choi, S. V. Hanly, A. Lozano, A. CK. Soong, and J. C. Zhang, "What will 5G be?," *IEEE Journal in Selected Areas Communications*, vol. 32, no. 6, pp. 1065–1082, 2014.

[9] T. Pham, T. Le-Ngoc, G. Woodward, and P. Martin, "Channel Estimation and Data Detection for Insufficient Cyclic Prefix MIMO-OFDM," *IEEE Transactions on Vehicular Technology*, 2016.

[10] D. W. Bliss, T. Hancock, and P. Schniter, "Hardware Phenomenological Effects on Cochannel Full-duplex MIMO Relay Performance," in *Asilomar Conference on Signals, Systems and Computers*. IEEE, 2012, pp. 34–39.

[11] Q. Zou, A. Tarighat, and A. H. Sayed, "Joint compensation of IQ Imbalance and Phase Noise in OFDM Wireless Systems," *IEEE Transactions on Communications*, vol. 57, no. 2, pp. 404–414, 2009.

[12] Y. Xin and et al., "Technical report on full duplex for 802.11," Tech. Rep., IEEE802.11-18/0498r6, Sep. 2018.

[13] D. López-Pérez, A. Garcia-Rodriguez, L. Galati-Giordano, M. Kasslin, and K. Doppler, "IEEE 802.11 be − Extremely High Throughput: The Next Generation of Wi-Fi Technology Beyond 802.11 ax," *arXiv preprint arXiv:1902.04320*, 2019.

[14] A. Sabharwal, P. Schniter, D. Guo, D. W. Bliss, S. Rangarajan, and R. Wichman, "In-Band Full-Duplex wireless: Challenges and Opportunities," *IEEE Journal on Select. Areas in Comm.*, vol. 32, no. 9, pp. 1637–1652, 2014.

[15] D. Kim, H. Lee, and D. Hong, "A Survey of In-Band Full-Duplex Transmission: From the Perspective of PHY and MAC Layers," *IEEE Communication Surveys Tutorials*, vol. 17, no. 4, pp. 2017–2046, 2015.

[16] G. Liu, F. R. Yu, H. Ji, Victor C. M. Leung, et al., "In-Band Full-Duplex Relaying: A Survey, Research Issues and Challenges," *IEEE Communication Surveys Tutorials*, vol. 17, no. 2, pp. 500–524, 2015.

[17] M. Heino, D. Korpi, T. Huusari, E. Antonio-Rodriguez, S. Venkatasubramanian, T. Riihonen, L. Anttila, C. Icheln, K. Haneda, R. Wichman, et al., "Recent Advances in Antenna Design and Interference Cancellation Algorithms for In-Band

Full Duplex Relays," *IEEE Communication Magazine*, vol. 53, no. 5, pp. 91–101, 2015.

[18] J. I. Choi, M. Jain, K. Srinivasan, P. Levis, and S. Katti, "Achieving Single Channel, Full Duplex Wireless Communication," in *16th annual International Conference on Mobile Computing and Networks*. ACM, 2010, pp. 1–12.

[19] M. Duarte, A. Sabharwal, V. Aggarwal, R. K. Jana, K. Ramakrishnan, Christopher W. Rice, and N. K. Shankaranarayanan, "Design and Characterization of a Full-Duplex Multiantenna System for WiFi Networks," *IEEE Transactions on Vehicular Technology*, vol. 63, no. 3, pp. 1160–1177, 2014.

[20] D. Bharadia, E. McMilin, and S. Katti, "Full Duplex Radios," *ACM SIGCOMM Computer Comm. Rev.*, vol. 43, no. 4, pp. 375–386, 2013.

[21] V. Syrjala, M. Valkama, L. Anttila, T. Riihonen, and D. Korpi, "Analysis of Oscillator Phase-Noise Effects on Self-Interference Cancellation in Full-Duplex OFDM Radio Transceivers," *IEEE Trans. on Wireless Comm.*, vol. 13, no. 6, pp. 2977–2990, 2014.

[22] D. Korpi, L.i Anttila, V. Syrjälä, and M. Valkama, "Widely Linear Digital Self-Interference Cancellation in Direct-Conversion Full-Duplex Transceiver," *IEEE Journal on Selected Areas in Communications*, vol. 32, no. 9, pp. 1674–1687, 2014.

[23] T. Riihonen, S. Werner, and R. Wichman, "Mitigation of Loopback Self-interference in Full-duplex MIMO Relays," *IEEE Transactions on Signal Processing*, vol. 59, no. 12, pp. 5983–5993, 2011.

[24] T. Riihonen, S. Werner, and R. Wichman, "Optimized Gain Control for Single-frequency Rrelaying With Loop Interference," *IEEE Transactions on Wireless Communications*, vol. 8, no. 6, 2009.

[25] I. Krikidis, H. A Suraweera, P. J. Smith, and C. Yuen, "Full-duplex Relay Selection for Amplify-and-forward Cooperative Networks," *IEEE Transactions on Wireless Communications*, vol. 11, no. 12, pp. 4381–4393, 2012.

[26] P. C. Sofotasios, M. K. Fikadu, S. Muhaidat, S. Freear, G. K. Karagiannidis, and M. Valkama, "Relay Selection Based Full-Duplex Cooperative Systems Under Adaptive Transmission," *IEEE Wireless Communications Letters*, vol. 6, no. 5, pp. 602–605, 2017.

[27] H. Cui, M. Ma, L. Song, and B. Jiao, "Relay Selection for Two-Way Full Duplex Relay Networks with Amplify-and-Forward Protocol," *IEEE Transactions on Wireless Communications*, vol. 13, no. 7, pp. 3768–3777, 2014.

[28] T. Riihonen, S. Werner, and R. Wichman, "Hybrid Full-duplex/Half-duplex Relaying with Transmit Power Adaptation," *IEEE Transactions on Wireless Communications*, vol. 10, no. 9, pp. 3074–3085, 2011.

[29] T. Kwon, S. Lim, S. Choi, and D. Hong, "Optimal Duplex Mode for DF Relay in Terms of the Outage Probability," *IEEE Transactions on Vehicular Technology*, vol. 59, no. 7, pp. 3628–3634, 2010.

[30] T. Riihonen, P. Mathecken, and R. Wichman, "Effect of Oscillator Phase Noise and Processing Delay in Full-duplex OFDM Repeaters," in *Asilomar Conference on Signals, Systems and Computers*. IEEE, 2012, pp. 1947–1951.

[31] G. J. González and et al., "Full-duplex amplify-and-forward relays with optimized transmission power under imperfect transceiver electronics," *EURASIP Journal on Wireless Communications and Networking*, vol. 2017, no. 1, pp. 76, 2017.

[32] A. Gomaa and N. Al-Dhahir, "Multi-user SC-FDMA Systems Under IQ Imbalance: EVM and Subcarrier Mapping Impact," in *Global Communications Conference*. IEEE, 2011, pp. 1–5.

[33] L. Blanco and M. Nájar, "Sparse Multiple Relay Selection for Network Beamforming with Individual Power Constraints Using Semidefinite Relaxation," *IEEE Transactions on Wireless Communications*, vol. 15, no. 2, pp. 1206–1217, 2016.

[34] E. Dahlman, S. Parkvall, and J. Skold, *4G: LTE/LTE-advanced for Mobile Broadband*, Academic press, 2013.

[35] D. Tse and P. Viswanath, *Fundamentals of Wireless Communication*, Cambridge university press, 2005.

[36] W. Zhong and Z. Mao, "Efficient Time-domain Residual ISI Cancellation for OFDM-based WLAN Systems," *IEEE Transactions on Consumer Electronics*, vol. 52, no. 2, pp. 321–326, 2006.

[37] G. Parsace, A. Yarali, and H. Ebrahimzad, "MMSE-DFE Equalizer Design for OFDM Systems with Insufficient Cyclic Prefix," in *Vehicular Technology Conference (VTC)*. IEEE, 2004, vol. 6, pp. 3828–3832.

[38] G. Arslan, B. Evans, and S. Kiaei, "Equalization for Discrete Multitone Transceivers to Maximize Bit Rate," *IEEE Transactions on Signal Processing*, vol. 49, no. 12, pp. 3123–3135, 2001.

[39] H. Zamiri-Jafarian, H. Khoshbin, and S. Pasupathy, "Time-domain Equalizer for OFDM Systems Based on SINR Maximization," *IEEE Transactions on Communications*, vol. 53, no. 6, pp. 924–929, 2005.

[40] Naofal Al-Dhahir and John M Cioffi, "Optimum Finite-length Equalization for Multicarrier Transceivers," *IEEE Transactions on Communications*, vol. 44, no. 1, pp. 56–64, 1996.

[41] P. J.W. Melsa, R. C. Younce, and C. E. Rohrs, "Impulse Response Shortening for Discrete Multitone Transceivers," *IEEE Transactions on Communications*, vol. 44, no. 12, pp. 1662–1672, 1996.

[42] J. Zhang and W. Ser, "A new Algorithm for Time Domain Equalization in OFDM Systems," in *VTC'02*. IEEE, 2002, vol. 2, pp. 904–907.

[43] Y. Jin and X. Xia, "An Interference Nulling Based Channel Independent Precoding for MIMO-OFDM Systems with Insufficient Cyclic Prefix," *IEEE Transactions on Communications*, vol. 61, no. 1, pp. 131–143, 2013.

[44] T. Pham, T. Le-Ngoc, G. Woodward, P. A. Martin, and K. T. Phan, "Equalization for MIMO-OFDM Systems with Insufficient Cyclic Prefix," in *Vehicular Technology Conference (VTC)*. IEEE, 2016, pp. 1–5.

[45] A. Gomaa and N. Al-Dhahir, "A New Design Framework for Sparse FIR MIMO Equalizers," *IEEE Transaction on Communications*, vol. 59, no. 8, pp. 2132–2140, 2011.

[46] A. Al-Abbasi, R. Hamila, W. Bajwa, and N. Al-Dhahir, "A General Framework for the Design and Analysis of Sparse FIR Linear Equalizers," in *Global Conference on Signal and Information Processing (GlobalSIP)*. IEEE, 2015, pp. 834–838.

[47] A. Alabbasi, R. Hamila, W. U. Bajwa, and N. Al-Dhahir, "Design and Analysis of Sparsifying Dictionaries for FIR MIMO Equalizers," *IEEE Transactions on Wireless Communications*, 2017.

[48] D. Petrovic, W. Rave, and G. Fettweis, "Limits of Phase Noise Suppression in OFDM," in *European Wireless Conference*. VDE, 2005, pp. 1–6.

[49] S. Bittner, M. Krondorf, and G. Fettweis, "Numerical Performance Evaluation of OFDM Systems Affected by Transmitter Nonlinearities, Phase Noise and Channel Estimation Errors," in *Global Communications Conference (GLOBECOM)*. IEEE, 2008, pp. 1–6.

[50] P. Mathecken, T. Riihonen, S. Werner, and R. Wichman, "Performance Analysis of OFDM with Wiener Phase Noise and Frequency Selective Fading Channel," *IEEE Transactions on Communications*, vol. 59, no. 5, pp. 1321–1331, 2011.

[51] S. Stefanatos, F. Foukalas, and T. Khattab, "On the Achievable Rates of OFDM With Common Phase Error Compensation in Phase Noise Channels," *IEEE Transactions on Communications*, vol. 65, no. 8, pp. 3509–3521, 2017.

[52] K. Nikitopoulos and A. Polydoros, "Phase-impairment Effects and Compensation Algorithms for OFDM Systems," *IEEE Transactions on Communications*, vol. 53, no. 4, pp. 698–707, 2005.

[53] S. Wu and Y. Bar-Ness, "OFDM Systems in the Presence of Phase Noise: Consequences and Solutions," *IEEE Transactions on Communications*, vol. 52, no. 11, pp. 1988–1996, 2004.

[54] D. Petrovic, W. Rave, and G. Fettweis, "Effects of Phase Noise on OFDM Systems with and without PLL: Characterization and Compensation," *IEEE Transactions on Communications*, vol. 55, no. 8, pp. 1607–1616, 2007.

[55] V. Syrjala, M. Valkama, N. Tchamov, and J. Rinne, "Phase Noise Modelling and Mitigation Techniques in OFDM Communications Systems," in *Wireless Telecommunications Symposium*. IEEE, 2009, pp. 1–7.

[56] P. Mathecken, T. Riihonen, S. Werner, and R. Wichman, "Phase Noise Estimation in OFDM: Utilizing its Associated Spectral Geometry," *IEEE Transactions on Signal Processing*, vol. 64, no. 8, pp. 1999–2012, 2016.

[57] P. Mathecken, T. Riihonen, S. Werner, and R. Wichman, "Constrained Phase Noise Estimation in OFDM Using Scattered Pilots Without Decision Feedback," *IEEE Transactions on Signal Processing*, vol. 65, no. 9, pp. 2348–2362, 2017.

[58] L. Samara, M. Mokhtar, Özgür Ö., R. Hamila, and T. Khattab, "Residual Self-Interference Analysis for Full-Duplex OFDM Transceivers Under Phase Noise and I/Q Imbalance," *IEEE Communications Letters*, vol. 21, no. 2, pp. 314–317, 2017.

[59] L. Samara, A. Gouissem, and R. Hamila, "Hybrid Full-Duplex and Alternate Multiple Relay Selection and Beamforming in AF Cooperative Networks," *IEEE Access*, vol. 6, pp. 28467–28477, 2018.

[60] L. Samara, A. O. Alabassi, R. Hamila, and N. Al-Dhahir, "Sparse equalizers for ofdm signals with insufficient cyclic prefix," *IEEE Access*, vol. 6, pp. 11076–11085, 2018.

[61] L. Samara, A. O. Al-Abbasi, R. Hamila, and N. Al-Dhahir, "Reduced-complexity sparsity-aware joint phase noise mitigation and channel equalization in ofdm receivers," *Physical Communication*, vol. 30, pp. 50–57, 2018.

[62] T. Schenk, "RF Impairments in Multiple Antenna OFDM: Influence and Mitigation," 2006.

[63] A. Tarighat, R. Bagheri, and A. H. Sayed, "Compensation Schemes and Performance Analysis of IQ Imbalances in OFDM Receivers," *IEEE Transactions on Signal Processing*, vol. 53, no. 8, pp. 3257–3268, 2005.

[64] W. Cheng, X. Zhang, and H. Zhang, "Optimal Dynamic Power Control for Full-duplex Bidirectional-channel Based Wireless Networks," in *International Conference on Computer Communications*. IEEE, 2013, pp. 3120–3128.

[65] L. Samara, R. Hamila, T. Khattab, and Ö. Özdemir, "Mean squared error analysis for ofdma signals under joint tx/rx iq imbalance," in *2018 International Conference on Advanced Communication Technologies and Networking (CommNet)*. IEEE, 2018, pp. 1–7.

[66] Z. Chen, L. X. Cai, Y. Cheng, and H. Shan, "Sustainable Cooperative Communication in Wireless Powered Networks with Energy Harvesting Relay," *IEEE Transactions on Wireless Communications*, 2017.

[67] Z. Yi and I.-M. Kim, "Optimum Beamforming in the Broadcasting Phase of Bidirectional Cooperative Communication with Multiple Decode-and-forward Relays," *IEEE Transactions on Wireless Communications*, vol. 8, no. 12, 2009.

[68] A. Alsharoa, H. Ghazzai, A. E. Kamal, and A. Kadri, "Optimization of a Power Splitting Protocol for Two-Way Multiple Energy Harvesting Relay System," *IEEE Transactions on Green Communications and Networking*, vol. 1, no. 4, pp. 444–457, 2017.

[69] B. V. Nguyen and K. Kim, "Single Relay Selection for Secure Communication in a Cooperative System with Multiple Full-duplex Decode-and-forward Relays," in *Information Forensics and Security (WIFS)*. IEEE, 2015, pp. 1–6.

[70] V. Havary-Nassab, S. Shahbazpanahi, A. Grami, and Z. Luo, "Distributed Beamforming for Relay Networks Based on Second-Order Statistics of the channel State Information," *IEEE Transactions on Signal Processing*, vol. 56, no. 9, pp. 4306–4316, 2008.

[71] J. Lee and N. Al-Dhahir, "Exploiting Sparsity for Multiple Relay Selection with Relay Gain Control in Large AF Relay Networks," *IEEE Wireless Communications Letters*, vol. 2, no. 3, pp. 347–350, 2013.

[72] A. Gouissem, R. Hamila, N. Al-Dhahir, and S. Foufou, "A sparsity-aware approach for nbi estimation and mitigation in large cognitive radio networks," in *Vehicular Technology Conference (VTC)*, Sept 2016, pp. 1–7.

[73] A. Y. Wang and C. G. Sodini, "On the Energy Efficiency of Wireless Transceivers," in *International Conference on Communications (ICC)*. IEEE, 2006, vol. 8, pp. 3783–3788.

[74] J. Tropp and A. Gilbert, "Signal Recovery from Random Measurements via Orthogonal Matching Pursuit," *IEEE Transactions on Information Theory*, vol. 53, no. 12, pp. 4655–4666, 2007.

[75] V. Strassen, "Gaussian Elimination is not Optimal," *Numerische mathematik*, vol. 13, no. 4, pp. 354–356, 1969.

[76] H. Henderson and S. Searle, "On deriving the inverse of a sum of matrices," *Siam Review*, vol. 23, no. 1, pp. 53–60, 1981.

[77] K. Petersen, Michael S. Pedersen, et al., "The Matrix Cookbook," *Technical University of Denmark*, vol. 7, pp. 15, 2008.

[78] M. Mokhtar, W. U Bajwa, and N. Al-Dhahir, "Sparsity-aware Joint Narrowband Interference and Impulse Noise Mitigation for Hybrid Powerline-wireless Transmission," in *Wireless Communications and Networking Conference (WCNC)*. IEEE, 2015, pp. 615–620.

[79] F. Wang, A. Ghosh, C. Sankaran, P. J. Fleming, F. Hsieh, and S. J. Benes, "Mobile WiMAX Systems: Performance and Evolution," *IEEE Communications Magazine*, vol. 46, no. 10, 2008.

[80] A. Al-Dweik, F. Kalbat, S. Muhaidat, O. Filio, and S. M. Ali, "Robust MIMO-OFDM System for Frequency-selective Mobile Wireless Channels," *IEEE Transactions on Vehicular Technology*, vol. 64, no. 5, pp. 1739–1749, 2015.

[81] L. Samara, V. Syrjälä, R. Hamila, and M. Valkama, "Phase Noise Mitigation in OFDMA Uplink," in *6th International Symposium on Communications, Control and Signal Processing (ISCCSP)*. IEEE, 2014, pp. 344–347.

[82] P. Rabiei, W. Namgoong, and N. Al-Dhahir, "Reduced-Complexity joint Baseband Compensation of Phase Noise and I/Q Imbalance for MIMO-OFDM Systems," *IEEE Transactions on Wireless Communications*, vol. 9, no. 11, pp. 3450–3460, 2010.

[83] Ö. Özdemir, R. Hamila, and N. Al-Dhahir, "Exact Average OFDM Subcarrier SINR Analysis Under Joint Transmit–Receive I/Q Imbalance," *IEEE Transactions on Vehicular Technology*, vol. 63, no. 8, pp. 4125–4130, 2014.

[84] S. Krone and G. Fettweis, "Capacity Analysis for OFDM Systems with Transceiver I/Q Imbalance," in *Global Communication Conference (GLOBECOM)*. IEEE, 2008, pp. 1–6.

[85] V. Syrjala, "Accurate Characterization of Oscillator Phase-Noise Corrupted OFDMA-Uplink," *IEEE Communication letters*, vol. 17, no. 10, pp. 1968–1971, 2013.

[86] W. U. Bajwa and A. Pezeshki, "Finite Frames for Sparse Signal Processing," in *Finite Frames*, pp. 303–335. Springer, 2013.

[87] W. Bajwa, R. Calderbank, and S. Jafarpour, "Why Gabor Frames? Two Fundamental Measures of Coherence and their Role in Model Selection," *Journal of Communications and Networks*, vol. 12, no. 4, pp. 289–307, 2010.

[88] W. Bajwa, R. Calderbank, and D. Mixon, "Two are Better than One: Fundamental Parameters of Frame Coherence," *Applied and Computational Harmonic Analysis*, vol. 33, no. 1, pp. 58–78, 2012.

[89] H. Ye, Geoffrey Y. Li, and B. Juang, "Power of deep learning for channel estimation and signal detection in ofdm systems," *IEEE Wireless Communications Letters*, vol. 7, no. 1, pp. 114–117, 2018.

[90] Z. Qin, H. Ye, G. Y. Li, and B. F. Juang, "Deep Learning in Physical Layer Communications," *arXiv preprint arXiv:1807.11713*, 2018.

[91] A. Balatsoukas-Stimming, "Non-linear Digital Self-interference Cancellation for In-band Full-duplex Radios Using Neural Networks," in *International Workshop on Signal Processing Advances in Wireless Communications (SPAWC)*. IEEE, 2018, pp. 1–5.

[92] Ö. Özdemir, R. Hamila, and N. Al-Dhahir, "A USRP-based Experimental Testbed for OFDM Systems Impaired by I/Q Imbalance," in *GCC Conference and Exhibition*. IEEE, 2013, pp. 98–102.

[93] A. Gouissem, L. Samara, R. Hamila, N. Al-Dhahir, L. Ben-Brahim, and A. Gastli, "Machine-Learning Based Relay Selection in AF Cooperative Networks," in *Wireless Communication and Networking Conference (WCNC)*. IEEE, 2019.

APPENDIX A: AVERAGE RESIDUAL SI POWER ANALYSIS IN OFDM SYSTEMS AFFECTED BY UNDER PN AND IQI

Towards deriving the average residual SI power, several cross-terms arise due to the co-existence of PN and IQI, which vanish to zero. For the sake of completeness, the following is the proof.

The frequency-domain received signal in the presence of PN and IQ imbalance can be written as

$$Y(k) = \sum_{c=0}^{L}\sum_{l=0}^{N-1} a_c e^{-j(w_m(cT_s+\delta)+2\pi kc/N)} \times (\mu_{rx}\mu_{tx}S[l] + \mu_{rx}\nu_{tx}S^*[l']) \times P^1_{k-l} \quad (1)$$
$$+ \sum_{c=0}^{L}\sum_{l=0}^{N-1} a_c^* e^{j(w_m(cT_s+\delta)+2\pi kc/N)} \nu_{rx}\mu_{tx}^* S^*[l'] \times P^2_{k-l}.$$

Taking the expected value of the absolute square of (1) yields

$$\mathbb{E}\left\{|Y(k)|^2\right\} = |\mu_{rx}\mu_{tx}|^2 \underbrace{\mathbb{E}\left\{\left|\sum_{c=0}^{L}\sum_{l=0}^{N-1} a_c e^{-j(w_m(cT_s+\delta)+2\pi kc/N)} S[l]P^1_{k-l}\right|^2\right\}}_{t_1} \quad (2)$$
$$+|\mu_{rx}\nu_{tx}|^2 \underbrace{\mathbb{E}\left\{\left|\sum_{c=0}^{L}\sum_{l=0}^{N-1} a_c e^{-j(w_m(cT_s+\delta)+2\pi kc/N)} S^*[l']P^1_{k-l}\right|^2\right\}}_{t_2}$$
$$+|\nu_{rx}\mu_{tx}^*|^2 \underbrace{\mathbb{E}\left\{\left|\sum_{c=0}^{L}\sum_{l=0}^{N-1} a_c^* e^{j(w_m(cT_s+\delta)+2\pi kc/N)} S^*[l']P^2_{k-l}\right|^2\right\}}_{t_3}$$
$$+ g_1\Re\left\{t_4\right\} + g_2\Re\left\{t_5\right\} + g_3\Re\left\{t_6\right\},$$

where

$$t_4 = \mathbb{E}\Bigg\{ \sum_{c_1=0}^{L}\sum_{l_1=0}^{N-1}\sum_{c_2=0}^{L}\sum_{l_2=0}^{N-1} a_{c_1} e^{-j(w_m(c_1T_s+\delta)+2\pi kc_1/N)} S[l_1]P^1_{k-l_1}a^*_{c_2} \quad (3)$$
$$\times e^{j(w_m(c_2T_s+\delta)+2\pi kc_2/N)} S[l_2](P^1_{k-l_2})^* \Bigg\},$$

$$t_5 = \mathbb{E}\Bigg\{ \sum_{c_1=0}^{L} \sum_{l_1=0}^{N-1} \sum_{c_2=0}^{L} \sum_{l_2=0}^{N-1} a_{c_1} e^{-j(w_m(c_1 T_s+\delta)+2\pi k c_1/N)} S[l_1] P^1_{k-l_1} a_{c_2} \times e^{-j(w_m(c_2 T_s+\delta)+2\pi k c_2/N)} S[l_2] (P^2_{k-l_2})^* \Bigg\}, \tag{4}$$

$$t_6 = \mathbb{E}\Bigg\{ \sum_{c_1=0}^{L} \sum_{l_1=0}^{N-1} \sum_{c_2=0}^{L} \sum_{l_2=0}^{N-1} a_{c_1} e^{-j(w_m(c_1 T_s+\delta)+2\pi k c_1/N)} S^*[l'_1] P^1_{k-l_1} a_{c_2} \times e^{-j(w_m(c_2 T_s+\delta)+2\pi k c_2/N)} S[l_2] (P^2_{k-l_2})^* \Bigg\}, \tag{5}$$

$g_1 = 2\mu_{rx}|\mu_{tx}|^2\nu^*_{tx}$, $g_2 = 2\mu_{rx}\mu^2_{tx}\nu^*_{rx}$ and $g_3 = 2\mu_{rx}\nu_{tx}\nu^*_{rx}\mu_{tx}$. The terms t_1, t_2 and t_3 reduce to the closed form expression in Eq. (2.10), while the cross terms t_4, t_5 and t_6 go to zero as shown next.

For the term t_4, given that the data, channel and PN processes are statistically independent, the following can be written

$$t_4 = \sum_{c_1=0}^{L} \sum_{l_1=0}^{N-1} \sum_{c_2=0}^{L} \sum_{l_2=0}^{N-1} \mathbb{E}\Bigg\{ a_{c_1} a^*_{c_2} e^{-j(w_m(c_1 T_s+\delta)+2\pi k c_1/N)} \times \mathbb{E}\left\{S[l_1]S[l_2]\right\} P^1_{k-l_1} e^{j(w_m(c_2 T_s+\delta)+2\pi k c_2/N)} (P^1_{k-l_2})^* \Bigg\}. \tag{6}$$

Since $\mathbb{E}\left\{S[l_1]S[l_2]\right\} = 0 \,\forall\, l_1,\, l_2$ (the data is a zero-mean complex random variable with $\mathbb{E}\{S[l_1]S[l_2]^*\} = \sigma^2_S \delta(l_1 - l_2)$). Even when $l_1 = l_2$, the result is

$$\begin{aligned} \mathbb{E}\left\{S[l_1]S[l_2]\right\} &= \mathbb{E}\left\{S^2[l]\right\} = \mathbb{E}\{(S_I[l] + jS_Q[l])^2\} \\ &= \mathbb{E}\{S^2_I[l]\} - \mathbb{E}\{S^2_Q[l]\} + 2j\mathbb{E}\{S_I[l]S_Q[l]\}. \end{aligned} \tag{7}$$

With symmetric constellation points, $\mathbb{E}\{S_I[l]\} = \mathbb{E}\{S_Q[l]\} = 0$. Moreover, the real and imaginary parts of $S[l]$ have the same energy, i.e., $\mathbb{E}\{S^2_I[l]\} = \mathbb{E}\{S^2_Q[l]\}$. Hence, the quantity $\mathbb{E}\{S^2[l]\} = 0$ and the term t_4 vanishes. Similarly, the term t_5 will vanish because of using zero-mean constellation points with both real and imagery parts having the same energy.

The term t_6 is written as follows

$$t_6 = \mathbb{E}\Bigg\{ \sum_{c_1=0}^{L} \sum_{l_1=0}^{N-1} \sum_{c_2=0}^{L} \sum_{l_2=0}^{N-1} \mathbb{E}\left\{a_{c_1} a_{c_2}\right\} e^{-j(w_m(c_1 T_s+\delta)+2\pi k c_1/N)} \times S^*[l_1'] P^1_{k-l_1} e^{-j(w_m(c_2 T_s+\delta)+2\pi k c_2/N)} S[l_2](P^2_{k-l_2})^* \Bigg\}, \tag{8}$$

where $\mathbb{E}\left\{a_{c_1} a_{c_2}\right\} = 0 \; \forall \; c_1, \; c_2$ are the channel tap's coefficients which are modeled as zero-mean circularly-symmetric Gaussian complex random variables. Similar to 7, it can be easily shown that $\mathbb{E}\{a_{c1} a_{c2}\} = 0 \; \forall \; c_1, \; c_2$. Consequently, the term t_6 is equal to zero even when $\mathbb{E}\{|S[l]|^2\} \neq 0$ when $l_1' = l_2 = l$. Hence, the residual SI power of an OFDM signal where a FD transceiver is impaired by PN and IQI reduces to the result in 2.10. Q.E.D.

APPENDIX B: RECURSIVE RELATION OF THE RESIDUAL SI IN FD AF RELAY WITH BEAMFORMING

This appendix is intended to prove the correctness of (3.2) by using a recursion approach. Recalling that the received signal $r_{R_i}[n]$ at the relay R_i is written as

$$r_{R_i}[n] = h_{SR_i}[n]x[n] + v_{R_i}[n] + I_{R_i}[n]. \tag{9}$$

The residual SI $I_{R_i}[n+1]$ at time instant $n+1$ can be written as

$$\begin{aligned} I_{R_i}[n+1] &= \tilde{h}_{R_i}[n+1]w_{R_i}[n+1]r_{R_i}[n], \\ &= \tilde{h}_{R_i}[n+1]w_{R_i}[n+1]\Big(h_{SR_i}[n]x[n] + v_{R_i}[n] + I_{R_i}[n]\Big), \\ &= \alpha[n+1]\Big(\beta[n] + I_{R_i}[n]\Big). \end{aligned} \tag{10}$$

where $\alpha[n] = \tilde{h}_{R_i}[n]w_{R_i}[n]$ and $\beta[n] = h_{SR_i}[n]x[n] + v_{R_i}[n]$. Note that when $n = 1$, the relay does not suffer from SI, i.e. $I_{R_i}[1] = 0$. This is true since the relay starts transmitting at time slot 1.

Next, it is proved by recurrence that (3.2) is correct $\forall n$. When using the notation in (10), $I_{R_i}[n]$ is written as

$$I_{R_i}[n] = \sum_{m=1}^{n-1}\Big(\prod_{p=n-m+1}^{n}\alpha[p]\Big)\beta[n-m]. \tag{11}$$

When $n = 2$, (11) is expanded by writing

$$\begin{aligned} I_{R_i}[2] &= \sum_{m=1}^{2-1}\Big(\prod_{p=2-m+1}^{2}\alpha[p]\Big)\beta[n-m] \\ &= \alpha[2]\beta[1]. \end{aligned} \tag{12}$$

Since $I_{R_i}[1] = 0$, it is deduced from (12) and (10) that (11) is verified when $n = 2$. Next, assuming (11) is correct for n, (11) needs to be verified also for $n+1$. In particular, it

is deduced from (10) that

$$I_{R_i}[n+1] = \alpha[n+1]\Big(\beta[n] + I_{R_i}[n]\Big), \tag{13}$$

$$= \alpha[n+1]\left(\beta[n] + \sum_{m=1}^{n-1}\Big(\prod_{p=n-m+1}^{n}\alpha[p]\Big)\beta[n-m]\right), \tag{14}$$

$$= \alpha[n+1]\beta[n] + \sum_{m=1}^{n-1}\Big(\prod_{p=n-m+1}^{n+1}\alpha[p]\Big)\beta[n-m]. \tag{15}$$

Applying the change of variables $q = m + 1$,

$$I_{R_i}[n+1] = \alpha[n+1]\beta[n] + \sum_{q=2}^{n}\Big(\prod_{p=n-q+2}^{n+1}\alpha[p]\Big)\beta[n-q+1],$$

$$= \sum_{q=1}^{n}\Big(\prod_{p=n-q+2}^{n+1}\alpha[p]\Big)\beta[n-q+1], \tag{16}$$

which is equal to (11) for the $n+1$'s time slot. Q.E.D.

APPENDIX C: LIST OF PUBLICATIONS

This appendix includes the list publications that were disseminated throughout the course of my studies:

Journal Articles

1. Samara, L., Mokhtar, M., Ozdemir, O., Hamila, R., and Khattab, T. (2017). Residual self-interference analysis for full-duplex OFDM transceivers under phase noise and I/Q imbalance. IEEE Communications Letters, 21(2), 314-317.

2. Samara, L., Gouissem, A., and Hamila, R. (2018). Hybrid Full-Duplex and Alternate Multiple Relay Selection and Beamforming in AF Cooperative Networks. IEEE Access, 6, 28467-28477.

3. Samara, L., Alabassi, A. O., Hamila, R., and Al-Dhahir, N. (2018). Sparse Equalizers for OFDM Signals With Insufficient Cyclic Prefix. IEEE Access, 6, 11076-11085.

4. Gouissem, A., Samara, L., Hamila, R., Al-Dhahir, N., and Foufou, S. (2018). Multiple Relay Selection and Beamforming in Dual-Hop Amplify-and-Forward Relay Networks. IEEE Systems Journal.

5. Samara, L., Al-Abbasi, A. O., Hamila, R., and Al-Dhahir, N. (2018). Reduced-complexity sparsity-aware joint phase noise mitigation and channel equalization in OFDM receivers. Physical Communication, 30, 50-57.

6. Samara, L., Gouissem, A., Hamila, R., Hasna, M. O., Al-Dhahir, N., Full-Duplex AF Relaying Under IQ Imbalance, submitted to IEEE Transactions on Vehicular Technology, 2018.

Proceedings

1. Samara, L., Ozdemir, O., Mokhtar, M., Hamila, R., and Khattab, T. (2016, March). Analysis of In-band Full-Duplex OFDM Signals Affected by Phase Noise and I/Q Imbalance. In Qatar Foundation Annual Research Conference Proceedings (Vol. 2016, No. 1, p. ICTOP2684). Qatar: HBKU Press.

2. Gouissem, A., Samara, L., Hamila, R., Al-Dhahir, N., and Foufou, S. (2017, October). Relay selection in FDD amplify-and-forward cooperative networks. Annual International Symposium on Personal, Indoor, and Mobile Radio Communications (PIMRC), (pp. 1-7). IEEE.

3. Samara, L., Hamila, R., Khattab, T., and Ozdemir, O. (2018, April). Mean squared error analysis for OFDMA signals under joint Tx/Rx IQ imbalance. International Conference on Advanced Communication Technologies and Networking (CommNet), (pp. 1-7). IEEE.

4. Gouissem, A., Samara, L., Hamila, R., Al-Dhahir, N., Ben-Brahim, L., Gastli, A. (2019, April). Machine-Learning Based Relay Selection in AF Cooperative Networks, accepted at Wireless Communications and Networking Conference (WCNC), (pp. 1-7). IEEE.